Interference Mitigation Techniques for Wireless OFDM

A Thesis Submitted in Fulfillment of the Requirements
for the Degree of Doctor of Philosophy

Khaizuran Abdullah

M.Eng, B.Sc.E.E

School of Electrical and Computer Engineering
Science, Engineering and Technology Portfolio
RMIT University

August 2009

Declaration

I certify that except where due acknowledgement has been made, the work is that of the author alone; the work has not been submitted previously, in whole or in part, to qualify for any other academic award; the content of the thesis is the result of work which has been carried out since the official commencement date of the approved research program; and, any editorial work, paid or unpaid, carried out by a third party is acknowledged.

Khaizuran Abdullah

August 2009

This dissertation is dedicated to my father who passed away during my PhD candidature, and also to my wife Julia Azrina whose unlimited love and support, and my children, including the newborn daughter, whose uncountable source of joy

Acknowledgements

I wish to express my sincere gratitude to my supervisor Associate Professor Zahir Hussain for his support and guidance throughout the duration of my study at RMIT University. I admire and appreciate the technical knowledge and personal experiences that he has shared with me. I also highly appreciate the help and comments Dr Seedahmed, a DSP engineer at Future Fiber Technologies Ltd. His supports also make me stronger to survive and understand more about DSP. I wish to greatly thank to my research colleagues, namely Fawaz, Katrina, Arun, Khalifa, Noura and Mehdi for being accompany for encouragement and supports.

Publications

Below are the publications in conjunction with the author's PhD candidacy:

Journal Publications

1. K. Abdullah, S. Mahmoud and Z.M. Hussain, "Performance Analysis of an Optimal Circular 16-QAM for Wavelet Based OFDM Systems", *International Journal of Communications, Network and System Sciences (IJCNS)*,Vol. 2, No. 9, Dec 24, 2009.

Journal Publications(Under Revision)

1. K. Abdullah, S. Mahmoud and Z.M. Hussain, "Exact BER Analysis of Circular 16-QAM", *submitted to Antenna and Wireless Propagation Letters*. Under revision.
2. K. Abdullah, and Z.M. Hussain, "An Interference Mitigation Technique for OFDM Systems", *submitted to Eurasip Journal on Wireless Communications and Networking*. Under revision.

Refereed Conference Publications

1. K. Abdullah and Z. M. Hussain, "Performance of Fourier-Based and Wavelet-Based OFDM for DVB-T Systems", *IEEE Australasian Telecommunication Networks and Applications Conference*, Christchurch New Zealand, Dec 2007.

2. K. Abdullah, K. L. Neville and Z. M. Hussain, "An Interference Cancelation Algorithm for Fourier-Based and Wavelet-Based OFDM Systems", *IEEE International Conference on Advance Technologies for Communications*, Hanoi Vietnam, Oct 2008.
3. K. Abdullah and Z. M. Hussain, "Impulsive Noise Effects on DWT- and WPT-OFDM versus FFT-OFDM", *IEEE International Conference on Communication, Computer and Power*, Muscat Oman, Feb 2009.
4. K. Abdullah and Z. M. Hussain, "Studies on DWT-OFDM and FFT-OFDM Systems", *IEEE International Conference on Communication, Computer and Power*, Muscat Oman, Feb 2009.
5. K. Abdullah, N.A. Hinai, A.Z. Sadik and Z. M. Hussain, "Circular 16-QAM Modulation Scheme for Wavelet and Fourier Based OFDM Systems", *The 5th IEEE GCC Conference*, Kuwait, March 2009.
6. K. Abdullah, A.Z. Sadik and Z. M. Hussain, "On the DWT- and WPT-OFDM versus FFT-OFDM", *The 5th IEEE GCC Conference*, Kuwait, March 2009.
7. S. M. Lajervadi, K. Abdullah and Z. M. Hussain, "Modulation Comparison Over OFDM Channel Facial Expression Recognition", *IEEE International Conference on Advance Technologies for Communications*, Hai Phong Vietnam, Oct 2009.
8. A. K. Gurung, F. S. Al-Qahtani, K. Abdullah and Z. M. Hussain, "Closed-Form Expressions for Symbol Error Rates of MIMO-MRC with Channel Estimation Error", *IEEE International Conference on Advance Technologies for Communications*, Hai Phong Vietnam, Oct 2009.
9. K. Abdullah, S. M. Lajervadi and Z. M. Hussain, "QAM Modulations over Wavelet based OFDM Channel for Facial Expression Recognition", *IEEE Australasian Telecommunication Networks and Applications Conference*, Canberra Australia, Nov 2009.

Keywords

Fourier Based OFDM, Wavelet based OFDM, 16-QAM, Discrete Wavelet Transform, Wavelet Packet Transform, Discrete Multitone Modulation, Discrete Wavelet Multitone Modulation, Wavelet OFDM, FFT-OFDM, Multicarrier Modulation, Fourier based Multicarrier Modulation, Orthogonal Wavelets, Biorthogonal Wavelets.

Preface

This dissertation considers two OFDM systems; Fourier and wavelet based OFDM systems. Fourier based OFDM system is referred to an OFDM technique that uses Fourier transform in the transceiver. On the other hand, wavelet based OFDM system is used when an OFDM transceiver uses wavelet transform. Conventional OFDM system uses inverse fast Fourier transform (IFFT) and fast Fourier transform (FFT) in the transmitter and receiver respectively for simultaneous parallel multiplexing of signals in the transmitter and receiver. Simultaneous subchannels are orthogonal to each other during the transmission. In time domain, the subchannels are in rectangular pulses next to each other, on the other hand, these subchannels are in sinc pulses in frequency domain. The peak amplitude of the sinc pulse is at null's of other sinc pulse. By having this property, the orthogonality is achieved. However, OFDM bandpass signal in reality suffers distorted signals. The received signal becomes distorted or not perfect due to time varying channel or multipath fading. This situation can also be called a nonuniform OFDM system. In this case, the spacing between two adjacent subcarriers is not constant because of intersymbol interference (ISI) and intercarrier interference (ICI). To combat these interference, guard interval (GI) which is the length of cyclic prefix (CP) is implemented in an OFDM system in such that it is longer than the channel impulse response. However, longer GI may reduce channel efficiency. For example, in digital video broadcasting-terrestrial (DVB-T) system there are 4 available GI, $\frac{1}{4}$,$\frac{1}{8}$, $\frac{1}{16}$ and $\frac{1}{32}$. Using $\frac{1}{4}$ results the best protection but the data

rate is the lowest. On the other hand, using $\frac{1}{32}$ gives the highest data rate but results in the least protection. An alternative solution without using a CP is to use wavelet transform. The channel efficiency is obviously enhanced if the system does not use CP. According to the Institute of Electrical and Electronics Engineers (IEEE) broadband wireless standard [34], avoiding the CP gives Wavelet OFDM an advantage of roughly 20 percent in bandwidth efficiency [78]. Further discussion of Fourier based OFDM is in chapter 2, whereas, chapter 3 describes more about wavelet based OFDM.

Circular and square 16-quadrature amplitude modulation (QAM) techniques, Narrowband interference models and mitigation techniques, interference cancelation algorithm, impulse noise interference effects, and DVB-T system are discussed in this dissertation. All chapters include both OFDM systems except chapters 2 and 5. Since modulation technique is a part of wireless multicarrier communication system, chapter 4 includes the discussion of circular and square 16-QAM schemes. Although there are many modulation techniques used by OFDM systems, a common and simple technique is to use binary pulse shift keying (BPSK) signaling. Incoming signal is modulated to $+1$ and -1 before transmission and recovered back to the original signal after demodulation in the receiver. Examples of good related works that use BPSK can be obtained from [2], [62]. But, this type of modulation limits a bandwidth usage. A better technique is to use M-ary QAM. A 2 bit per OFDM symbol can be performed using 4-QAM. The data signal is mapped into 4 levels which are $\pm 1 \pm j$. At the receiver, the signal needs to be detected and demodulated for recovery. Performance studies can be done to compare the bit error. The next QAM technique is 16-QAM which uses 16 levels for modulating an incoming signal. The incoming signal is mapped into 16 possible levels from combinations of $\pm 1 \pm j$, $\pm 3 \pm j3$, $\pm 1 \pm j3$, and $\pm 3 \pm j$. At the receiver, the signal needs to be detected and demodulated for recovery. Since the number of levels are larger than 4-QAM and suffering of multipath effect, the bit error rate (BER) would be larger than that of 4-QAM. Other QAMs are 64-, 128-

and 256-QAM. The more the levels of QAM, the more complex the receiver needs to demodulate for the recovery. This will result more bit errors as the system becomes more complex. Most of literatures discuss the square QAM scheme. For this reason, a niche modulation technique needs to focus for the comparisons between Fourier and wavelet based OFDM. The 16-QAM modulation is a good choice for this study with comparisons of circular and square 16-QAM schemes in both OFDM systems.

Another important issue is the effect of narrowband interference to the OFDM systems. The definition of the narrowband interference is that its spectrum is far less than the signal transmission bandwidth occupied by the data. This means that few subcarriers are affected by the interference. Another term of narrowband interference is sinusoidal interference. BER performance can be improved if a mitigation technique is introduced in the systems. Thus, the literature surveys of models and mitigation techniques are discussed in chapter 5, and chapter 6 introduces the proposed technique to reduce or mitigate the interference.

The impulse noise interference is also considered in this dissertation. Unlike the density noise which is normally based on Gaussian distribution, the impulse noise is considered as Poisson distribution. A recurrence Poisson parameter and a ratio of impulse noise power over Gaussian noise power are taken into considerations when observing impulse noise affecting both OFDM systems. Two situations heavily disturbed and less disturbed should be considered. Comparisons of BER results are performed in both OFDM systems, Fourier and wavelet based OFDM systems. Further discussion can be viewed in chapter 7.

Application of OFDM systems in DVB-T is also studied in chapter 8. The DVB-T in 2k mode under the European Telecommunications Standards Institute (ETSI) standard is considered. In this case, 1705 subcarriers for one OFDM symbol are generated within 8 kHz bandwidth. Generations of the signals are considered in additive white Gaussian noise (AWGN) channel and

also multipath fading. Simulation results are done in Fourier based OFDM system as well as in wavelet based OFDM system. Facial expression recognition (FER) application which is used as input message is considered also in this last chapter.

I hope that this dissertation would be used as a source of study and inspire further research in these fields.

Khaizuran Abdullah

Melbourne

August 2009

Contents

List of Figures

List of Tables

List of Acronyms and Principal Symbols

T_s	OFDM symbol period
T_{s1}	OFDM symbol period first block
T_{s2}	OFDM symbol period second block
T_F	Effective OFDM symbol period or the FFT/IFFT duration
T_{CP}	Guard time
f	Frequency
B	Bandwidth
ΔB	Excess bandwidth
f_c	Carrier Frequency
f_d	Doppler spread Frequency
f_n	Nyquist bandwidth
f_s	Sampling Frequency
R	Transmission rate
P_{ave}	Power average of transmitted signal
$\Phi_{nn}(f)$	Ratio power spectral density of the additive Gaussian noise
$\|C(f)\|^2$	Square absolute value of the capacity
α	Gain parameter
$<,>$	Dot product

$(.)^T$	Transposition
$(.)^*$	Conjugation
$(.)^H$	Hermitian transposition
CA	Low pass filter (approximated) coefficients for DWT transmitter
CD	High pass filter (detail) coefficients for DWT transmitter
ca	Low pass filter (approximated) coefficients for DWT receiver
cd	High pass filter (detail) coefficients for DWT receiver
a	Poisson recurrence parameter
d	Message signal
g	Low pass filter coefficients
h	High pass filter coefficients
M	Length of an oversampled FIR filter
m	Length of Nyquist rate FIR filter
N	Number of subcarriers
ns	Number of symbols
r	ratio impulsive noise power over Gaussian noise power
U_k	DWT-receiver incoming signal
U_m	QAM demodulator input signal
uu	serial output signal from DWT
X_m	QAM modulator output signal
xx	serial input signal for IDWT
X_k	DWT-transmitter outgoing signal
β	Roll-off factor
μ	Step-size of algorithm adaptation
ν	Mobile speed
Ω	Normalized Radian Frequency
ϕ	Scaling function
ψ	Wavelet function
ρ	SNR improvement
σ	Variance of a signal
c	Speed of light

ADC	Analog-to-Digital Converter
BER	Bit Error Rate
BPSK	Binary Pulse Shift Keying
CP	Cyclic Prefix
DAB	Digital Audio Broadcasting
DAC	Digital-to-Analog Converter
DFE	Decision feedback equaliser
DFT	Discrete Fourier Transform
DMT	Discrete Multitone Modulation
DSP	Digital Signal Processing
DVB-T	Digital Video Broadcasting - Terrestrial
DWMT	Discrete Wavelet Multitone Modulation
DWT	Discrete Wavelet Transform
EbN0	Energy Bit over Density Noise ratio
ETSI	European Telecommunications Standard Institute
FDM	Frequency division multiplexing
FER	Facial Expression Recognition
FFT	Fast Fourier Transform
FFT-OFDM	Fast Fourier Transform OFDM
FIR	Finite-Impulse Response
GI	Guard Interval
HiperLAN	High Performance LAN
HPF	High Pass Filter
ICA	Interference Cancelation Algorithm
ICI	Intercarrier Interference
IIR	Infinite-Impulse Response
IDFT	Inverse Discrete Fourier Transform
IDWT	Inverse Discrete Wavelet Transform

IEEE	Institute of Electrical and Electronics Engineers
IFFT	Inverse Fast Fourier Transform
ISI	Intersymbol Interference
LAN	Local Area Network
LPF	Low Pass Filter
MSE	Mean-Square Error
MSM	Multiscale Wavelet Modulation
OFDM	Orthogonal Frequency Division Multiplexing
PAPR	Peak-to-Average Power Ratio
PAM	Pulse Amplitude Modulation
PDF	Probability Density Function
QAM	Quadrature Amplitude Modulation
RBS	Radio Base Station
RFI	Radio Frequency Interference
RS	Reed Solomon
SNR	Signal-to-noise ratio
WOFDM	Wavelet based Orthogonal Frequency Division Multiplexing
WPT	Wavelet Packet Transform

Abstract

Orthogonal Frequency Division Multiplexing (OFDM) is a promising multi-carrier wireless system for transmission of high-rate data stream with spectral efficiency and fading immunity. Conventional OFDM system use efficient IFFT and FFT to multiplex the signals in parallel at the transmitter and receiver respectively. On the other hand, wavelet based OFDM system uses orthonormal wavelets which are derived from a multistage tree-structured wavelet family. The Fourier based and wavelet based OFDM systems are studied in this dissertation. Two types of QAM schemes, circular and square modulations are used to compare the performance in both OFDM systems. A new approach of determining exact BER for optimal circular QAM is proposed. In addition, the presence of narrowband interference (NBI) degrades the performance of OFDM systems. Thus, a mitigation technique is necessary to suppress NBI in an OFDM system. Recent mitigation techniques can be broadly categorised into frequency domain cancellation, receiver windowing and excision filtering. However, none of the techniques considers wavelet based OFDM. Therefore, an interference cancelation algorithm has been proposed to work for both OFDM platforms. The performance results of two OFDM schemes applicable to digital video broadcasting (DVB)-terrestrial system and under the effect of impulsive noise interference are also included. BER performances are obtained in all results. It has been shown that wavelet based OFDM system has outperformed Fourier based OFDM system in many cases.

Twelve papers have been published/submitted during this candidature.

Chapter 1

Introduction

1.1 Introduction

OFDM can be considered as a multicarrier modulation system. The transmission channel is divided into a number of subchannel in which each subchannel is assigned a subcarrier. When a signal is transmitted through a non-ideal channel, intersymbol interference (ISI) will occur such that the system performance is degraded. The degree of the performance depends on the frequency response characteristics of the channel. Due to this ISI effect, the complexity of the receiver will also be increased [49]. Two factors of constraints are usually required for designing the system, they are the transmitted power constraints and receiver complexity constraints. Within these constraints, a designer has to efficiently use the channel bandwidth availability in order to transmit the information reliably. When a single carrier system is employed in which the sequence of messaging data is transmitted in serial at some specified transmission rate R symbols per second, the time dispersion of the non-ideal channel is normally much greater than the symbol duration. Hence, ISI will greatly affect the receiver system. For this reason, an equaliser is required to compensate for the system. Examples of equalisers in the receiver are discussed in [29], [43], [44], [79]. The principle task of an equaliser is to flatten the channel over the used bandwidth. This is possible by using a digital filter at the receiver. This means that the channel becomes linear satisfying the

water pouring optimisation theory. According to [42], the bits per channel assigned to each narrowband frequency bin is flat before transmission. After transmitting via a non-linear channel, the received signals become unflattened or have deep fades due to cross talk or interference. To recover the signals, the equalisers in the receiver must compensate for the defect. A decision feedback equaliser (DFE) generally improves the performance by minimising the ISI by converting the channel into a minimum phase channel and then subtracting the resulting channel output from an emulated ISI pattern provided in its feedback path [79]. Detailed discussions are in [48] and [42] about the water-pouring interpretation in which the average transmitted power (P_ave) as the same amount of pouring water into a bowl. The ratio of the power spectral density of the additive white Gaussian noise ($\Phi_{nn}(f)$) over the square absolute value of the capacity ($|C(f)|^2$) is interpreted as the bottom of a bowl of unit depth. The water which is interpreted as P_{ave} will distribute itself into the bowl to achieve the capacity. To make the frequency response becomes flat, the transmitted power in each subchannel should be a constant value for all subchannels over specified bandwidth. Furthermore, it is suggested by [48] that the transmission data of a single modulated carrier with an equaliser at the receiver is difficult to achieve at a high transmission rate. Thus, a multicarrier transmission technique such as OFDM can possibly compensate for the problem by assigning parallel transmission of quadrature amplitude modulation (QAM) symbols with an inverse fast Fourier transform (IFFT) and fast Fourier transform (FFT) operations in the transmitter and the receiver respectively. OFDM consists of N independent QAM channels which are called subcarriers, each operating at the same symbol rate $\frac{1}{T}$ within distinct constellation points having complex-valued signals. The IFFT and FFT are employed to modulate and demodulate the N subcarriers into QAM information symbols at the transmitter and receiver respectively. However, one limitation of this conventional based OFDM is that it suffers relatively large spectral sidelobes. The first sidelobe is only 13 dB down from the peak at the

desired subchannel [48]. As a result, the Fourier based implementations are vulnerable to interchannel interference (ICI). It is suggested that substantially lower sidelobes need to be achieved to deal with such channel anomalies. An attractive alternative is to use wavelet based filters which satisfy the perfect reconstruction property [83], [48].

Recently, wavelet based OFDM has became popular in much of the literature. Wavelet OFDM can better combat narrowband interference and is inherently robust to ICI compared to FFT filters, this is due to the fact that its filters offer very high spectral containment properties [82], [88], [100], [106], [118]. In this dissertation, we are discussing the study on the comparisons of conventional OFDM, which is Fourier based OFDM, with wavelet based OFDM. Another term which can be used for Fourier based OFDM is FFT-OFDM since it is referring to FFT filters in the OFDM transceiver. Sometimes, this conventional OFDM is also called discrete multitone modulation (DMT) because it also uses Fourier filters in both transmitter and receiver. On the other hand, other names of wavelet based OFDM are discrete wavelet transform (DWT)-OFDM. This alternative implementation is also sometimes called discrete wavelet multitone modulation (DWMT).

Recent trends and developments in the use of wavelets in wireless communications are reviewed in [78]. Among other uses of wavelets are source and channel coding, channel modeling, data compression, signal denoising, and design of transceivers. It is reported that the flexibility and ability to characterize signals accurately is the main property of wavelets in these applications. Having such property makes wavelets a strong candidate for future use in the wireless field. The meaning of wavelet originally came from construction of small waves since the derivation of the word wavelet is from the French researcher, Jean Morlet, who used the French word *ondelette* meaning a *small wave* [85]. Then, the word was transformed from *onde* into *wave* combining with *lette* to become "wavelets". From the definition of its name, it is suggested that wavelets are small waves with an oscillating non-zero signal

for limited periods of time governed by mathematical properties. Fourier and wavelet transforms are almost the same in performing their tasks because they decomposes signals into elementary waveforms or basis of frequency components. However, their basis functions are different. Fourier transform has sines and cosines as its elementary functions. On the other hand, wavelet transform has the basis elements in terms of low pass and high pass filter coefficients. Due to the characteristics of the basis functions, wavelet has the ability to analyse the local properties of the input signal, such as edges or transients. In this case, Fourier transform is not an efficient tool to analyse the local property such as the edge or transient. The wavelet transform is represented by the scale and time analysis whereas the Fourier transform is represented in time and frequency domain. In general, a wavelet transform uses an irregular shape of scaling and wavelet functions to represent sharp change and local feature of a signal. At low frequencies, wavelet transform gives a good frequency resolution and poor time resolution, whereas, at high frequencies, it gives good time resolution and poor frequency resolution. This principle is correct since a signal can be considered as having high frequency components for short durations and low frequency components for long durations.

1.2 Fourier Versus Wavelet based OFDM

Fig. 1.1 shows an overall system block diagram for a wavelet based and Fourier based OFDM systems. The system is considered wavelet based OFDM if it uses IDWT and DWT blocks in place of the blocks labelled 'inverse transform' and 'forward transform' respectively. On the other hand, it is considered as Fourier based OFDM when it uses IFFT and FFT blocks in place of the blocks labelled 'inverse transform' and 'forward transform' accordingly. Let us discuss the wavelet based OFDM first. The transmitter in the top part of Fig. 1.1, accepts serial data d, in the form of time-division multiplexed (TDM) data, and converts it into several lower rate sequences of channel symbols in the

QAM modulator. It is then passed in parallel to the inverse discrete wavelet transform(IDWT) block as X_m. A single signal sequence X_k is the output after IDWT and is being frequency division multiplexed (FDM) before being passed to a DAC (digital to analog converter) for transmission. Then, the transmitted signal passes through the communication channel such as an additive White Gaussian noise channel (AWGN) or multipath channel. At the wavelet based OFDM receiver, shown in the bottom part of Fig. 1.1, multicarrier demodulation is performed with a discrete wavelet transform (DWT). The decoded data sequences are then converted back to a single TDM stream, d_m, and passed through the data recovery process.

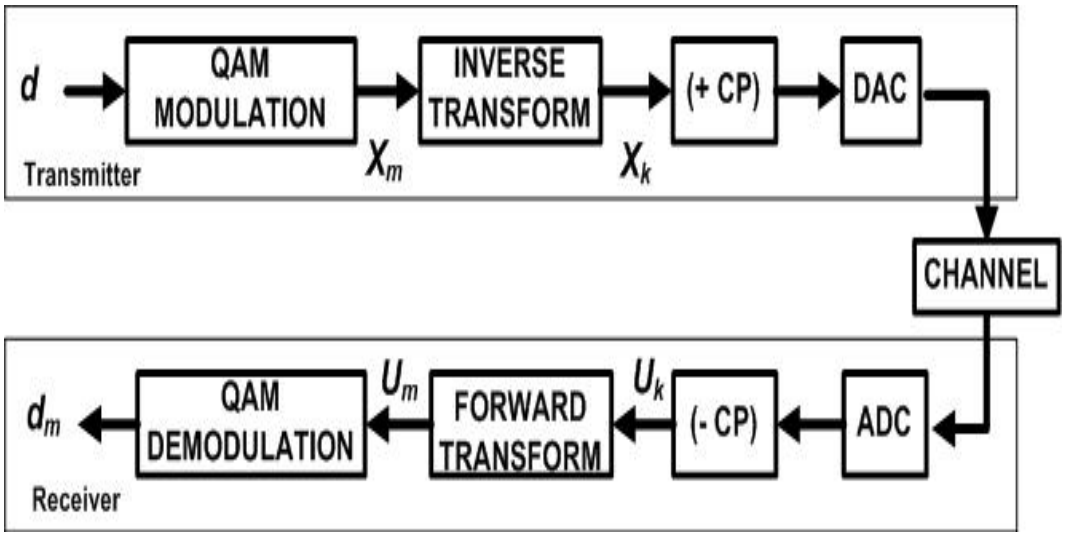

Figure 1.1: An OFDM transceiver. Note that the bracket sign of the components (+CP) and (-CP) are referring to the system does not require CP for wavelet based OFDM, whereas, it requires CP for Fourier based OFDM. The plus and negative signs indicate 'add' and 'remove' CP when it deals with Fourier based OFDM.

For the Fourier based OFDM system, the transform blocks' implementations are with an inverse and forward FFT, rather than with an inverse and forward wavelet transform. Other system block functions are similar to DWT-OFDM system. In following two chapters, both OFDM systems are discussed in details.

1.3 Orthogonal versus Biorthogonal

The Fourier transform has exponential parts consisting of cosine and sine signal bases which are orthogonal to each other. The wavelet transform also has orthogonal bases. Its bases are low pass and high pass filters which are associated with the scaling and wavelet function respectively. Since Fourier and wavelet transforms are orthogonal, their BER results will show similar performances in an AWGN channel. Currently, we are not interested in discussing the results but in section 3.4, a more detailed of performance of this will be presented. The purpose of this section is to introduce the concepts of orthogonal and biorthogonal bases and why they are fundamental to the work in this dissertation.

The wavelet transform can be classified either orthogonal or biorthogonal [86]. Using the MATLAB command *wavename('orth')* or *wavename('bior')*, we can check whether a wavelet family is orthogonal or biorthogonal. Among orthogonal wavelets are Daubechies, Coiflets, Morlet and Meyer. On the other hand, biorthogonal wavelets are different than orthogonal wavelets because they have biorthogonal bases meaning that their bases have symmetric perfect reconstruction properties with compactly support. In order to work as biorthogonal functions, their scaling and wavelet filters have duality properties. In this case, there are two duality functions for each scaling and wavelet, they are ϕ and $\hat{\phi}$ for the scaling filters, and ψ and $\hat{\psi}$ for the wavelet filters accordingly. In MATLAB, we have built-in functions such as bior1.1, bior2.2 , bior5.5 , rbio1.1, rbio2.2 and rbio5.5. The number next to its name is referring to the length of the filter in the decomposition and reconstruction filters.

1.4 Research Problem

Conventional OFDM uses a Fourier based transform in this case the system requires a cyclic prefix (CP) to minimize ISI. However, by having this CP in the symbol transmission, the bandwidth usage would be inefficient. An

alternative way is to use the wavelet transform which will allow the overlapping of subcarriers in the symbol transmission and not require the CP. Due to time overlap wavelet based OFDM system can not use cyclic prefix (CP) or any kind of guard interval (GI) that is commonly used in conventinal OFDM system [28]. By not requiring the CP, the bandwidth would be more efficiently used. According to [118], wavelet based OFDM gives more advantage in spectral containment compared to Fourier based OFDM due to the overlapped nature offered by wavelets. The higher the overlapping factor g, the better the spectral containment [89], [118]. The comparisons of frequency responses is shown in Fig. 1.2.

A similar comparison between the frequency responses of wavelet based and Fourier based OFDM also can be found in [88], [89]. The first side lobe for a wavelet based OFDM subchannel is 45 dB down from the main lobe, on the other hand, it is only 13 dB down from the main lobe for Fourier based OFDM. It is worth mentioning that the great reduction in sidelobe levels is the main motivation behind the recent trend of using wavelet filters in OFDM systems. Wavelet filters provide better spectral containment than its Fourier counterpart. When orthogonality between carriers is lost after the transmitted signal passes through a non-uniform channel, the amount of interference between carriers in wavelet systems is much lower than in Fourier systems since the sidelobes contain much less energy. This improved spectral containment reduces ICI. The notion of a CP (and the necessary 1-tap equalizers at the receiver) does not make sense in the context of wavelet OFDM, due to the overlapped nature of the signaling. Reduced ICI without the need for a CP is an attractive feature of wavelet OFDM. It allows data rates to be pushed past those of Fourier OFDM, which relies heavily on the CP and 1-tap filters to mitigate the effects of ICI.

This dissertation also tackles impulsive noise interference which can be considered as one of the major drawbacks that degrade OFDM system performance. Impulsive noise interference is a primary source of performance degra-

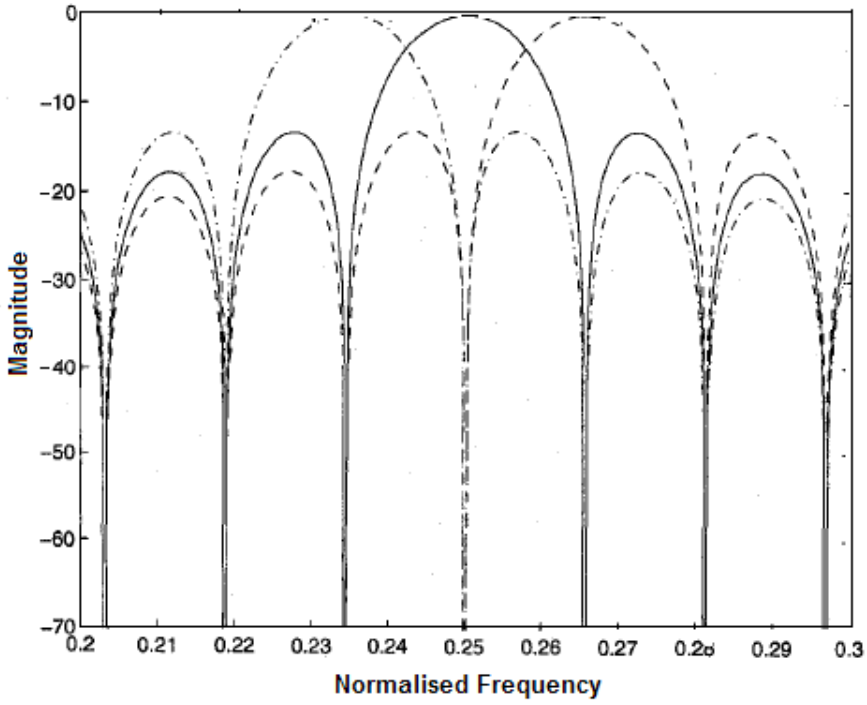

(a) DMT transmission

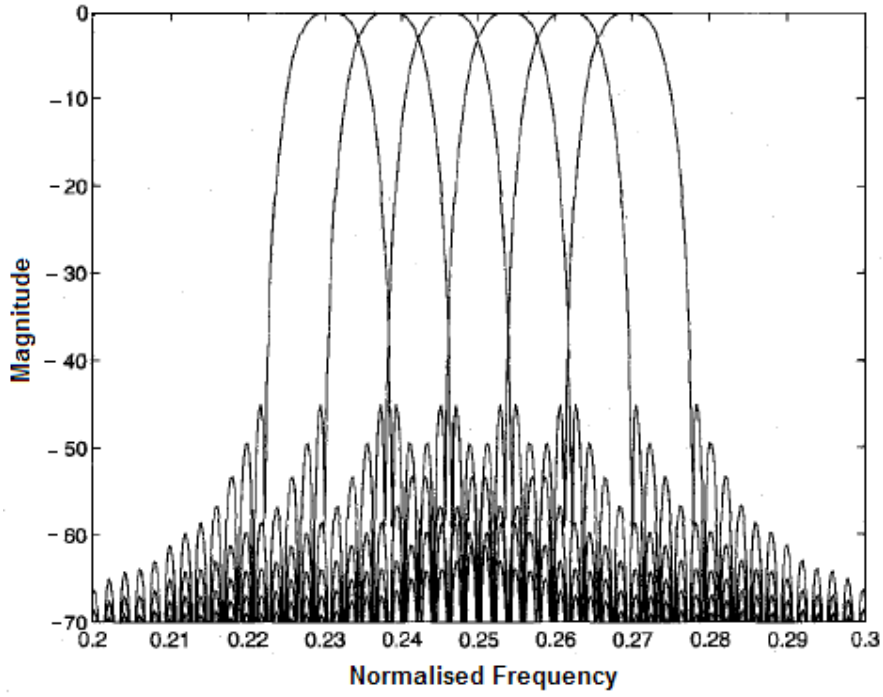

(b) DWMT transmission

Figure 1.2: Illustrating the frequency response comparisons of six spectrally contiguous subchannel pulse sequences between Fourier (DMT transmission) and wavelet based OFDM (DWMT transmission) taken from [118].

dation in several applications, including data transmission over telephone networks and its effects on various digital communication schemes have received considerable attention [62], [75], [91], [111], [115]. A noise burst is considered impulsive if it causes a response in the RF filter portion of a receiver which is essentially identical in shape to the impulse response of the RF filter, i.e., differs from it at most by a complex gain. Thus the essential requirement for a noise burst to be called impulsive is that its spectrum be flat across the passband of the RF filter studied. It appears that for a wide range of communication receivers and pulse-like disturbances found in their vicinity, the above impulsive noise definition should be quite satisfactory. Broadly speaking, in the case of radio links the impulsive interference is caused by a combination of atmospheric noise and man-made noise for frequencies up to 100 MHz and is almost exclusively man-made for frequencies above 100 MHz. In telephone lines the impulsive interference is also caused by several sources: lightning, switching transients, and accidental hits during maintenance work. Thus, the study is to generate impulsive noise contamination to both OFDM systems; Fourier and wavelet. In this case, Poisson distribution is considered for the impulsive noise distribution. To generate impulsive noise with Poisson distribution, a Poisson recurrence parameter a, is considered along with a ratio r which is the ratio of impulsive noise power over Gaussian noise power. Considering this distribution, a Poisson recurrence parameter a is observed in two cases when a is small and a is large. This problem is shown in Fig. 1.3.

Another important issue is the effect of radio frequency interference (RFI) to the OFDM systems. RFI can be divided into two types; narrowband interference and broadband interference [96]. The sources of narrowband interference are produced from intentional transmissions such as radio and TV stations, pager transmitters, baby monitors, microwave ovens, garage door openers and cell/cordless phones [2], [96]. Narrowband interference can be defined as a bandpass signal that has a bandwidth much less than the bandwidth of an OFDM signal [48]. This definition is also approximately close

to the definition of narrowband interference in a spread spectrum system described by [47]. The narrowband interference spectrum may reside within an OFDM spectrum. The OFDM subcarriers which are adjacent to it may be affected. Due to this effect, the performance of OFDM systems becomes degraded. On the other hand, broadband interference is caused by the devices with a rich harmonic content which interferes over a very broad spectrum, due to this characteristics, the interference spectra is embedded within almost every subcarrier in an OFDM symbol. The receiver will also be less effective to filter the interference. This dissertation focusses mainly on mitigating the narrowband interference. The broadband interference mitigation may be left for future research.

1.5 Thesis Objectives

The objective section is divided into two parts: main objective and specific objectives. The main objective consists of reviewing the study of wavelet based OFDM as an alternative replacement to the conventional OFDM system, Fourier based OFDM. With the alternative approach, wavelet based OFDM, DWT and IDWT operations replace the IFFT and FFT blocks.

The specific objectives are described as follows. Firstly, to observe the circular M-ary modulation type for Fourier and wavelet based OFDM. The circular scheme needs to be compared with the conventional square scheme in both OFDM platforms. Since there are many types of modulations such as BPSK, QPSK, and M-ary QAM, one type is chosen to have a niche area of study, this being 16-QAM modulation. This modulation type is chosen for this research based on the fact it is commonly used in the standard OFDM modulation schemes such as terrestrial Digital Video Broadcasting (DVB), Digital Audio Broadcasting (DAB) and High Performance Radio LAN Version 2 (HIPERLAN/2) [108]. It is also a moderate modulation scheme of obtaining the results between 4-QAM and 64-QAM [48].

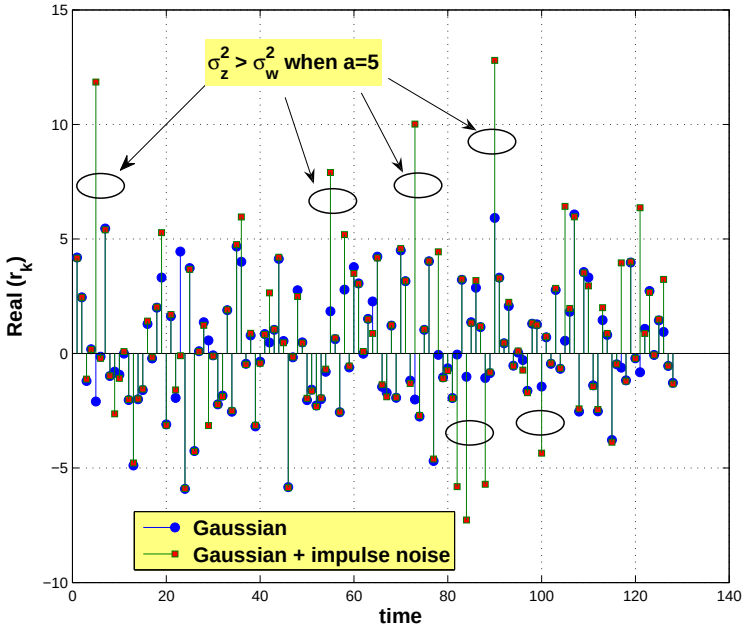

(a) Impulsive noise effect when a=5

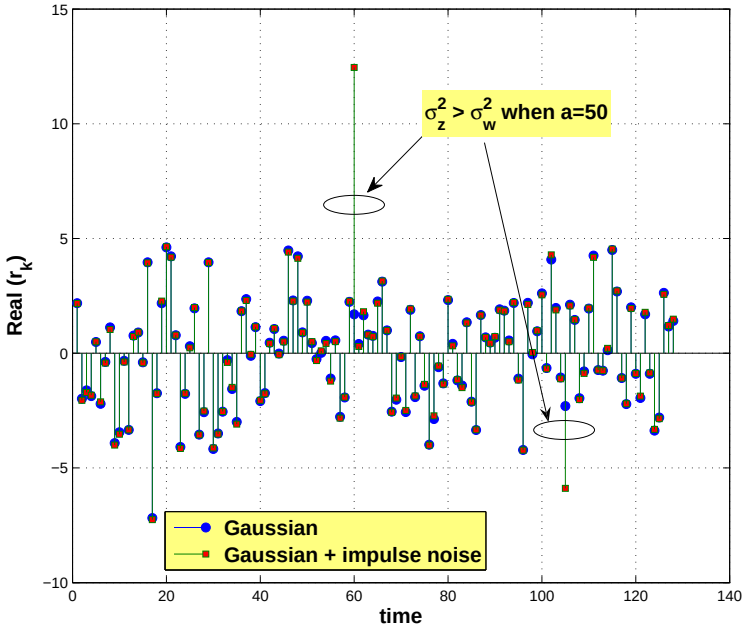

(b) Impulsive noise effect when a=50

Figure 1.3: Sequence Samples of two OFDM symbols with impulsive noise effect, (a) small a, i.e. $a = 5$ and (b) large a, i.e. $a = 50$.

The second specific objective is to study the effect of impulsive noise interference in both OFDM systems. Studies indicate that OFDM systems are affected by impulsive noise following a Poisson distribution. Considering this distribution, a Poisson recurrence parameter, a is observed. Two scenarios; a is small and a is large are investigated. From these situations, performance of results among Fourier and wavelet based OFDM are obtained.

The third specific objective is to mitigate interference in Fourier and wavelet based OFDM. A sinusoidal interference, which is an unknown signal component, is considered to affect both OFDM systems. An interference cancelation algorithm is developed to minimise or mitigate that unknown signal. For this problem of study, we propose two situations; an ideal case which is when the received signal mixes with a known interference signal, and a non-ideal case where the received signal is contaminated with an unknown interference signal. Both cases are determined under the two OFDM systems, Fourier and wavelet based OFDM. Performance of results are obtained to observe which system outperforms the other.

The last specific objective is to study the application of DVB-T for both OFDM systems. To simulate the system, the standard parameters approved by ETSI in 2k mode or 8k mode should be considered. The study should perform the comparative BER performances between wavelet (DWT) based OFDM and Fourier (FFT) based OFDM. It also will include both AWGN and Rayleigh fading channels.

1.6 Original Contributions

The main contributions of this dissertation are as follows:

1. A new approach of study on calculation of exact and closed-form of BER for circular 16-QAM constellation based on the four types of the decision boundaries is developed. Each decision boundary is classified based on minimum distance d, following the pdf Gaussian distribution

with respect to the in-phase and quadrature components n_I and n_Q respectively. The BER analysis is extended to determine the exact BER for other M-ary QAM. It is shown that all the simulation results have met the theoretical calculations for all M-ary QAM modulations. This led to the submission of publication in *IEEE Antenna and Wireless Propagation Letters* in August 2009.

2. A new approach of study on the circular 16-QAM constellation that has been performed in the previous point is developed and applied to the Fourier and wavelet based OFDM systems. The error performance is done between circular and square schemes. The BER performance also includes comparisons of wavelet families; orthogonal and biorthogonal wavelets. This contribution was presented at *The 5th IEEE GCC Conference* in March 2009.
3. A new approach on designing the wavelet-based OFDM for DVB-T system is performed. DVB-T system is conventionally done using Fourier based OFDM. By using the same OFDM parameters of DVB-T (2k mode) compliance with ETSI standard as in Fourier based, the wavelet based OFDM is considered. Comparative BER performances are included. It is shown that the DWT-OFDM outperforms FFT-OFDM in AWGN and also in Rayleigh fading channels. This study was published in *IEEE Australasian Telecommunication Networks and Applications Conference* (ATNAC) in 2007 [55]. This new approach also can be viewed in IEEE xplore.
4. A new interference cancelation algorithm (ICA) for Fourier and wavelet based OFDM is proposed. This ICA is considered in two cases, ideal and non-ideal. In the ideal case, we assume the reference signal is an unwanted sinusoidal signal (the input to our ICA algorithm). In the non-ideal case, we assume the received OFDM signal is contaminated with sinusoidal interference. From these two cases, we indicate that the proposed ICA exhibits outstanding performance since the BER results

obtained in both cases are almost the same. The wavelet based OFDM outperformed the Fourier-based OFDM in both cases. The findings of this work was published in *IEEE International Conference on Advance Technologies for Communications (ATC)* in 2008 [56]. This paper is available in IEEE xplore.

5. The impulsive noise effect on OFDM system is one of the challenging issues faced by OFDM studies, therefore, designing the steps of how to simulate flexible transformed models of DWT- and WPT-OFDM as alternative replacements of FFT-OFDM under the effect of impulsive noise is one of the new approaches in this dissertation. The development of DWT and WPT models are the keys of study. This work led to the publication in the *IEEE International Conference on Communication, Computer and Power* in February 2009 [57].
6. A model for DWT-OFDM is designed, this includes zero-padding and vector transpose for transmitting the OFDM signal. In order to act as an alternative replacement for conventional OFDM system, the wavelet based OFDM has to fulfill the perfect reconstruction properties. A modified version of the perfect reconstruction property was designed. This includes the analytical proof of mathematical equations involving the input and output variables of the low pass and high pass filters to illustrate the PR property's operation are discussed. This material was published in *IEEE International Conference on Communication, Computer and Power* in February 2009 [58].
7. A novel study is conducted on the performance of two different types of QAM modulations, 4 and 16 QAM, using FFT-OFDM system and facial expression recognition. The result shows that the image as an input source has been correctly detected by the receiver as expected. This has been proved when the empirical results obtain about the same as the theoretical results. This work was published in *IEEE International Conference on Advance Technologies for Communications (ATC) 2009*

[114].

8. The previous item is modified and developed so as to allow a study of BER performance when DWT-OFDM and facial expression recognition is conducted. Two types of wavelet transform; orthogonal (using db2) and biorthogonal (using bior5.5) are used for two different types of QAM modulations, 4 and 16 QAM, considering DWT-OFDM system. The result shows that bior5.5 performs better than db2 BER. This is due to the fact that biorthogonal wavelets offer more advantages by having symmetrical scaling and wavelet functions. This new idea was published in *IEEE Australasian Telecommunication Networks and Applications Conference (ATNAC) 2009* [61].

1.7 Thesis Organisation

This dissertation consists of nine chapters, organised as follows:

Chapter 2: Fourier Based OFDM

An overview of the conventional OFDM is made in this chapter. As this OFDM system is a multicarrier system, it has many advantages to deal with multipath effect by having a cyclic prefix. This prefix must be longer than the channel impulse response to reduce ISI. This chapter provides system process and model of FFT-OFDM. It also discusses the orthogonality, cyclic prefix, IFFT and FFT operations. The peak-to-average power ratio of FFT-OFDM is also provided at the end of the chapter.

Chapter 3: Wavelet Based OFDM

In this chapter wavelet based OFDM, which is an alternative candidate to replace conventional OFDM, is introduced. It is suggested by much literatures that it has high spectral containment due to not needing a cyclic prefix. This chapter discusses the wavelet OFDM principles for orthogonal and biorthogonal wavelets. It also gives a system model of DWT-OFDM and discusses

the property of perfect reconstruction. The peak-to-average power ratio of DWT-OFDM is discussed at the end of this chapter to reflex the PAPR in the previous chapter.

Chapter 4: Circular and Square Quadrature Amplitude Modulations

In this chapter, two modulation schemes are compared. The conventional scheme is the square 16-QAM. The alternative scheme is the circular 16-QAM. The derivation of the constellations points is provided and the BER analysis for the circular scheme is also given. The results and discussion of BER performances in both OFDM systems are provided at the end of the chapter.

Chapter 5: Narrowband Interference Models and Mitigation Techniques

The interference models and mitigation techniques are included in this chapter. This is an overview of the current research of the interference in an OFDM system. The narrowband interference models are discussed to see the interference characteristics in terms of parameters such as the amplitude, frequency, and phase. By investigating these parameters, the interference can be estimated. This leads to the mitigation that is proposed in the next chapter.

Chapter 6: The Proposed Interference Cancelation Algorithm

This chapter proposes a new interference cancelation algorithm. This algorithm is implemented to minimise the narrowband interference. Two cases, ideal and non-ideal are considered. Analysis and simulation are provided for each case. The performance results are also provided to evaluate the cancelation algorithm.

Chapter 7: Impulsive Noise Interference effects in OFDM Systems

In this chapter, we attempt to see the impulsive noise effects to the OFDM systems, and observe how wavelet OFDM perform better than Fourier OFDM. The experimental results and discussions are divided into two scenarios depending on the Poisson recurrence parameter and the ratio of impulsive noise

power over Gaussian noise power.

Chapter 8: Performance OFDM Systems in DVB-T and FER

In this chapter, applications of DVB-T and FER are included for both OFDM systems. The study of DVB-T using 2T mode of OFDM parameters following the ETSI standards is discussed followed by the application of FER for OFDM channels.

Chapter 9: Conclusions and Future Work

This chapter summarises the main conclusions of this dissertation and presents possible future directions. Suggestions and ways of improvement for the future research are also given.

Chapter 2

Fourier Based OFDM

2.1 Introduction

A conventional multicarrier technique such as frequency-division multiplexing (FDM) takes a parallel data system and divides it into N frequency subchannels which do not spectrally overlap [11], [35], [39],[40], [67], [109] ,[108], [116] and [131]. The separation of the subchannels is possible using three available schemes [131]:

1. Using filters to completely separate subbands. This method was borrowed from the conventional FDM technology. The limitation of filter implementation forces the bandwidth of each subband to be equal to $(N+\beta)f_n$, where N is the number of subcarrier, β is the roll-off factor and f_n, is the Nyquist bandwidth. Another disadvantage is that it is difficult to assemble a set of matched filter when the number of carriers are large.
2. Using staggered QAM to increase the efficiency of band usage. In this way the individual spectra of the modulated carriers still use an excess bandwidth of ΔB, but they are overlapped at the 3 dB frequency. The advantage is that the composite spectrum is flat. The separability or orthogonality is achieved by staggering the data (offset the data by half a symbol). The requirement for filter design is less critical than that for the first scheme.

3. Using the discrete Fourier transform (DFT) to modulate and demodulate parallel data. The individual spectra are now sinc functions and are not bandlimited. The FDM is achieved, not by bandpass filtering, but by baseband processing. Using this method, both transmitter and receiver can be implemented using efficient FFT techniques which reduce the number of operations from N^2 in DFT down to about $N \log_2 N$.

The separation of the subchannels is necessary in order to avoid spectral overlap of channels to eliminate interchannel interference. However, the available spectrum is not efficiently being used. To cope with this problem, an overlapping multicarrier modulation technique, such as OFDM, can be used. By implementing this technique, almost half of the available bandwidth can be saved [108]. This is illustrated in Figs. 2.1 and 2.2. According to Fig. 2.1, the total frequency bandwidth B_{FDM} is divided into nonoverlapping frequencies i.e 8 subchannels. The number on top of each subchannel corresponds to the channel number. Each subchannel is modulated with a separate carrier and then the 8 subchannels are frequency-multiplexed. Whereas in Fig. 2.2, the total frequency bandwidth B_{OFDM} which is about half of B_{FDM} is divided into the same number of subchannel with orthogonally overlapping frequency subchannels. The significant point here is the orthogonality between the different modulated subchannels or subcarriers. Basically, the name 'Orthogonal Frequency Division Multiplexing' comes from that concept.

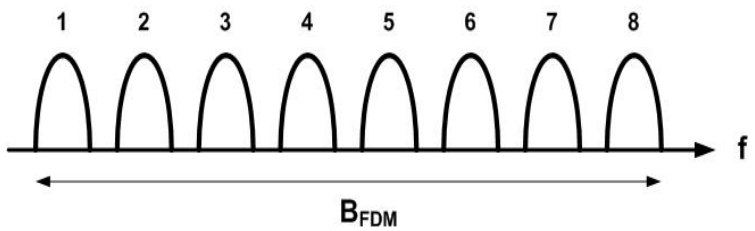

Figure 2.1: Non-overlapping subchannels in a conventional multicarrier technique such as FDM.

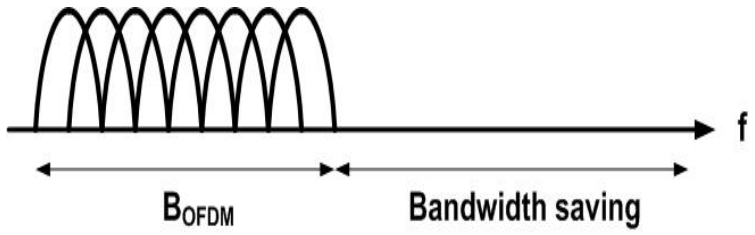

Figure 2.2: Overlapping subchannels in an orthogonal multicarrier technique such as OFDM yielding to bandwidth saving.

The multiplexing OFDM subcarriers are possible using the inverse discrete Fourier transform (IDFT) and discrete Fourier transform (DFT) in the transmitter and receiver respectively. Some literatures use IFFT and FFT operations instead of IDFT and DFT. The reason is that the computation algorithm of DFT which is N^2 is slower than FFT which is $N \log_2 N$ [102], [131]. A further discussion is illustrated in Table 2.1.

Table 2.1: Calculation Complexity between DFT and FFT.

$\frac{Bits}{OFDMSymbol}$	N	DFT	FFT
1	2	4	2
2	4	16	8
3	8	64	24
4	16	256	64
5	32	1024	160
6	64	4096	384
7	128	16384	896
8	256	65536	2048
9	512	262144	4608
10	1024	1048576	10240

The OFDM system also employs guard intervals or cyclic prefixes (CP) so that the delay spread of the channel becomes longer than the channel impulse response [10], [11], [35], [38], [40], [108], [116] and [131]. The purpose of this is to minimize inter-symbol interference (ISI), however a CP reduces the power efficiency and data throughput. In this case, the system must make sure that the cyclic prefix is a small fraction of the per carrier symbol duration

[30], [38], [122]. The CP also has the disadvantage of reducing the spectral containment of the channels [88], [100], [106] and [118]. Due to these problems, an alternative method is to use a wavelet transform to replace the IFFT and FFT blocks [6], [88], [100], [106], [118]. By using these transforms, the spectral containment of the channels is better since they are not using CP [88], [100], [106], [118]. The wavelet OFDM will be discussed in details in the next chapter.

This chapter is organised as follows. The next section describes the process of a typical FFT-OFDM system followed by section 2.3 discussing the general model of FFT-OFDM. Section 2.4 studies the orthogonality of a Fourier based OFDM system. The discussion of Fourier transform in an OFDM transceiver is presented in section 2.5. Section 2.6 analyses the cyclic prefix and the final section, section 2.7 completes this chapter and discusses the PAPR in FFT-OFDM.

2.2 FFT-OFDM System Process

An OFDM transceiver system is shown in Fig. 2.3. The inverse and forward transform blocks are the operations that will be focussed on since they can be FFT-based or DWT-based OFDM. Signal generator will produce a sequence of binary numbers, d, consisting of binary 0s and 1s. Depending on the system transmission rate, the output from the generator will determine the bit rate for the transmission. For example, if the system requires 16-QAM then the binary output will have 4 bits per OFDM symbol. The binary number is in multiple of 2 since it has a random probability of a 0 or 1. From this example, we can observe that there are 4 bits representing an OFDM symbol. If MATLAB produces a random integer using the randint built-in function, the integer will have a random probability of a number between 0 and 15.

After generating binary number d, the mapping process is performed. An OFDM symbol is mapped from a binary to a complex signal with an amplitude and phase represented by a real and imaginary number. This is then encoded

and interleaved so as to produce a matrix to be mapped onto QAM values in the form of amplitude and phase. In the case that the system uses 16-QAM, it maps 4 binary bits to 16 constellation points, X_m. This involves taking N parallel streams of QAM symbols (N being the number of sub-carriers used in the transmission of the data) and performing an IFFT operation. The output of the IFFT operation in discrete time is as follows:

$$X_{k(n)} = \frac{1}{\sqrt{N}} \sum_{i=0}^{N-1} X_{m(i)} \exp\left(j2\pi \frac{n}{N} i\right) \tag{2.1}$$

where $X_{m(i)}|0 \leq i \leq N-1$ are complex numbers in the discrete frequency domain and $X_{k(n)}|0 \leq n \leq N-1$ is a sequence in the discrete time domain.

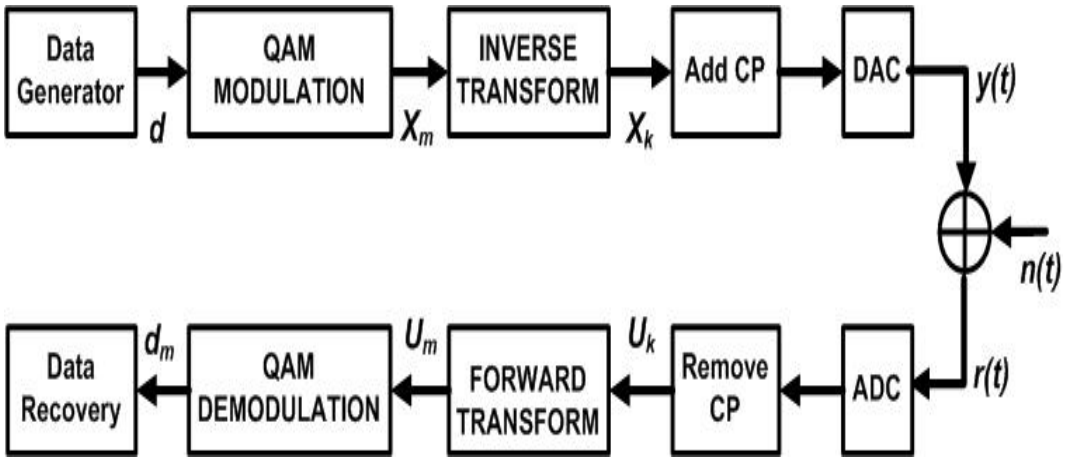

Figure 2.3: An OFDM transceiver illustrating the process of Fourier and wavelet based OFDM systems in an AWGN channel with n(t) representing the Gaussian noise.

The cyclic prefix (CP) is lastly added before transmission to minimize the inter-symbol interference (ISI). At the receiver, the process is reversed to obtain the decoded data. The CP is removed to obtain the data in the discrete time domain and then processed using the FFT for data recovery. The output of the FFT in the frequency domain is as follows:

$$U_{m(i)} = \sum_{n=0}^{N-1} U_{k(n)} \exp\left(-j2\pi \frac{n}{N} i\right) \tag{2.2}$$

Samples of one OFDM symbol processed in the FFT-OFDM system shown in Fig. 2.3 are shown in Figs. 2.4 and 2.5.

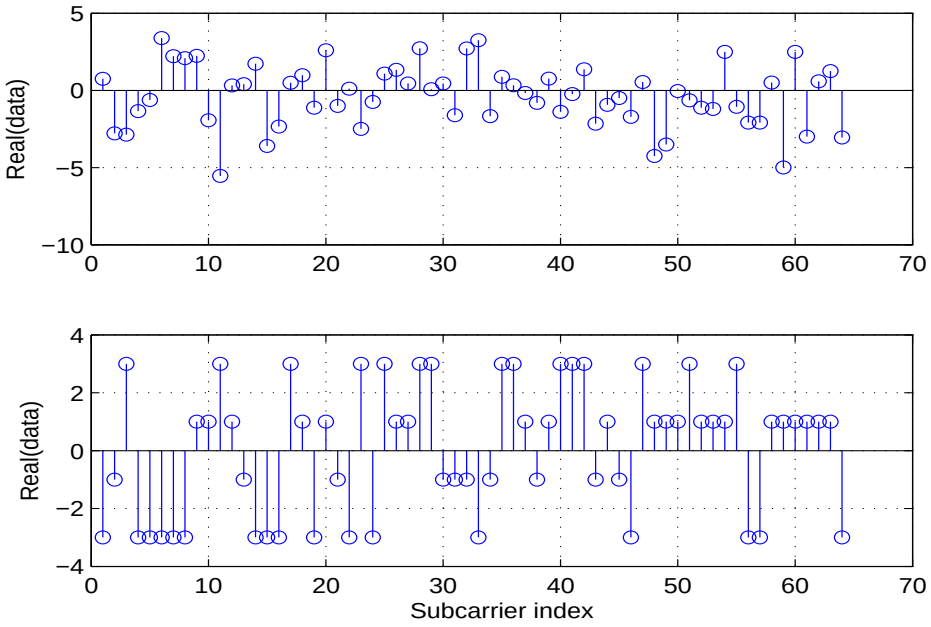

Figure 2.4: Tx data: X_m (Below), X_k (Top).

2.3 System Model of FFT-OFDM

The block diagram in Fig. 2.3 is a typical system conventional OFDM. It is assumed that there is no frequency offset so that the FFT itself acts as a matched filter at the receiver. To determine the data in sub-channel k, we match the transmitted waveform with carrier i [88]:

$$\langle y(t), f_i(t)\rangle = \sum_{k=0}^{K-1} d_k \langle f_k(t), f_i(t)\rangle \tag{2.3}$$

where $y(t)$ is the transmitted data via IFFT, $f_k(t)$ are complex exponentials or it can be written as $e^{j2\pi km/K}$ (K being the size of FFT), d_k is the data projected onto each carrier, $\langle f_k(t), f_i(t)\rangle$ equals 1 when $k = i$ and 0 when $k \neq i$.

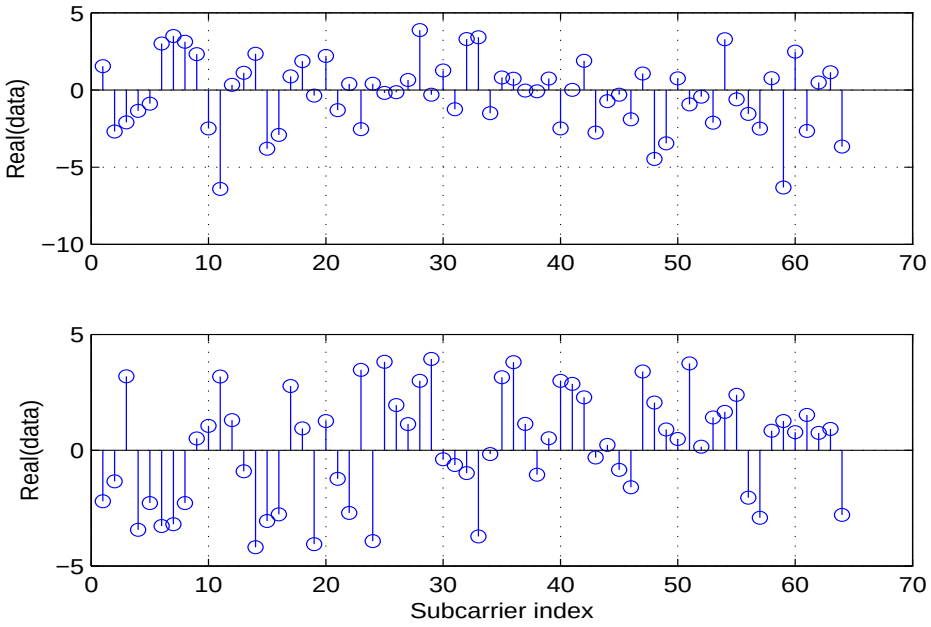

Figure 2.5: Rx data: U_m (Below) U_k (Top).

In a typical communication system, data is transmitted over a dispersive channel. The impulse response of a deterministic (and possibly time-varying) channel can be modelled by a linear filter $h(t)$:

$$\begin{aligned} r(t) &= y(t) * h(t) + n(t) \\ &= \sum_{k=0}^{K-1} d_k x'_k(t) + n(t) \end{aligned} \tag{2.4}$$

where $x'_k(t) = x_k(t) * h(t)$. When matching the transmitted waveform with carrier i, we have

$$\begin{aligned} \langle y(t), f_i(t) \rangle &= \sum_{k=0}^{K-1} d_k \langle x'_k(t), f_i(t) \rangle + \langle n(t), f_i(t) \rangle \\ &= \sum_{k=0}^{K-1} d_k \rho_{k,0}(0) + \langle n(t), f_i(t) \rangle \\ &= d_K \rho_{i,i}(0) + \sum_{\substack{k=0 \\ k \neq i}}^{K-1} d_k \rho_{k,i}(0) + n''(t) \end{aligned} \tag{2.5}$$

where $d_K\rho_{i,i}(0)$ is the recovered data with correlation term $\rho_{i,i}(0)$ and $n''(t)$ is uncorrelated Gaussian noise. The interference term, $i(t) = \sum_{k=0,k\neq i}^{K-1} d_k\rho_{k,i}(0)$, degrades the system performance. It causes the filter to be distorted and causes the data to no longer be orthogonal to one another with correlation terms $\rho_{k,i}(0)$. If the channel has no distortion, this term becomes 0 and would decode exactly what was transmitted plus a Gaussian noise term.

2.4 Orthogonality

Orthogonality for an OFDM signal allows multiple overlapping information signals to be transmitted perfectly without suffering interference. This happens when the signals have integer number of cycles per OFDM symbol. By having them cyclic, it yields to have an integer number of samples within the IFFT/FFT interval. Equation (2.6) below indicates that there is a precise mathematical relationship between the subcarriers to preserve orthogonality in the system;

$$\int_0^{T_s} \sin(n\omega t)\sin(m\omega t)dt = \{^{1 \quad n=m}_{0 \quad n\neq m} \tag{2.6}$$

where $\omega = 2\pi f$, f is the carrier spacing, m and n are the number of carriers and T_s is the effective OFDM symbol period excluding the guard interval. It is worth mentioning that equation (2.6) is the same principle as the equation defined in [123]. According to equation (2.6), the integral indicates that the integer number n and m must not be equal so that the integration is zero. In this case the integration over a period of symbol duration T_s satisfies the orthogonality property. If the integer n is equal to m, the integration over a period T_s cannot be zero, thus, it will not be orthogonal. The integral limit is taken for one OFDM symbol period, T_s and consists of four subcarriers as plotted in Fig. 2.6.

The number of the subcarriers depends on the requirement of the bit rate and the OFDM symbol rate in a multiple of 2 and it is not necessary for

the subcarriers to be four. The integration of any two signals from any four subcarriers is zero. Note that all these subcarriers are zero phase and each subcarrier has an integer number of cycles per effective OFDM symbol. Here, we can define that the effective OFDM symbol is the IFFT/FFT duration excluding the guard interval. The subcarriers: $\sin(\omega t)$ has one cycle, $\sin(2\omega t)$ has two cycles, $\sin(3\omega t)$ has three cycles, and $\sin(4\omega t)$ has four cycles. If the integer number of subcarriers are equal, i.e $m = n$, then the integration over the OFDM symbol period T_s cannot be equal to zero. Hence, orthogonality cannot be fulfilled. If the integer number of subcarriers are not equal, that is $m \neq n$, then the integration over the OFDM symbol period T_s can be equal to zero. For example, two signals such as $\sin(\omega t)$ and $\sin(2\omega t)$, which are indicated in Fig. 2.6, fulfill the orthogonality by determining the integration over an effective OFDM symbol period T_s as shown in Appendix A. Additional understanding of orthogonality can be thought of as a set of harmonic sine and cosine functions, such as $\sin(nt)$ and $\cos(nt)$ on any specified interval range with any integer value of n [85]. This is possible because they are square-integrable functions over specified interval ranges which form an orthogonal basis used in the Fourier series expansion.

The orthogonality property of OFDM signals can also be viewed by looking at its frequency spectrum. Fig. 2.6 shows the first 4 OFDM subcarriers where N is the number of subcarriers per OFDM symbol. Each OFDM subcarrier has a $\mathrm{sinc}(f)$ or $\frac{\sin(x)}{(x)}$ spectrum where x is πf. This is the result of the symbol time corresponding to the inverse of the carrier spacing $\frac{1}{T}$ Hz, where T is the duration time for fast Fourier transform which is a fraction of the OFDM symbol period T_s. The spectrum of an effective OFDM signal is, in fact, obtained by the convolution of a sinc function, which is the spectrum of a single subcarrier, with a sequence of dirac pulses $\delta(f)$ equispacing with Δf. The sinc function has a narrow main lobe at the centre with many side-lobes that decay slowly with the magnitude of the frequency difference away from the centre. Each subcarrier has a peak at the centre frequency and nulls evenly

spaced with a frequency gap equal to the carrier spacing. From Fig. 2.6, it can be seen that the first subcarrier, peak occurs at 0 subcarrier frequency and zeroes at other subcarrier frequencies 1, 2, 3 until N, the same principle applies to the adjacent subcarriers 2, 3, until N. It shows that the orthogonal nature of the transmission is a result of the peak of each sub carrier corresponding to the nulls of all other sub carriers.

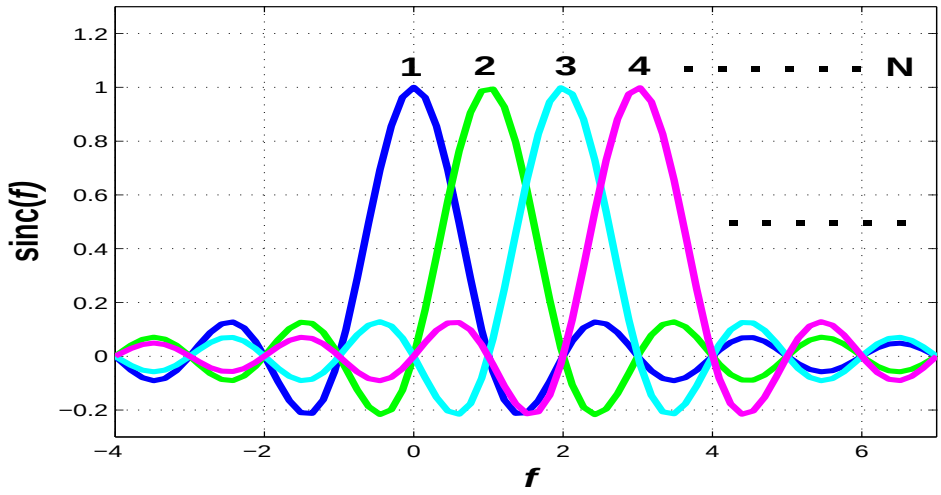

Figure 2.6: Overlapping spectra of subcarriers per OFDM symbol.

2.5 IFFT and FFT Operations

The IFFT performs the same operations as an IDFT, except that it is much more computational efficient, and so is used in many practical systems. For example, using the radix-2 algorithm, IFFT performs $(\frac{N}{2})\log_2 N$ complex multiplications [101], [108]. For 64 number of samples, it requires 192 multiplications. The number of multiplications can be less if the system uses the radix-4 algorithm which performs $(\frac{3}{8})N\log_2 N - 2$. For 64 number of samples, the system requires only 96 multiplications if it uses radix-4 algorithm which is about 50 percent less. This is illustrated in Table 2.2.

An example of performing radix-4 algorithm for N subcarriers in a four-

Table 2.2: FFT: Radix-2 and Radix-4 Complex Multiplication Comparisons.

N	Radix-2 FFT	Radix-4 FFT
8	12	3
16	32	12
32	80	36
64	192	96
128	448	240
256	1024	576

point IFFT is shown as follows:

$$\frac{1}{N}\begin{bmatrix} 1 & 1 & 1 & 1 \\ 1 & j & -1 & -j \\ 1 & -1 & 1 & -1 \\ 1 & -j & -1 & j \end{bmatrix} \begin{bmatrix} x_0 \\ x_1 \\ x_2 \\ x_3 \end{bmatrix} = \frac{1}{N} \begin{bmatrix} y_0 \\ y_1 \\ y_2 \\ y_3 \end{bmatrix} \tag{2.7}$$

This equation can be rewritten as

$$\frac{1}{N} A \cdot x = \frac{1}{N} \cdot y \tag{2.8}$$

where A is the matrix consisting of IFFT algorithm values, x is the input vector, y is the IFFT output vector per OFDM symbol and N is the number of subcarrier. A further example illustrating the above matrix is discussed next. Let us assume that our aim is to transmit four binary values $[-1 \quad 1 \quad -1 \quad -1]$ on four subcarriers. Then, the matrix operation will be as follows:

$$\frac{1}{4}\begin{bmatrix} 1 & 1 & 1 & 1 \\ 1 & j & -1 & -j \\ 1 & -1 & 1 & -1 \\ 1 & -j & -1 & j \end{bmatrix} \begin{bmatrix} -1 \\ 1 \\ -1 \\ -1 \end{bmatrix} = \frac{1}{4} \begin{bmatrix} -2 \\ 2j \\ -2 \\ -2j \end{bmatrix} \tag{2.9}$$

Thus, there are four IFFT outputs that form one OFDM symbol. If eight binary values are generated, the IFFT part should have [8x8] matrix with [8x1] output matrix. The N point IFFT corresponding to the number of subcarriers

will generate one OFDM symbol. For example, the [8x1] input matrix [1 1 1 -1 1 1 -1 1] will be processed to produce an OFDM symbol yielding to [8x1] output matrix. This is shown as follows [108]:

$$\frac{1}{8}\begin{bmatrix} 1 & 1 & 1 & 1 & 1 & 1 & 1 & 1 \\ 1 & \xi_a & j & \xi_b & -1 & \xi_c & -j & \xi_d \\ 1 & j & -1 & -j & 1 & j & -1 & -j \\ 1 & \xi_b & -j & \xi_a & -1 & \xi_d & j & \xi_c \\ 1 & -1 & 1 & -1 & 1 & -1 & 1 & -1 \\ 1 & \xi_c & j & \xi_d & -1 & \xi_a & -j & \xi_b \\ 1 & -j & -1 & j & 1 & -j & -1 & j \\ 1 & \xi_d & -j & \xi_c & -1 & \xi_b & j & \xi_a \end{bmatrix} \begin{bmatrix} 1 \\ 1 \\ 1 \\ -1 \\ 1 \\ 1 \\ -1 \\ 1 \end{bmatrix} = \frac{1}{8}\begin{bmatrix} 4 \\ \sqrt{2}(1+\gamma_a) \\ 2+2j \\ -\sqrt{2}(1+\gamma_b) \\ 0 \\ -\sqrt{2}(1-\gamma_b) \\ 2-2j \\ \sqrt{2}(1-\gamma_a) \end{bmatrix} \tag{2.10}$$

where $\xi_a = \frac{1}{2}\sqrt{2}(1+j)$, $\xi_b = \frac{1}{2}\sqrt{2}(-1+j)$, $\xi_c = \frac{1}{2}\sqrt{2}(-1-j)$, $\xi_d = \frac{1}{2}\sqrt{2}(1-j)$, $\gamma_a = j(\sqrt{2}-1)$ and $\gamma_b = j(\sqrt{2}+1)$.

After performing the IFFT, the OFDM signal is required to have a cyclic extension followed by windowing to combat interchannel interference (ICI). A proper windowing of OFDM signals is important to mitigate the effect of frequency offset and to control the transmitted signal spectrum. Finally, the calculated time domain signal is mixed with the required frequency in a RF amplifier component before being passed to the antenna for transmission. Note that OFDM is a linear modulation technique which requires the amplifier to operate in its linear region which has low power efficiency.

In the receiver path, the system basically performs the reverse operation of the transmitter. The receiving antenna converts the electromagnetic signals to electrical signals, then it demodulates the RF signal to an OFDM baseband signal for processing to obtain the original signal. The amplitude and phase of the subcarriers is then picked out and converted back to digital data within an analog-to-digital converter. In reality, the interferences between OFDM subcarriers such as ICI caused by frequency offset and ISI caused by timing offset

cannot be negligible. A proper windowing such as a raised-cosine windowing can control ICI and ISI trade-off. In practical systems, a simple linear windowing approach is commonly taken to shape the spectrum, in order to eliminate cyclic extension, the discrete time signals corresponding to the cyclic/guard interval has to be removed. The IFFT and the FFT are complementary function and the most appropriate term depends on whether the signal is being received or generated, using the IFFT at the transmitter and FFT at the transmitter corresponds to the idea that multicarrier signals at the transmitter are in the frequency domain and IFFT is used to transform the frequency domain into a time domain signal. Actually, the FFT and IFFT can be interchanged. With respect to DSP, using FFT or IFFT will not make any difference as long as they are performed in pairs. For example, if the transmitter uses FFT, then the receiver can use IFFT or vice versa. Then, the process continues about the same as transmission but it is in reverse operations such as demapping QAM, deinterleaving and decoding before returning to the original data.

2.6 Cyclic Prefix

OFDM is a multicarrier transmission technique. A multipath propagation causes multipath delay spread in which inter-symbol interference occurs. The higher the ratio of the delay time over the time duration of transmission, the worse the inter-symbol interference is. However, OFDM can deal with this interference in an efficient way by using a guard time for each of its symbols. In this case, to avoid interference between each OFDM symbols, the guard time must be at least four times larger than the expected delay spread. A typical OFDM block showing guard time, the effective OFDM symbol period or the FFT/IFFT duration and the total OFDM symbol period is shown in Fig. 2.7.

Consideration must be taken that the chosen duration of the guard time must be optimum, otherwise, the OFDM transmission would have lost sub-

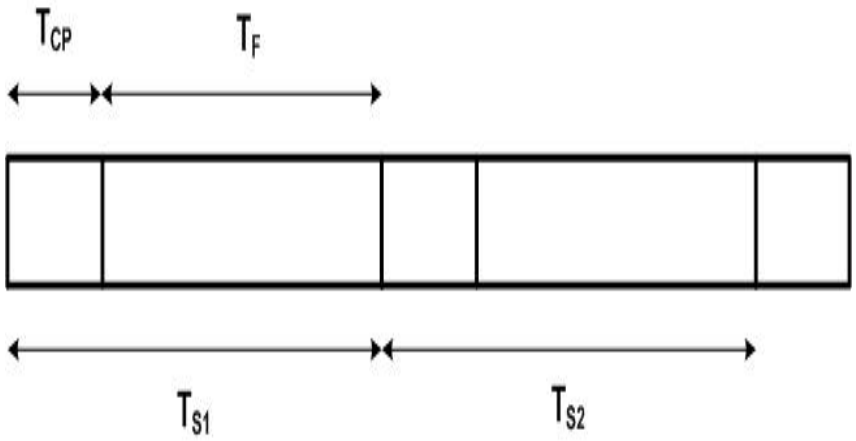

Figure 2.7: A typical of perfect OFDM block showing the guard time (T_{CP}), the effective OFDM symbol period or the FFT/IFFT duration (T_F) and the total OFDM symbol period ($T_{CP} + T_F$). T_{S1} is the first OFDM symbol while T_{S2} is the second OFDM symbol.

stantial power. The guard time should be assumed to be part of the signal so that orthogonality can be achieved. In the case that there is no signal within the guard time, the orthogonality cannot be satisfied in the presence of multipath components. This situation results in intercarrier interference (ICI) in the form of crosstalk between different subcarriers.

Doppler spread in frequency is one example of a phenomenon that creates crosstalk. When a transmitter and/or receiver is in motion, Doppler shifts from different incoming waves cause Doppler spread, f_d, to occur. For example, a transmitting wave from a stationary transmitter such as Radio Base Station (RBS) to a moving receiver such as a mobile phone located inside an automobile causes Doppler spread, f_d. The maximum Doppler shift ($\frac{\nu}{\lambda}$ or $\nu \times \frac{f_c}{c}$) can be determined when the incoming wave from the RBS is in the same direction as the automobile. In this case, $f_d = \nu \times \frac{f_c}{c}$, where f_c is the received carrier frequency, ν is the mobile speed and c is the speed of light. The higher the speed of the mobile unit, the more Doppler spread. As a result, the crosstalk becomes worse which mean that ICI increases. However, OFDM can minimize ICI by using a cyclic extension in the guard time. By having the cyclic extension, the delayed replicas of the OFDM symbol always have

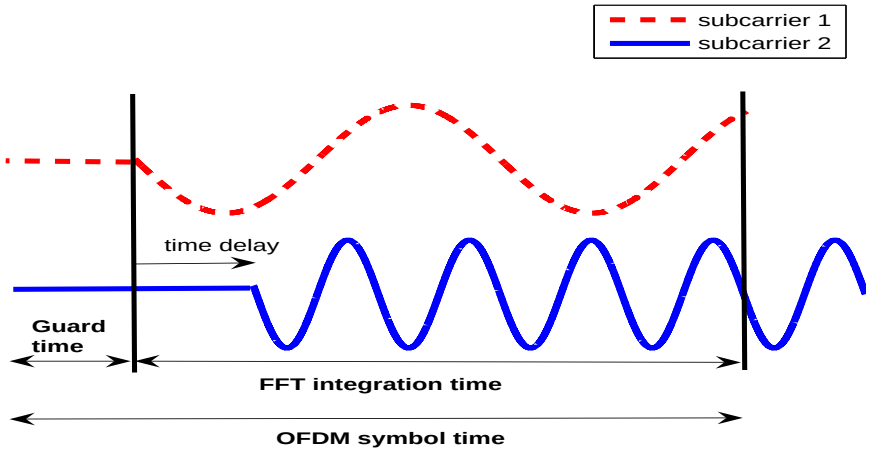

Figure 2.8: A diagram showing part of subcarrier 2 causing ICI on subcarrier 1 because of the delay time.

an integer number of cycles within the FFT interval provided that the guard time is larger than the delay. This is illustrated in Fig. 2.9.

2.7 Peak-to-Average Power Ratio FFT-OFDM

PAPR is well known as one of the drawbacks that inevitably occur in FFT-OFDM, hence, it is considered in this section in order to keep updating with its current issue. According to [108], PAPR can substantially occur because the OFDM signal is an addition of a number of independently modulated subcarriers. When a number of N signals is added with the same phase, it produces a peak power that is N time the average power. Due to PAPR problem, the complexity of the analog-to-digital converter (ADC) and digital-to-analog converter (DAC) is consequently increased and it also reduces the RF power amplifier efficiency [108]. A well discussion of PAPR also can be found in [21]. Some reduction or mitigation methods suggested by [21] are:

1. Clipping technique consisting of decision-aided reconstruction, oversampling and frequency domain filtering and iterative estimation and canceling. This clipping technique is also being discussed by [108] with

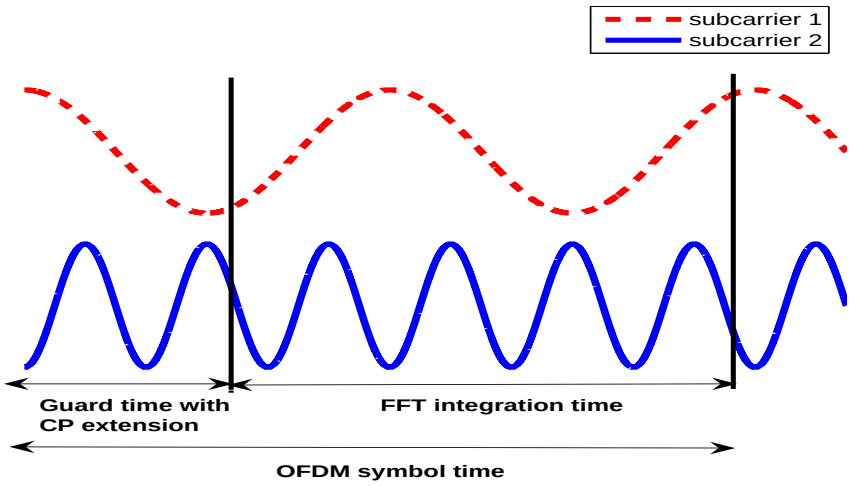

Figure 2.9: Orthogonality is preserved with cyclic extension is done for the guard time. This will make sure that the guard time is larger than the multipath delay.

an additional discussion that the peak amplitudes can be reduced by nonlinearly distorting the OFDM signal at or around them.

2. Amplitude alteration consisting of companding and complementary clipping transform; pre-IFFT data alteration consisting of selective mapping, repeated random phasor transform, selective scrambling, partial transmit sequence and dummy sequence insertion;
3. Coding consisting of parity-check coding, Rudin-Shapiro coding and Golay complementary sequences and Reed-Mueller codes. [108] includes the forward-error correcting code that excludes OFDM symbols with a large PAPR.

It is interesting to note that the last point above is also discussed by [52]. However, Anwar et. al. suggest the reduction technique are for wavelet based OFDM. One thing that we need to ask: Is the Fourier based OFDM offer the best of reduction PAPR? In this case, many studies such as in [32], [97] and [133] say that wavelet based has offered more advantage for PAPR reduction than the conventional OFDM system because it does not require CP and has more spectral containment. This will be further discussed at the end of next chapter.

2.8 Summary

Conventional frequency division multiplexing (FDM) system has the characteristics of separation of subchannels, which is necessary, to avoid spectral overlap of channels to eliminate interchannel interference. However, the available spectrum is not efficiently being used. To cope with this problem, an overlapping multicarrier modulation technique, such as OFDM, is used. In order to make this possible, IFFT and FFT are used in the multiplexing of transmitting and receiving OFDM data respectively. Thus, the IFFT and FFT process and operation are discussed in this chapter. One important property of an OFDM signal is orthogonality between subcarriers, thus, the concept of orthogonality in Fourier based OFDM is also included. In order to maintain the orthogonality, the cyclic prefix has to be longer than the channel impulse response. One of inevitable problem in OFDM system is PAPR. This problem brings disadvantage to an OFDM system, thus, an overview of PAPR is also discussed.

Chapter 3

Wavelet Based OFDM

3.1 Introduction

Multi-Carrier Modulation (MCM) is a data transmission technique where the data-stream is divided into several parallel bit streams, each at a lower bit rate, and using these substreams to modulate several carriers. Orthogonal Frequency Division Multiplexing or OFDM is a MCM scheme where the sub carriers are orthogonal sine/cosine waves. The major drawback of such an implementation is the rectangular window used, which creates high side lobes [78]. Moreover, the pulse shaping function used to modulate each subcarrier extends to infinity in the frequency domain [134], this leads to high interference and lower performance levels. The effect of wave-shaping of OFDM signals on ISI and ICI is reported in [26]. In [27] the optimal wavelet is designed for OFDM signals in order to minimize the total interference. The wavelet transforms have longer basis functions and can offer a higher degree of side lobe suppression [3]. With the promise of greater flexibility and improved performance against channel effects, wavelet based basis functions have emerged as strong candidates for MCM in wireless channels. A modified block diagram of the wavelet based OFDM for multicarrier communication system is shown in Fig. 3.5. This block diagram has been modified and simplified from [78] and [134].

Replacing the conventional Fourier-based complex exponential carriers of

a multicarrier system with orthonormal wavelets is suggested in many studies [13], [88], [106], [118], these wavelets are derived from a multistage tree-structured Haar and Daubechies orthonormal QMF bank and produce improved performance with respect to the reduction of the power of ISI and ICI. This work is extended in [137] by realizing a high-speed digital communication system over low voltage powerline, with empirical investigations on a model obtained from the measurements of a practical low-voltage power line communication channel, the authors reaffirm the effectiveness of wavelets for use in OFDM systems, especially with regard to ISI and ICI mitigation . Another real time application of the system is reported in [139]. According to this work, the bit error rate (BER) performance of the wavelet based V-BLAST system is superior to its Fourier based counterparts. In conventional systems, the ISI and ICI are reduced by adding a guard interval (GI) using a cyclic prefix (CP) to the start of the OFDM symbol, adding a CP can largely reduce the spectrum efficiency. Wavelet based OFDM schemes do not require a CP, thereby enhancing the spectral efficiency. Avoiding the CP gives Wavelet OFDM (WOFDM) an advantage of roughly 20 percent in bandwidth efficiency [97]. Moreover, as pilot tones are not necessary for wavelet based OFDM systems they perform better in comparison to existing OFDM systems like 802.1la or HiperLAN, where 4 out of 52 sub-bands are used for pilots. This gives WOFDM another 8 percent advantage over typical OFDM implementations. Even though wavelet can have many advantages, it is still has disadvantage in which it has high calculation complexity. [74] shows that wavelet filter calculation C_w is given by

$$C_w = 4N + Nlog_2N \tag{3.1}$$

where N is number of subcarriers. Wavelet filter performs higher complexity than FFT but lower than DFT. Table 3.1 shows the calculation complexity of DWT-OFDM using (3.1) as compared to FFT and DFT.

From Table 3.1, the calculation of wavelet filter requires 46.7% of percent-

Table 3.1: Calculation Complexity between DFT, FFT and DWT.

$\frac{Bits}{OFDMSymbol}$	N	DFT	FFT	DWT
1	2	4	2	10
2	4	16	8	24
3	8	64	24	56
4	16	256	64	128
5	32	1024	160	288
6	64	4096	384	640
7	128	16384	896	1408
8	256	65536	2048	3072
9	512	262144	4608	6656
10	1024	1048576	10240	14336

age error higher than FFT. However, DWT performs an efficient calculation more than 10 times of DFT in average. Nevertheless, when discussing the calculation complexity, one should relatively consider the computer processing capability when performing a computer simulation.

Despite the advantage and disadvantage of wavelet OFDM, types of its schemes are also discussed. According to [21], wavelet-OFDM or DWT-OFDM consists of five schemes. They are:

1. Fractal modulation, which is a type of diversity technique that transmit the same symbol using different symbol lengths in different subbands. Because of this feature, it is suitable for transmission over noisy channels of simultaneously over unknown duration and bandwidth.
2. The second is multiscale wavelet modulation (MSM), which has nonuniform subbands or it uses different time durations for symbols in different subchannels. Each OFDM symbol is shaped by a wavelet or scaling function to ensure orthogonality. Its purpose is the same as Fourier based OFDM, to overcome distortion caused by the frequency selective fading channel by having narrower subbands relative to the total bandwidth.
3. The third scheme is wavelet pulse shaping PAM signals. This scheme is

discussed in [80]. The purpose of this scheme is to improve bandwidth efficiency. This can be done by adding dyadic expansions to the mother wavelet used as a pulse shaper.

4. The fourth is the wavelet packet modulation (WPM). This scheme is discussed in [51], [62], [126], [127], [130]. Using this scheme, transmitting and receiving data are processed through synthesis and analysis filtering operations based on the tree structure algorithm. In MATLAB, a special built-in function, *wptree* with a syntax of $T = wptree(o, \iota, xx, wv)$ is used to invoke the structure. The parameter, o is the order number depending on the input signal xx and the second parameter, ι is the number of level depending on the size of xx, and wv is the type of a wavelet family.
5. The last one is the overlapped discrete wavelet multitone modulation (DWMT). This scheme, which is based on the application of wavelet filters with the baseband pulses for different data blocks overlap in time, is discussed in [69], [70], [71], [118].

As mentioned in the previous chapter, the inverse and forward block transforms are flexible and can be substituted with FFT, DWT or Wavelet Packet (WPT) transforms. We have discussed briefly FFT-OFDM, thus, this chapter describes wavelet based OFDM and is organised as follows. Description of wavelet based OFDM principle is in section 3.2. The DWT- and WPT-OFDM models and perfect reconstruction property are included in section 3.3 followed by simulation results in section 3.4. In the last section, PAPR problem in wavelet based OFDM is also discussed.

3.2 Wavelet OFDM Principles

A wavelet is normally assigned the variable $\psi(t)$ it is a square-integrable function [21]. In other literature [14], it is also indicated by $\psi(t)\epsilon L^2(\mathbf{R})$ where, L is a Lebesque integral and 2 signifies the integral of the square of the modulus

of the function, and **R** denotes the real number for integration of the independent variable t. In this section, we discuss two principles of wavelet transforms, orthogonal and biorthogonal wavelets as follows.

3.2.1 Orthogonal Wavelets

The Fourier transform has exponential parts consisting of cosine and sine signal bases. These bases are orthogonal to each other. The wavelet transform also has orthogonal bases. Its bases are low pass and high pass filters which are associated with the scaling and wavelet functions respectively. Among orthogonal wavelets are Daubechies, Coiflets, Morlet and Meyer [86].

Orthogonal wavelet functions can be generated by scaling and shifting properties as follows [21]:

$$\psi_{ab}(t) = \frac{1}{\sqrt{2}}\psi(\frac{t-b}{a}) \tag{3.2}$$

where a and b are the scaling and shifting real parameter values. According to [37], the wavelet transform is called continuous if a and b are continuous. The drawbacks of a continuos wavelet transform are redundancy and impracticality. To avoid these problems, those parameters have to be discretised as follows [5], [21]:

$$\begin{aligned} a &= a_0^m \\ b &= nb_0a_0^m \end{aligned} \tag{3.3}$$

where m and n indicates the exponential integers. From (3.2) and (3.3), the basis of the DWT can be formed as

$$\psi_{mn}(t) = a_0^{-\frac{m}{2}}\psi(a_0^{-m}t - nb_0) \tag{3.4}$$

Using $a_0 = 2$ and $b_0 = 1$, we can have the signal function

$$\begin{aligned} U(t) &= \sum_{n=-\infty}^{\infty} C_{L,n} 2^{-\frac{L}{2}} \phi(2^{-L}t - n) \\ &\quad + \sum_{m=1}^{L} \sum_{n=-\infty}^{\infty} D_{mn} 2^{-\frac{m}{2}} \psi(2^{-m}t - n) \end{aligned} \tag{3.5}$$

where the scaling coefficient $C_{L,n}$ is

$$\begin{aligned} C_{L,n} &= \langle U(t), \phi_{L,n}(t) \rangle \\ &= 2^{-\frac{L}{2}} \int U(t) \phi(2^{-L}t - n) dt \end{aligned} \tag{3.6}$$

where $\phi_{L,n(t)} = 2^{-L/2}\phi(2^{-L}t - n)$, and the wavelet coefficient D_{mn} is

$$\begin{aligned} D_{mn} &= \langle U(t), \psi_{mn}(t) \rangle \\ &= 2^{-\frac{L}{2}} \int U(t) \psi(2^{-L}t - n) dt \end{aligned} \tag{3.7}$$

In (3.5), the time domain signal $U(t)$ is DWT transformed to scales in which all the coefficients are denoted as the scales [21]. $U(t)$ can also be called the finite resolution wavelet representation [5]. The sum of scaled $\phi(2t)$ can make up the parent scaling function, and can be expressed as [14], [21]:

$$\phi(t) = \sqrt{2} \sum_{n} h_n \phi(2t - n) \tag{3.8}$$

where the coefficients $h(n)$ are a sequence of real or perhaps complex numbers called the scaling function(or scaling vector or filter). The use of $\sqrt{2}$ is to maintain the norm of the scaling function with the scale of 2. This scaling function in (3.8) can also be used for the multiresolution analysis (MMRA) [64]. A fundamental wavelet function can be expressed as a linear combination of translates of the scaling function as follows [5], [21]:

$$\psi(t) = \sqrt{2} \sum_{n} g_n \phi(2t - n) \tag{3.9}$$

where the wavelet coefficients g_n are related to the scaling coefficients h_n by

$$g(n) = (-1)^n h_{1-n} \tag{3.10}$$

An example of the application of (3.8) is the Haar scaling function which is given by [14] as follows:

$$\phi_H(t) = \phi(2t) + \phi(2t - 1) \tag{3.11}$$

It can be seen that $\phi(2t)$ can be used to construct $\phi_H(t)$. It also can be noted that (3.11) is the result of (3.8) for the first 2 sequence of discrete samples of n with coefficients $h(0) = \frac{1}{\sqrt{2}}$, $h(1) = \frac{1}{\sqrt{2}}$ [14]. Examples of Haar scaling and wavelet functions are shown in Fig. 3.1.

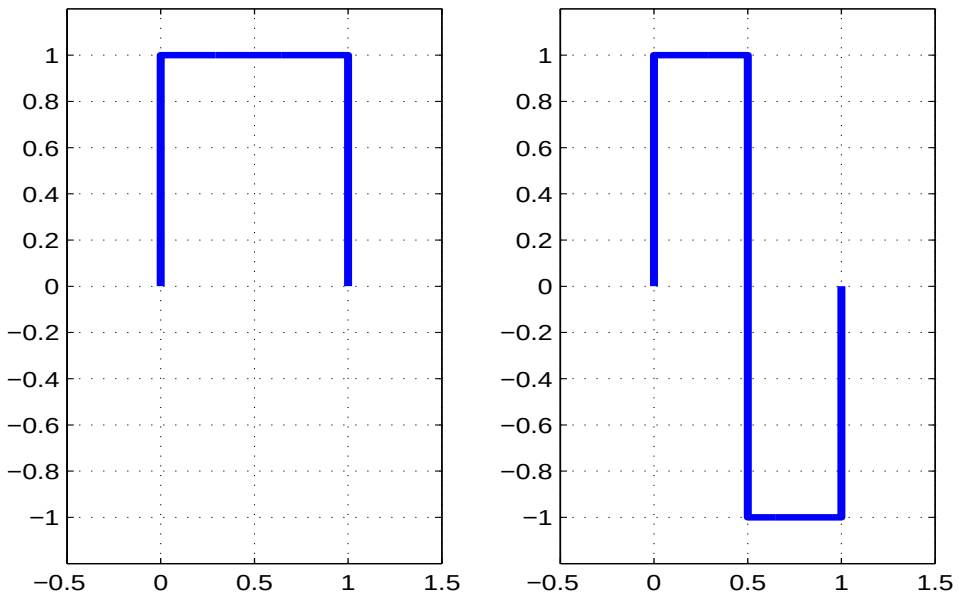

Figure 3.1: Haar (db1) scaling function $\phi(t)$ (left) and wavelet function $\psi(t)$ (right).

The Haar wavelet can be categorised as an orthogonal wavelet. All Daubechies wavelet families are categorised as orthogonal wavelets [86]. Another figure of

a Daubechie wavelet such as db2 is shown in Fig. 3.2.

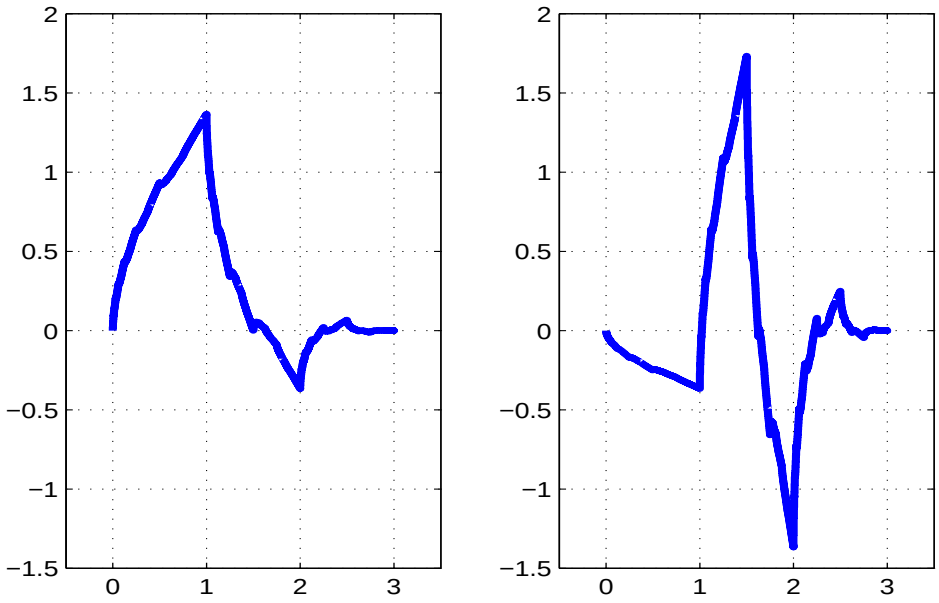

Figure 3.2: db2 scaling function $\phi(t)$ (left) and wavelet function $\psi(t)$ (right). Note that this plot is similar to [36] p. 197 and [14] p. 81.

3.2.2 Biorthogonal Wavelets

Biorthogonal wavelets are different than orthogonal wavelets because they have biorthogonal bases. Their bases have symmetric perfect reconstruction properties with compactly support. They also have two duality functions for each scaling and wavelet functions which are ϕ and $\hat{\phi}$ for the scaling filters, and ψ and $\hat{\psi}$ for the wavelet filters accordingly. In MATLAB, we have built-in functions such as bior1.1, bior2.2 , bior5.5 , rbio1.1, rbio2.2 and rbio5.5. The number next to the wavelet name refers to the length of the filter in the decomposition and reconstruction filters respectively.

Biorthogonal wavelets can be constructed from orthogonal wavelets by considering the duality concept. Let $\phi(t)$ and $\hat{\phi}(t)$ be two scaling functions and let $\psi(t)$ and $\hat{\psi}(t)$ be two wavelet functions, then we can express the biorthogonal scaling and wavelet functions as follows [36], [107]:

$$\begin{aligned}\langle \phi(t), \hat{\phi}(t-n) \rangle &= \delta n \\ \langle \psi(t), \hat{\psi}(t-k) \rangle &= \delta k \\ \langle \psi(t), \hat{\phi}(t-n) \rangle &= 0 \\ \langle \hat{\psi}(t), \phi(t-n) \rangle &= 0 \end{aligned} \tag{3.12}$$

where $\hat{\phi}(t) = \sqrt{2}\sum_n \hat{h_n}\hat{\phi}(2t-n)$ and $\hat{\psi}(t) = \sqrt{2}\sum_n \hat{h_n}\hat{\psi}(2t-n)$ with δn and δk are the results of biorthogonal bases. The last two equations in (3.12) satisfy the orthogonality properties. One advantage of using biorthogonal wavelets is that the scaling and wavelet functions are symmetric due to the duality concept [14], [36], therefore, biorthogonal wavelets provide an advantage over orthogonal wavelets because they offer not only orthogonality but also symmetry. In [104], comparing orthogonal transforms, biorthogonal transforms relax some of the constraints on the mother wavelet(or filters) and allow the mother wavelet to be symmetric and have linear phase. The plots of biorthogonal scaling and wavelet functions are shown in Figs. 3.3 and 3.4.

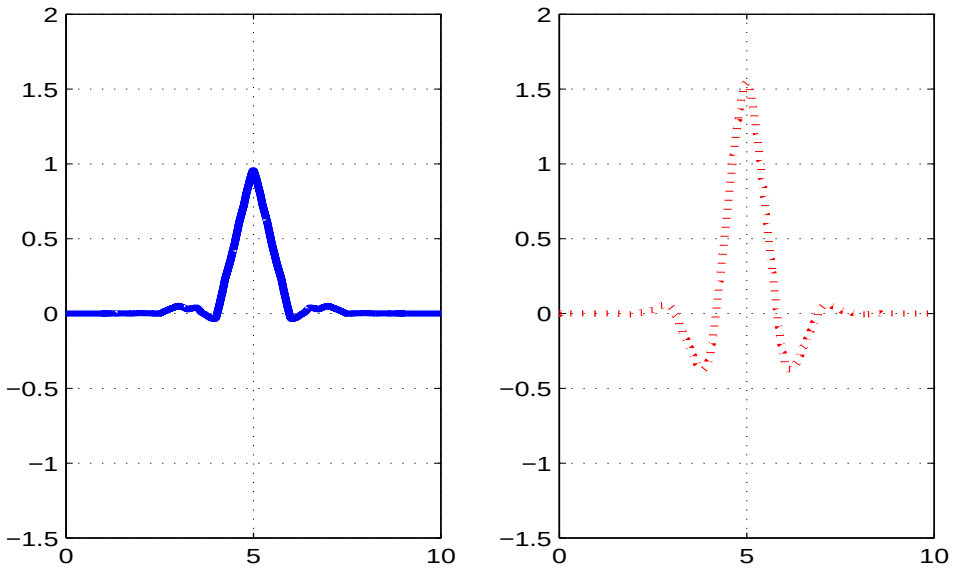

Figure 3.3: bior5.5 shows duality concept with two scaling functions, $\hat{\phi}(t)$ (left) and $\phi(t)$ (right). Note that this plot is similar to [36] p. 280.

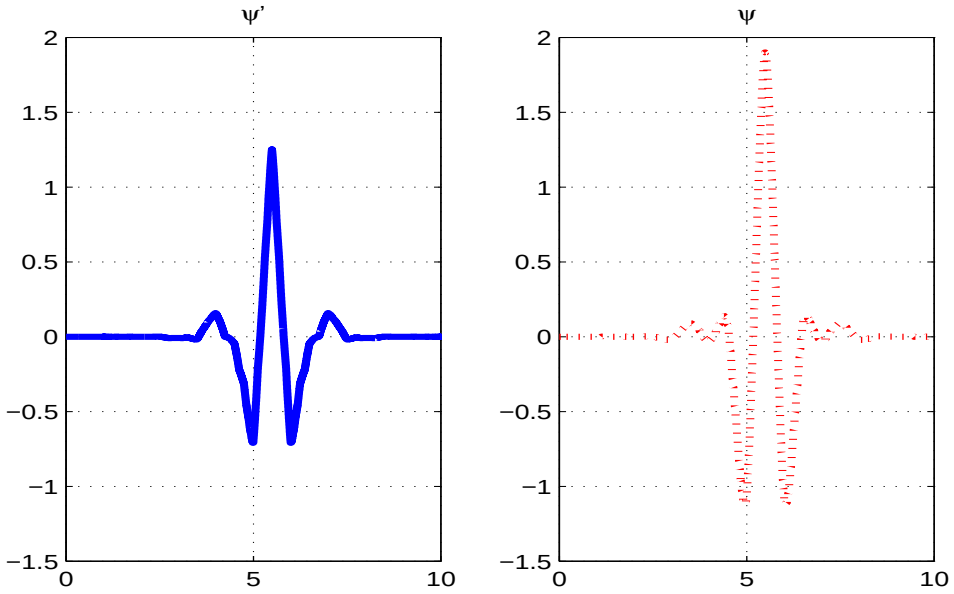

Figure 3.4: bior5.5 shows duality concept with two wavelet functions, $\hat{\psi}(t)$ (left) and $\psi(t)$ (right). Note that this plot is similar to [36] p. 280.

In wavelet OFDM, the binary data is processed by M-ary quadrature amplitude modulation (QAM) to map the raw binary data to appropriate QAM symbols. The term M here means the number of binary inputs to the QAM modulator. In the case of 4-QAM, M is equal to 2 bits. This allows four possible symbols to be transmitted in parallel in an OFDM channel for this type of QAM. On the other hand, M is equal to 4 bits if 16-QAM is considered, where, there are sixteen possible symbols that can be transmitted in parallel. These symbols are then input into an inverse discrete wavelet transform (IDWT). This involves taking N parallel streams of QAM symbols (N being the number of sub-carriers used in the transmission of the data) and performing an IDWT operation on this parallel stream. The IDWT operation acts as a synthesis filtering in the transmitter while the DWT operation acts as an analysis filter at the receiver respectively.

3.3 System Model of Wavelet-Based OFDM

The wavelet transform blocks comprise of an inverse discrete wavelet transform (IDWT) at the transmitter and a discrete wavelet transform (DWT) at the receiver as shown in Fig. 3.5.

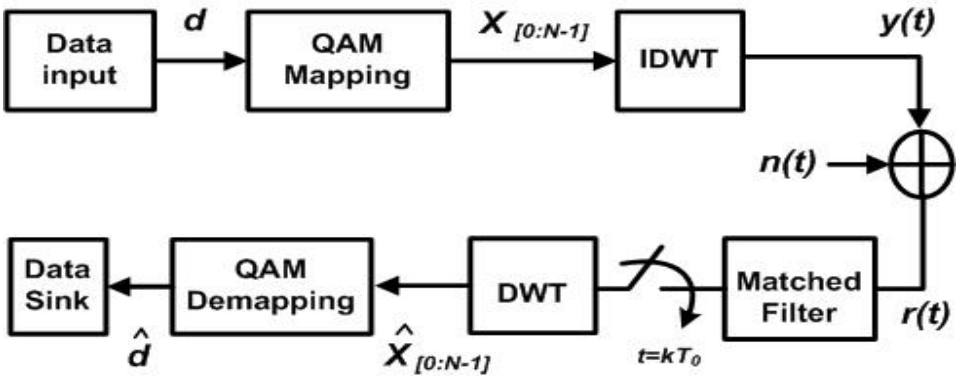

Figure 3.5: The system model of Wavelet based OFDM transceiver.

The IDWT and DWT blocks replace the IFFT and FFT blocks of Fourier based OFDM in Fig. 2.3 in Chapter 2. There is also no CP blocks in the transmitter or receiver. Due to the overlapping nature of wavelets, the wavelet-based OFDM has higher spectral containment and therefore does not need a cyclic prefix to deal with the delay spreads of the channel [106], [118]. The DWT-OFDM system model comprise of low pass filters (LPF) and high pass filters (HPF) in order to perform wavelet operations, this platform has to satisfy the orthonormal bases and perfect reconstruction properties. By assigning g as LPF filter coefficients and h as HPF filter coefficients, the orthonormal bases can be satisfied via four possible ways as follows [86]:

$$< g, g^* >= 1 \tag{3.13}$$

$$< h, h^* >= 1 \tag{3.14}$$

$$< g, h^* >= 0 \tag{3.15}$$

$$< h, g^* >= 0 \tag{3.16}$$

where (3.13) or (3.14) is related to the normal property and (3.15) or (3.16) is for orthogonal property accordingly. Both filters are assumed to have perfect reconstruction property. This means that the input and output of the two filters are expected to be the same. The g and h coefficients perform convolution process to perform as orthonormal wavelets, and can be expressed as follows [12]:

$$\begin{aligned} \alpha_i(n) &= h\left(\frac{n}{2^i}\right) * g\left(\frac{n}{2^i}\right) * ... * g\left(\frac{n}{2^{i-j}}\right) * ... * g(n) \\ \alpha_{N-1}(n) &= g\left(\frac{n}{2^{N-2}}\right) * g\left(\frac{n}{2^{N-1}}\right) * ... * g\left(\frac{n}{2^{i-j}}\right) * ... * g(n) \end{aligned} \tag{3.17}$$

where $(i-j)$ is a positive integer for $i, j \quad \epsilon \quad 0, 1, ..., N-2$. The signal is up-sampled and filtered by the LPF coefficients to become approximated coefficients.

In wavelet-based OFDM, the same analysis using matched filtering is performed except that the $f_k(t)$ and $f_i(t)$ in section 2.3 are replaced with $W_k(t)$ and $W_i(t)$; $W_k(t)$ being the wavelet carrier in the IDWT operation with k sub-channels to match with carrier i. Thus, the received signal is as follows:

$$\begin{aligned} r_W(t) &= y_W(t) * h(t) + n(t) \\ &= \sum_{k=0}^{K-1} d_k W'_k(t) \\ &\quad + \sum_{l=0}^{g-1} \sum_{k=0}^{K-1} d_{k,l} W'_k(t - lk) + n(t) \end{aligned} \tag{3.18}$$

where K is the wavelet filter rank (sampling rate), $W'_k(t) = W_k(t) * h(t)$, and g ($g > 1$) is the wavelet *genus* so that Kg is the filter order (number of taps

in that sub-band). After matched - filtering with carrier i, the signal becomes

$$\begin{aligned}
\langle r_W(t), W_i(t)\rangle &= \sum_{k=0}^{K-1} d_k \langle W'_k(t), W_i(t)\rangle \\
&\quad + \sum_{l=1}^{g}\sum_{k=0}^{K-1} d_{k,l}\langle W'_k(t-lk), W_i(t-lk)\rangle \\
&\quad + \langle n(t), f_i(t)\rangle \\
&= \sum_{k=0}^{K-1} d_k \rho_{k,0}(0) + \langle n(t), f_i(t)\rangle \\
&= d_K \rho_{i,i}(0) + \sum_{\substack{k=0 \\ k\neq i}}^{K-1} d_k \rho_{k,i}(0) \\
&\quad + \sum_{l=1}^{g}\sum_{\substack{k=0 \\ k\neq i}}^{K-1} d_{k,l}\rho_{k,i}(l) + n''(t)
\end{aligned} \tag{3.19}$$

where $d_K \rho_{i,i}(0)$ is the recovered data with correlation term $\rho_{i,i}(0)$. The second term which is $\sum_{k=0,k\neq i}^{K-1} d_k \rho_{k,i}(0)$ is the interference due to the distorted filters that are no longer orthogonal to one another with correlation terms $\rho_{k,i}(0)$, and $\sum_{l=1}^{g}\sum_{k=0,k\neq i}^{K-1} d_{k,l}\rho_{k,i}(l)$ is the interference term with correlation $\rho_{k,i}(l)$ due to the overlapped nature of the wavelet transform. If the channel has no distortion, only the first and last terms would appear, which result that the decoder would obtain almost the correct signal.

3.3.1 Discrete Wavelet Transform (DWT)

The transceiver of DWT-OFDM is shown in Fig. 3.6. In the top part, the transmitter first uses a digital modulator (i.e $16-QAM$) which maps the serial bits into symbols converting d_k into X_m, which consists of N parallel data stream $X_{m(i)}$ where $X_{m(i)}|0 \leq i \leq N-1$.

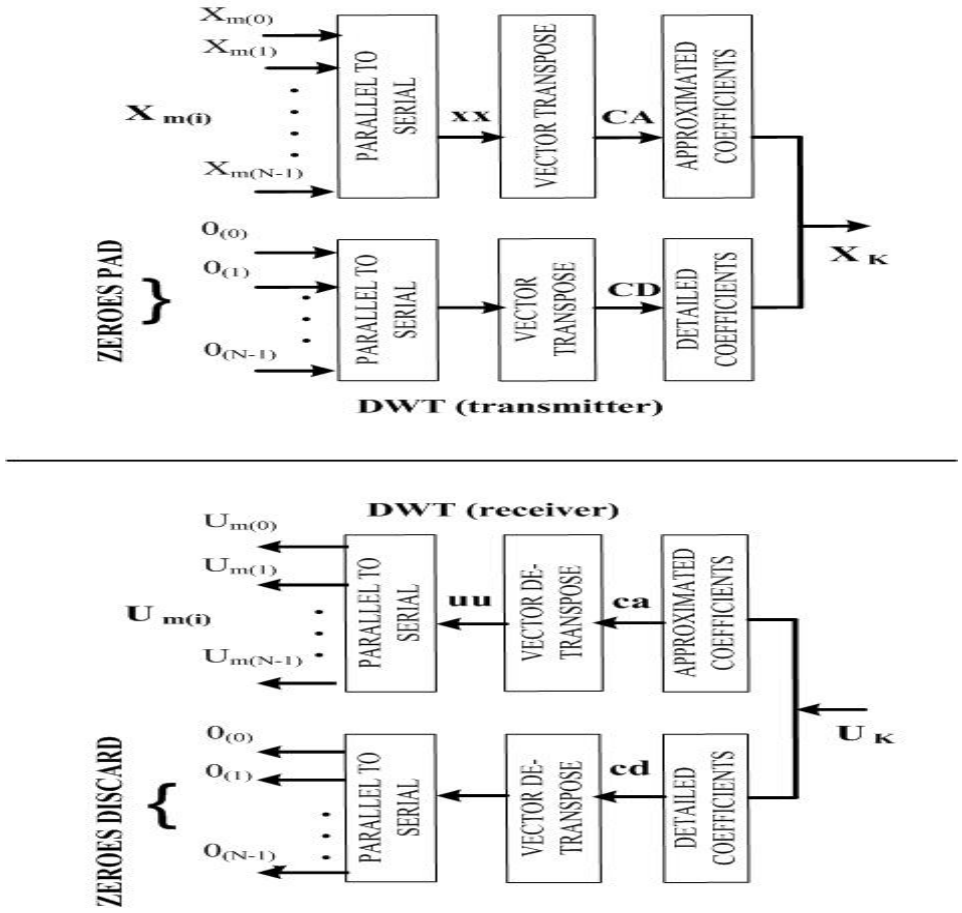

Figure 3.6: An Inverse and Forward Discrete Wavelet Transform DWT-OFDM model. The synthesis filters (transmitter part) are at the top and the analysis filters (receiver part) are at the bottom.

The main task of the transmitter is to perform the discrete wavelet modulation by constructing orthonormal wavelets. Each $X_{m(i)}$ is first converted to a serial representation labelled as a vector xx which will next be transposed into the vector labelled as CA. Then, the signal is up-sampled and filtered by the LPF coefficients or namely the approximation coefficients. Since our aim is to have low frequency signals, the modulated signals, xx, have a circular convolution performed with LPF filter whereas the HPF filter also performs the convolution with zeroes padding the signals, CD, respectively. Note that the HPF filter contains detail coefficients or wavelet coefficients. Different wavelet families have different filter length and values of approximation and detail co-

efficients. Both of these filters have to satisfy orthonormal bases in order to operate as a wavelet transform. This means that they must be orthogonal and normal to each other. By assigning g as LPF coefficients and h as HPF coefficients, the orthonormal bases can be satisfied via four possible ways as follows [86]:

$$< g, g^* >= 1 \tag{3.20}$$

$$< h, h^* >= 1 \tag{3.21}$$

$$< g, h^* >= 0 \tag{3.22}$$

$$< h, g^* >= 0 \tag{3.23}$$

where (3.20) or (3.21) is related to the normal property and (3.22) or (3.23) is realted to the orthogonal property respectively. The commas and star symbols in (3.20) to (3.23) are referring to the dot product and transposed vector accordingly. Both filters are also assumed to have perfect reconstruction property which means that the input and output of the two filters are expected to be the same. A further discussion of this can be found in section 3.3.3. In the transmitter block, the resultant signal is simulated using the MATLAB command $[X_k] = idwt(CA, CD, wv)$ where wv is the type of wavelet family. On the other hand, the reverse process is simulated using $[ca, cd] = dwt(U_k, wv)$ in the receiver. The resulting ca signal will be processed in the QAM demodulator for data recovery, however, the cd signal is discarded because it does not contain any useful information. One example of this block model is shown in Fig. 3.7.

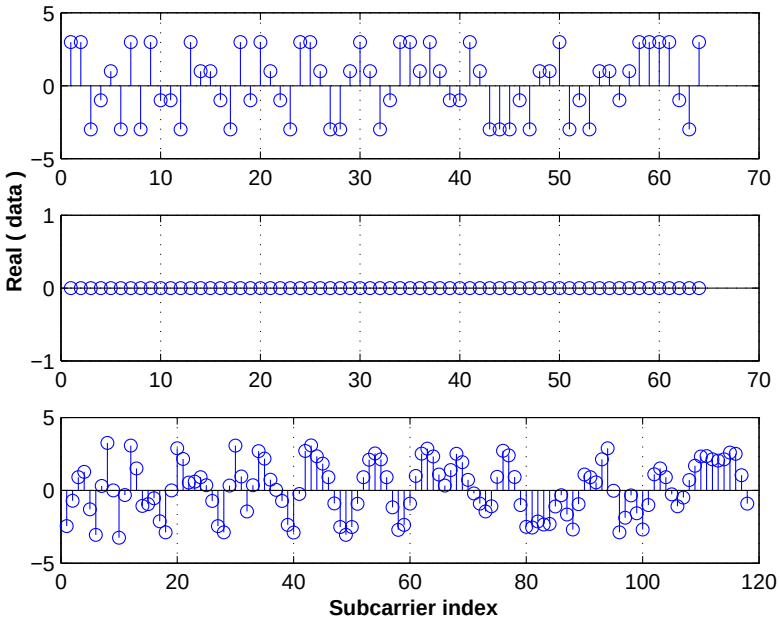

(a) Top: data CA. Middle: data CD. Bottom: data X_k

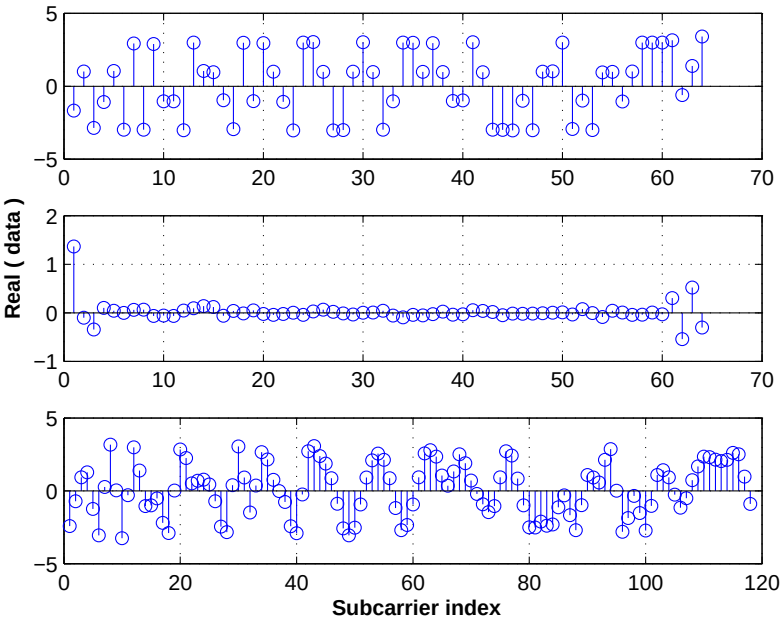

(b) Top: data ca. Middle: data cd. Bottom: data U_k

Figure 3.7: An example of the processed signals of one symbol in DWT-OFDM system using bior5.5. Part (a): DWT transmitter. Part (b): DWT receiver.

3.3.2 Wavelet Packet Transform (WPT)

A wavelet packet transform (WPT) block can be illustrated as in Fig. 3.8. The wavelet packet forming block can be simulated using the following MATLAB command, $T = wptree(2, 3, xx, wv)$. The purpose of this command is to create the wavelet packet tree T to be processed in the reconstruction block of the WPT.

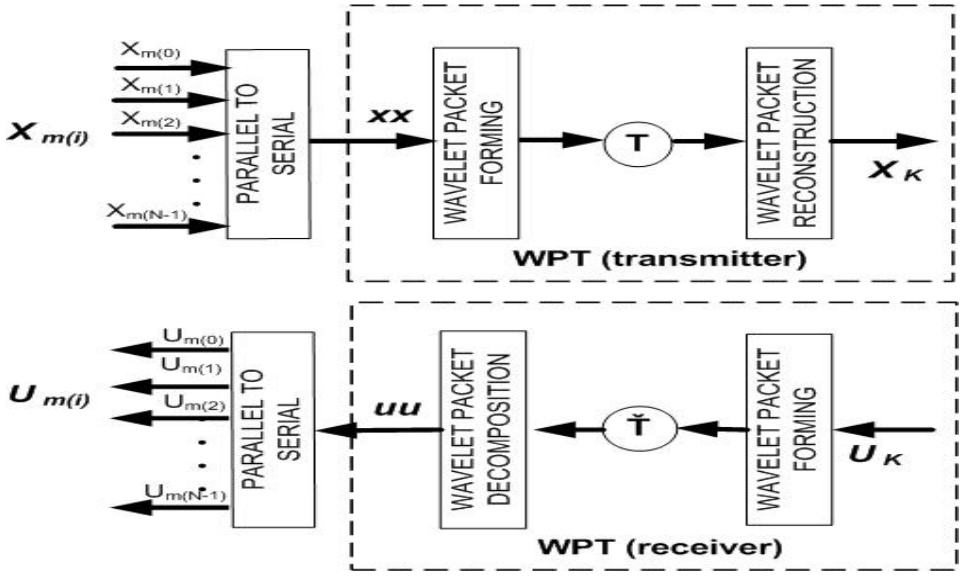

Figure 3.8: Inverse and Forward Wavelet Packet Transform WPT-OFDM model.

The first parameter 2 is the order number depending on the input signal xx. The second parameter 3 is the level number which is dependent on the size of the input data xx and lastly, wv is the wavelet family. The tree structure can be found in Fig. 3.9. Furthering process to this implementation, the MATLAB code $X_k = wprec(T, wv)$ is invoked. The input signals of WPT block has to be a wavelet packet tree, otherwise, the signal cannot be processed for transmission. At the front end of the receiver, the signals U_k is received by the system and processed by the WP forming block. Then the WPT decomposition block is used before the data is processed by the QAM demodulator. Examples of other WPT models can be found in [17] and [130]. An example of the signals that are processed by this block model is shown in Fig. 3.10.

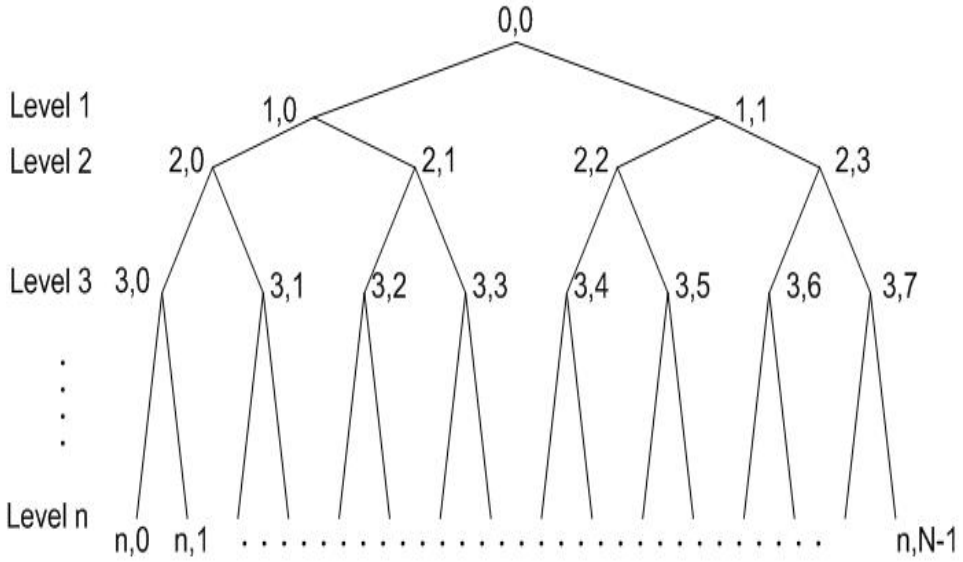

Figure 3.9: WPT-OFDM: the tree structure.

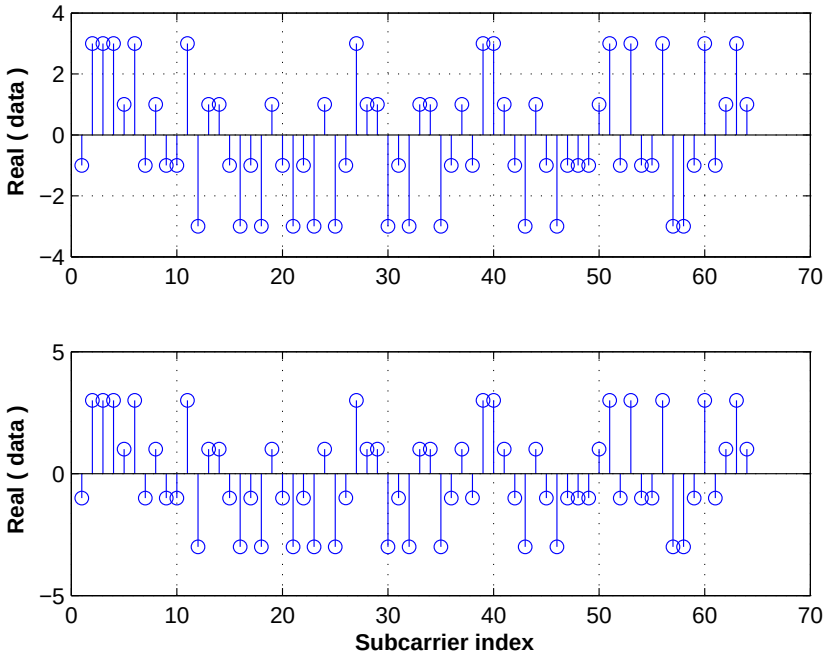

(a) Top: data XX. Bottom: data X_k

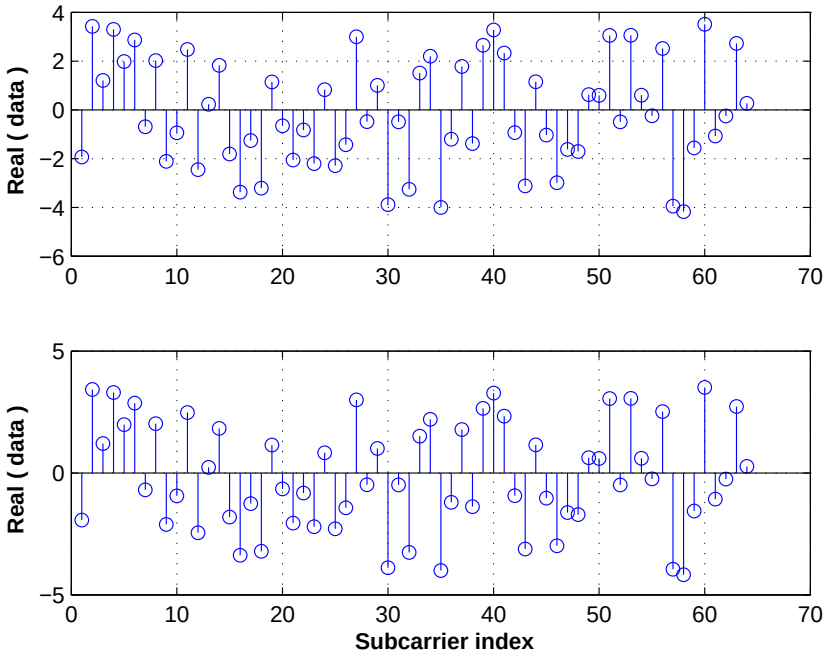

(b) Top: data uu. Bottom: data U_k

Figure 3.10: An example of the processed signals of one symbol in WPT-OFDM system using bior5.5. Part (a): WPT transmitter. Part (b): WPT receiver.

3.3.3 Perfect Reconstruction

A simple block diagram showing the perfect reconstruction (PR) property performed by a two-channel filter bank which is represented by the LPF and HPF is shown in Fig. 3.11.

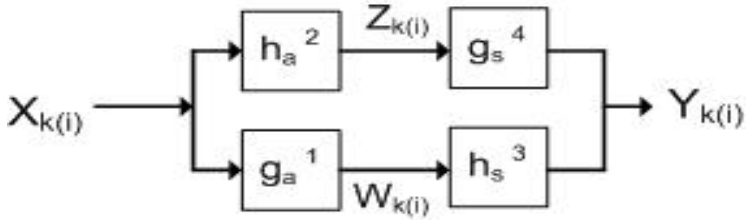

Figure 3.11: A two-channel filter bank illustrating a perfect reconstruction property with the superscript number is referring to the steps.

To satisfy a perfect reconstruction operation, the output $Y_{k(i)}$ is expected to be the same as $X_{k(i)}$. With the exception of a time delay, the input can be considered as $Y_{k(i)} = X_{k(i-n)}$ where 1 can be substituted into n to describe this simple task. The steps to perform the mathematical operation of PR can be summarised as follows [86]:

1. Selecting the filter coefficients for g_a, i.e., a and b. Thus, $g_a = \{a, b\}$.
2. h_a is a reversed version of g_a with every other value negated. Thus, $h_a = \{b, -a\}$. If the system has 4 filter coefficients with $g_a = \{a, b, c, d\}$, then $h_a = \{d, -c, b, -a\}$.
3. h_s is the reversed version of g_a, thus $h_s = \{b, a\}$.
4. g_s is also a reversed version of h_a, therefore $g_s = \{-a, b\}$.

The above steps can be rewritten as follows:

$$g_a = \{a, b\}, h_a = \{b, -a\}, h_s = \{b, a\}, g_s = \{-a, b\} \tag{3.24}$$

Considering that the input with delay are applied to h_a and g_a in Fig. 3.11, then the output of these filters are:

$$Z_{k(i)} = b(X_{k(i)}) - a(X_{k(i-1)}) \tag{3.25}$$

$$W_{k(i)} = a(X_{k(i)}) + b(X_{k(i-1)}) \tag{3.26}$$

Considering also that $Z_{k(i)}$ and $W_{k(i)}$ are delayed by 1, then i can be replaced by (i-1) as follows

$$Z_{k(i-1)} = a(X_{k(i-1)}) + b(X_{k(i-2)}) \tag{3.27}$$

$$W_{k(i-1)} = b(X_{k(i-1)}) - a(X_{k(i-2)}) \tag{3.28}$$

The output $Y_{k(i)}$ can be written as:

$$Y_{k(i)} = g_s Z_{k(i)} + h_s W_{k(i)} \tag{3.29}$$

or,

$$Y_{k(i)} = -aZ_{k(i)} + bZ_{k(i-1)} + bW_{k(i)} + aW_{k(i-1)} \tag{3.30}$$

Substituting equations (3.25), (3.26), (3.27) and (3.28) into (3.30) yields to

$$Y_{k(i)} = 2(a^2 + b^2)X_{k(i-1)} \tag{3.31}$$

The output $Y_{k(i)}$ is the same as the input $X_{k(i)}$ except that it is delayed by 1 if we substitute the coefficient factor $2(a^2 + b^2)$ by 1. The PR condition is satisfied.

3.4 Simulation Results

Simulation variables and their matrix values are shown in Table 3.2. The number of samples for the subcarriers N is 64, and the number of samples for the symbols, ns, is 1000. Due to computational complexity, the number of samples per symbol were limited. With a larger number of samples, a greater accuracy could be achieved. Other variables are listed according to their use as in Figs. 2.3, 3.6 and 3.8. Note that FFT-OFDM is considered when the inverse and forward transform blocks are replaced by IFFT and FFT in Fig. 2.3. Fig. 3.12 shows the OFDM symbols in time domain for the three transform

Table 3.2: Simulation variables and their matrix values.

	FFT-OFDM	**DWT-OFDM**	**WPT-OFDM**
Variables	**Matrix Values**	**Matrix Values**	**Matrix Values**
N	64	64	64
ns	1000	1000	1000
d $(N \times ns)$	64×1000	64×1000	64×1000
$X_m(N \times ns)$	64×1000	64×1000	64×1000
xx	1×64000	1×64000	1×64000
X_k	64000×1	128000×1	64000×1
U_k	64000×1	128000×1	64000×1
uu	1×64000	1×64000	1×64000
U_m $(N \times ns)$	64×1000	64×1000	64×1000
$d^{'}$ $(N \times ns)$	64×1000	64×1000	64×1000

platforms. Some of the simulation parameters related to this figure are: the OFDM symbol period $T_o = 9$ ms, the total simulation time $t = 10 \times T_o = 90$ ms, the sampling frequency $fs = 71.11$ kHz, the carriers spacing $\triangle N = 1.11$ kHz and the bandwidth $B = \triangle N \times 64 = 71.11$ kHz. All platforms used the same parameters. It is interesting to see that the DWT-OFDM symbol is the least mean of amplitude vectors as compared to others. This is due to the fact that zero - padding was performed in the DWT (transmitter) system model. As a result, most samples in the middle of its symbol are almost zero.

The DWT-OFDM performance can be observed from Fig. 3.13. The biorthogonal, Reverse-biorthogonal and Daubechies wavelet families are compared with FFT-OFDM. We have two parts in this figure since biorthogonal and reverse-biorthogonal wavelets produce results opposite to each other. It is shown that bior5.5 is superior among all in Fig. 3.13(a), it outperforms FFT and Daubechies by about 2 dB, and bior3.3 by 8 dB at 0.001 BER. On the other hand, Fig. 3.13(b) shows the result of using reverse-biorthogonal. The wavelet family rbior3.3 shows the least error as compared to others. At BER target of 0.001, it outperforms FFT and Daubechies by 4 dB, and rbior5.5 by 6 dB. It is also interesting to observe that all wavelets as well as FFT show similar results in Fig. 3.14. We use a level 3 wavelet decomposition and considered

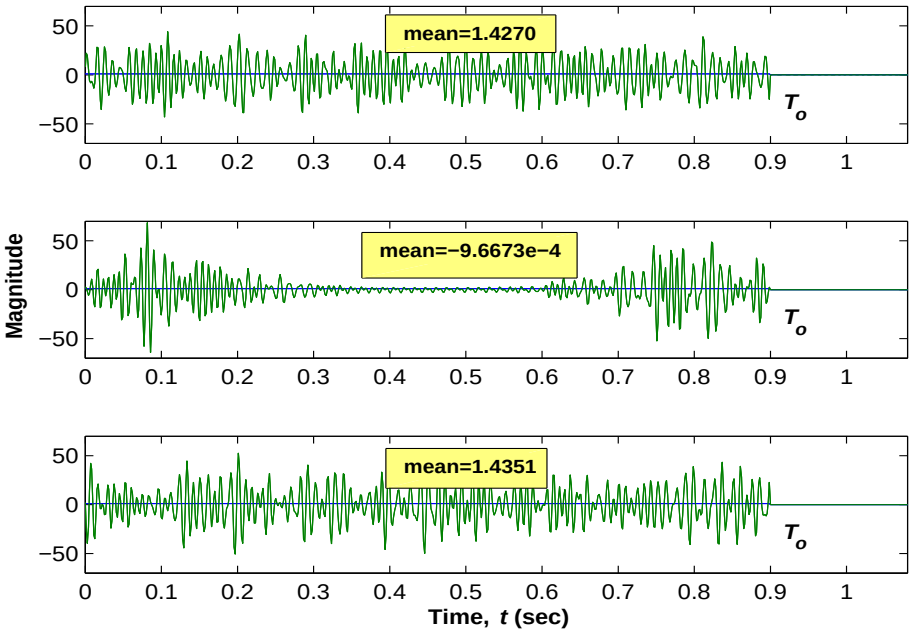

Figure 3.12: An OFDM symbol in Time domain for FFT-OFDM (Top), DWT-OFDM (Middle) and WPT-OFDM(Bottom).

white Gaussian noise only. The result is likely to be different if we could apply that to a higher level, however, this will make the system more complex and consume a longer period of time. Comparing the last two figures, we can say that Fig. 3.13 presents a better performance than that in Fig. 3.14. The reason for this is simply because we are using DWT-OFDM with zero - padding for the detail coefficients as we have a low-frequency signal; also DWT-OFDM satisfies orthonormal bases and perfect reconstruction properties. This leads to a better BER performance.

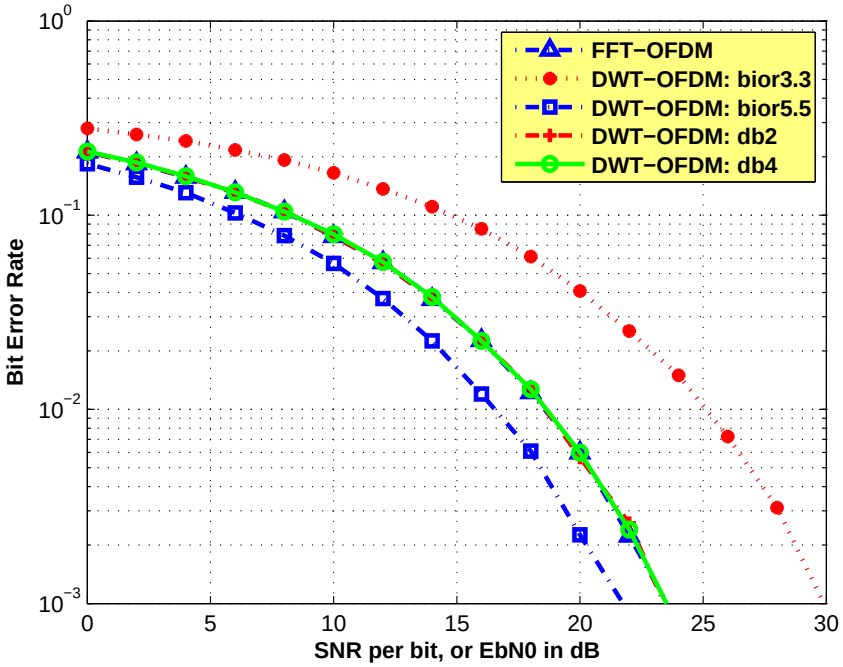

(a) Fourier based OFDM, biorthogonal (bior3.3 & bior5.5) and Orthogonal(db2 & db4) families

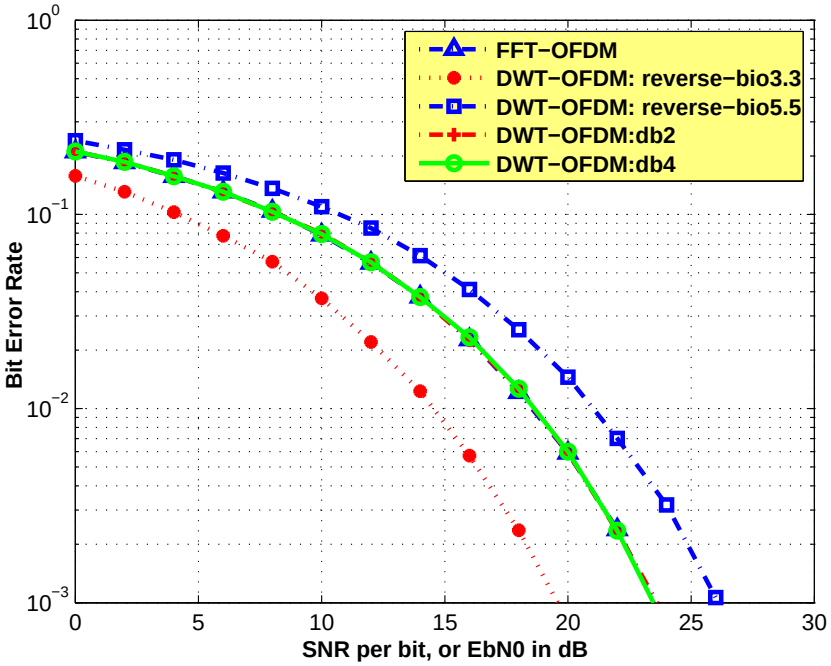

(b) Fourier based OFDM, reverse-biorthogonal(rbio3.3 & rbio5.5) and orthogonal(db2 & db4) families

Figure 3.13: BER performance for DWT-OFDM.

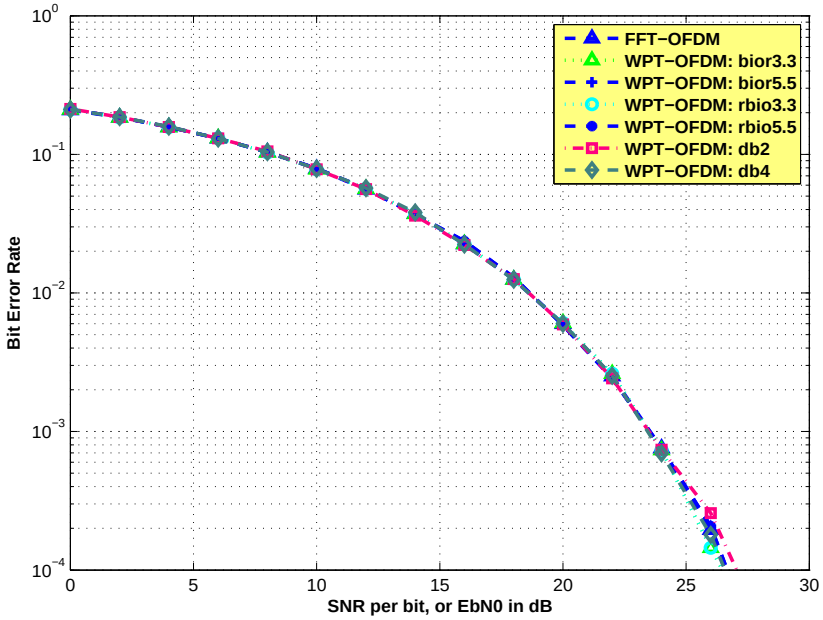

Figure 3.14: BER performance for WPT-OFDM.

3.5 Peak-to-Average Power Ratio DWT-OFDM

PAPR is well known as one of the drawbacks that inevitably occur not only to FFT-OFDM but also to DWT-OFDM system. Some literatures have discussed the PAPR problem in wavelet OFDM. They also include methods of PAPR reduction techniques. In [72], the reduction technique is introduced by deploying wavelet packet pre-processing of the QAM symbols. Another method is to use wavelet packet tree which is pruned via joining and splitting of terminal nodes to reduce PAPR [73]. This is specifically done by using alternative mappings of data symbols onto different generated tree structures, and the time domain sequence with the smallest PAPR is transmitted. However, none of these two literatures mention about the type of wavelet family that they use for the study. [127] discusses the type of wavelet families which are Daubechies (Db1, Db4 and Db 6), and introduces the searching algorithm for better wavelet packet tree structure. However, [127] did not include the com-

parison of study with FFT-OFDM. The comparisons of study between wavelet families and FFT-OFDM are done by [32]. For the future direction, a PAPR reduction technique that use different QAM modulation with different wavelet families and FFT-OFDM comparisons can be proposed. A further discussion of this can be found in chapter 8.

3.6 Summary

This chapter presents the wavelet based OFDM. It begins with the principle background, describes the DWT-OFDM model, includes orthogonality and perfect reconstruction properties. The simulation approaches for DWT-OFDM and WPT-OFDM as alternative substitutions for FFT-OFDM are described. At some points, the details of the MATLAB commands regarding the DWT-OFDM and WPT-OFDM platform models are also included. The results in terms of BER performance are also obtained. The DWT-OFDM system is shown to be superior to others, especially when the system uses bior5.5 or rbior3.3 wavelet family. An overview of PAPR discussion in the last section yields to the next current issue of wavelet based OFDM system that can be performed for future direction of research discussed in section 9.2.

Chapter 4

Circular and Square Quadrature Amplitude Modulations

4.1 Introduction

The quadrature amplitude modulation (QAM) scheme is a useful modulation technique in OFDM systems for achieving high data rate transmission. The task of QAM can be viewed as follows, in the transmitter, the output data of the OFDM generator is first mapped onto complex representations or constellation points by the QAM modulator. Each constellation point has a real and imaginary component which represents amplitude and phase of the carrier [48]. In the receiver, the bandpass signal will not be same as the output of the transmitted block because of ISI due to multipath channel effects. The task of the QAM demodulator is to recover the complex bandpass signal and hence the original data.

Some popular types of M-ary QAM are 4-QAM, 16-QAM and 64-QAM. The number of 4, 16 and 64 is corresponding to 2^2, 2^4 and 2^6. In these cases the superscript numbers 2, 4 and 6 are the bit rate per OFDM symbol respectively. Most of our simulations in this chapter use 16-QAM. One of the reasons for this is to give intermediate results between 4-and 64-QAM. 16-QAM is also considered one of the standard modulation schemes in OFDM applications such as terrestrial Digital Video Broadcasting (DVB), Digital Audio Broadcasting (DAB) and High Performance Radio LAN Version 2 (HIPERLAN/2)

[108]. This chapter is organised as follows: the derivations of the signal constellations for both square and circular 16-QAM are described in section 4.3, the derivation of the closed form bit error rate (BER) of the circular 16-QAM is also provided. Then, the results of the average power for the two modulation schemes are determined in section 4.5.1 as well as the BER performances are shown in section 4.5.2 and 4.5.3 respectively.

4.2 System Model of Wavelet-Based OFDM for Circular 16-QAM

The wavelet transform blocks comprise of an inverse discrete wavelet transform (IDWT) at the transmitter and a discrete wavelet transform (DWT) at the receiver as shown in Fig. 4.1. As discussed in previous chapters, no cyclic prefix block is necessary in this type of system [100], [118]. The DWT-OFDM system model comprise of low pass filters (LPF) and high pass filters (HPF), in order to perform wavelet operations, this platform has to satisfy the orthonormal bases and perfect reconstruction properties as discussed in chapter 3.

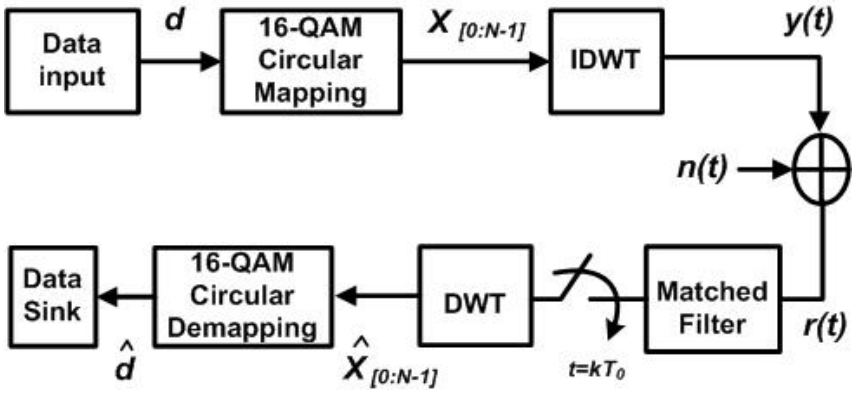

Figure 4.1: The system model of Wavelet based OFDM transceiver.

4.3 Derivation of 16-QAM Constellation Points

A circular signal point constellation has been discussed in [48], however, this case only covers for $M = 8$ constellations. While $M = 16$ can be inferred as sub-optimal, we extend the work for an optimal circular 16−QAM. Before we provide the work of circular 16-QAM, we will first derive the conventional square 16-QAM for the purpose of comparisons with the circular scheme in a programming-like language environment.

To obtain the square 16-QAM constellation points, we first define the minimum distance (dm) between the two symbols, which is $dm = 2d$. With the assumption that $d = 1$, then $dm = 2$. Let the number of circles be defined as S and the amplitude level define as R, this will give four circles associated with three different amplitudes R_1, R_2, R_2, R_3 (note that R_2 is repeated). Thus we have $S = 4$ with 4 points on the first circle with diameter R_1, 8 points on the second circle with diameter R_2 and 4 points on the third circle with diameter R_3. The calculations for the amplitudes associated with the diameter of the circles $d = 1$ are:

$$R_1 = \sqrt{d^2 + d^2} = \sqrt{2} \tag{4.1}$$

$$R_2 = \sqrt{d^2 + (3d)^2} = \sqrt{10} \tag{4.2}$$

$$R_3 = \sqrt{(3d)^2 + (3d)^2} = \sqrt{18} \tag{4.3}$$

By arranging (4.1), (4.2) and (4.3) in vector representation, we have:

$$V = d \times [R_1 \quad R_2 \quad R_2 \quad R_3] \tag{4.4}$$

Since every 4 points share one diameter, we repeat every amplitude 4 times. Thus,

$$v = V^T \times [1 \quad 1 \quad 1 \quad 1] \tag{4.5}$$

and the amplitude vector A_v for QAM representation will be,

$$A_v = v^T \tag{4.6}$$

where $\langle . \rangle^T$ is a transpose vector. Next, we need to derive the rotating phase for the constellation points. Let the first, second and third phases be associated with the circles R_1, R_2 and R_3 be P_{S1}, P_{S2} and P_{S3}. Then, we have

$$P_{S1} = [e_o \quad \pi - e_o \quad \pi + e_o \quad -e_o] \tag{4.7}$$

$$P_{S2} = [f_o \quad \frac{\pi}{2} - f_o \quad \frac{\pi}{2} + f_o \quad \pi + f_o \quad 3\frac{\pi}{2} - f_o \quad 3\frac{\pi}{2} + f_o \quad -f_o] \tag{4.8}$$

$$P_{S3} = [g_o \quad \pi - g_o \quad \pi + g_o \quad -g_o] \tag{4.9}$$

where $e_o = tan^{-1}[1]$, $f_o = tan^{-1}[\frac{1}{3}]$ and $g_o = tan^{-1}[1]$ Rearranging (4.7), (4.8) and (4.9) in vector representation yield to

$$P_S = [P_{S1} \quad P_{S2} \quad P_{S3}] \tag{4.10}$$

By transposing vector P_S, we have the phase vector P_v for QAM representation as follows

$$P_v = (P_S)^T \tag{4.11}$$

Combining (4.6) and (4.11), the square 16-QAM (S_{sq}) is expressed as

$$S_{sq} = A_v cos(P_v) \quad + \quad jA_v sin(P_v) \tag{4.12}$$

The next step is to derive our circular 16-QAM constellation points. In this case, the number of circles and amplitudes as compared to the square 16-QAM will be different. We have $S = 4$ with 4 points on all circles with different diameters r_1, r_2, r_3 and r_4. The calculations for the amplitudes related to the

diameter of the circles $d = 1$ are

$$r_1 = \sqrt{d^2 + d^2} = \sqrt{2} \tag{4.13}$$

$$r_2 = \sqrt{3d} = \sqrt{3} \tag{4.14}$$

$$r_3 = \sqrt{(1 + r_2)^2 + 2^2 - 4 * (1 + r_2) \times [cos(P_h)]} \tag{4.15}$$

where $P_h = \frac{\pi}{3} + P_o$ and $P_o = tan^{-1}(\frac{1}{r_2})$

$$r_4 = \sqrt{d_s^2 + r_1^2 - 2 \times [d_s] \times [r_1] \times [cos(\frac{P_p}{2} + P_{si})]} \tag{4.16}$$

where $d_s = \sqrt{(2d)^2 + (2d)^2 - (8d) \times [cos(b)]}$, $b = \pi - P_p$, $P_p = \phi - \frac{\pi}{3}$, $\phi = 2\pi - 2P_{si}$, $P_{si} = \pi - \frac{\pi}{4} - P_o$ and $P_o = tan^{-1}(\frac{1}{r_2})$. By rearranging (4.13), (4.14),(4.15) and (4.16) in vector representation, we have

$$V_c = d \times [r_1 \quad 1 + r_2 \quad r_3 \quad r_4] \tag{4.17}$$

Since every 4 points share one diameter, we repeat every amplitude 4 times. Therefore

$$v_c = (V_c)^T \times [1 \quad 1 \quad 1 \quad 1] \tag{4.18}$$

Hence the amplitude vector A_{vc} for all amplitudes of QAM constellation points will be

$$A_{vc} = (v_c)^T \tag{4.19}$$

Subsequently we need to derive the rotating phase for the constellation points. Thus,

$$P_{c1} = \frac{\pi}{4} \times [1 \quad 3 \quad 5 \quad 7 \quad 0 \quad 2 \quad 4 \quad 6]; \tag{4.20}$$

$$P_{c2} = [h_o \quad h_1 \quad h_2 \quad h_3] \tag{4.21}$$

where $h_o = sin^{-1}(\frac{2}{r_3}sin(p_h))$, $h_1 = \pi - h_o$, $h_2 = \pi + h_o$ and $h_3 = -h_o$

$$P_{c3} = [g_o \quad g_1 \quad g_2 \quad g_3] \tag{4.22}$$

where $g_o = \frac{\pi}{4} + sin^{-1}(\frac{d_s}{r_4}sin(\frac{P_p}{2} + P_{si}))$, $g_1 = \pi - g_o$, $g_2 = \pi + g_o$ and $g_3 = -g_o$. Rearranging (4.20), (4.21) and (4.22) in vector representation, we obtain

$$P_c = [P_{c1} \quad P_{c2} \quad P_{c3}] \tag{4.23}$$

where P_c has all angles of all constellation points. Combining the amplitude A_{vc} and the phase P_c, the final equation for the circular 16-QAM (S_{cir}) is expressed as

$$S_{cir} = A_{vc}cos(P_c) \quad + \quad jA_{vc}sin(P_c) \tag{4.24}$$

4.4 BER Analysis for Circular 16-QAM

Equation (4.24) can be generally rewritten as [48], [54]

$$S_{cir} = A_icos(2\pi f_c t) \quad + jA_jsin(2\pi f_c t) \tag{4.25}$$

where A_i and A_j are the real and imaginary components constituting the in-phase and quadrature phase components and f_c is the carrier frequency. The steps to determine P_e differ between the square and circular when considering the decision boundary. The diagram showing the decision boundaries for the circular scheme is shown in Fig. 4.2. In this section, we avoid the discussion of the probability of error derivation for the square scheme since it is available in many of the literatures.

We develop the exact calculation of P_e based on [48], [54] and equation (6) in [75]. From Fig. 4.2, we can observe that there are four types of boundary

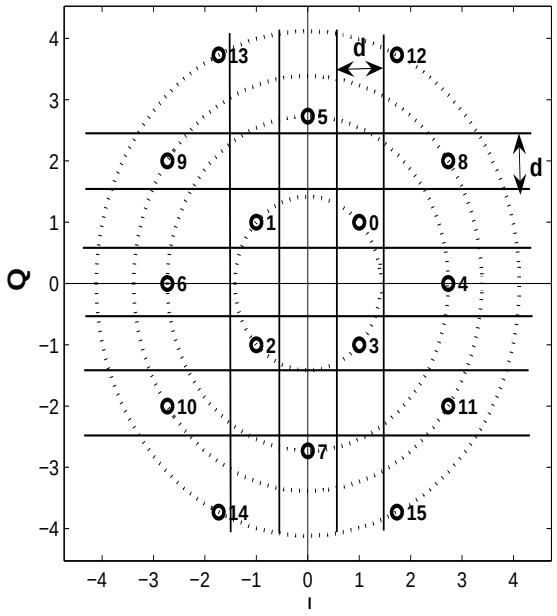

Figure 4.2: Signal-space diagram for circular 16-QAM.

regions. This boundary region theory is closely related to the definition of general Gaussian problem in [65] of Gaussian pattern vectors for M-class. In [65], decision regions in the observation space is given and the probability of error for the decision rule is calculated in terms of the probability of being correct. The general approach the probability of error can be expressed as follows [65]

$$P(error) = 1 - (\sum_{j=1}^{M} P(correct|C_j)P(C_j)) \tag{4.26}$$

where C is the class abide by the Gaussian probability density function.

In our case, all regions are also assumed to comply with the probability density function (pdf) in the direction of in-phase and quadrature components as the Gaussian distribution and can be written as n_I and n_Q respectively. The pdf associated with the decision boundaries is shown in Fig. C.2 [48]. Let us derive the first type of the boundary region. It is associated with the points located on the inner most circle. The probability of a correct decision made

by the receiver for Type I decision boundary in Fig. C.3 is written as

$$\begin{aligned} P_{c1} &= \left[1 - \left(P(n_I \leq -\frac{d}{2\sigma}) \quad + \quad P(n_I \geq \frac{d}{2\sigma})\right)\right] \\ &\quad \times \left[1 - \left(P(n_Q \geq \frac{d}{2\sigma}) \quad + \quad P(n_Q \leq -\frac{d}{2\sigma})\right)\right] \\ &= \left[1 - \left(2Q(\frac{d}{2\sigma})\right)\right]\left[1 - \left(2Q(\frac{d}{2\sigma})\right)\right] \end{aligned} \tag{4.27}$$

where

$$Q(x) = \frac{1}{\sqrt{2\pi}} \int_x^\infty e^{\frac{x^2}{2}} dx$$

Since there are 4 points associated with the same decision boundary, the probability of error for type I becomes

$$\begin{aligned} P_{e1} &= 4\left[1 - P_{c1}\right] \\ &= 4\left[1 - \left(1 - 2Q(\frac{d}{2\sigma})\right)^2\right] \end{aligned} \tag{4.28}$$

The next type is associated with the 2 points $\{5, 7\}$ on the second circle from the center. The boundary region is shown in Fig. C.4. The probability of a correct decision is determined as follows

$$\begin{aligned} P_{c2} &= \left[1 - \left(P(n_I \leq -\frac{d}{2\sigma}) \quad + \quad P(n_I \leq -\frac{d}{2\sigma})\right)\right] \\ &\quad \times \left[1 - \left(P(n_Q \leq \frac{0.232d}{\sigma})\right]\right. \\ &= \left[1 - (Q(\frac{d}{2\sigma}) + Q(\frac{d}{2\sigma}))\right]\left[1 - Q(\frac{0.232d}{\sigma})\right] \end{aligned} \tag{4.29}$$

Then, the probability of error for Type II is given by

$$\begin{aligned} P_{e2} &= 2\Big[1 - P_{c2}\Big] \\ &= 2\Big[1 - \Big(1 - 2Q(\frac{d}{2\sigma})\Big)\Big(1 - Q(\frac{0.232d}{\sigma})\Big)\Big] \end{aligned} \tag{4.30}$$

For Type III, there are six points $\{4, 6, 8, 9, 10, 11\}$ located on the second and third cirles. The decision boundary is shown in Fig. C.5. The probability of a correct decision is given by

$$\begin{aligned} P_{c3} &= \Big[1 - \Big(P(n_Q \geq \frac{0.5d}{\sigma}) \quad + \quad P(n_Q \leq -\frac{0.5d}{\sigma})\Big)\Big] \\ &\quad \times \Big[1 - \Big(P(n_I \leq -\frac{1.232d}{\sigma})\Big)\Big] \\ &= \Big[1 - \Big(Q(\frac{0.5d}{\sigma}) + Q(\frac{0.5d}{\sigma})\Big)\Big]\Big[1 - Q(\frac{1.232d}{\sigma})\Big] \\ &= \Big[1 - 2Q(\frac{0.5d}{\sigma})\Big]\Big[1 - Q(\frac{1.232d}{\sigma})\Big] \end{aligned} \tag{4.31}$$

From (4.31), we can write the probability of error for Type III as

$$\begin{aligned} P_{e3} &= 6\Big[1 - P_{c3}\Big] \\ &= 6\Big[1 - \Big(1 - 2Q(\frac{0.5d}{\sigma})\Big)\Big(1 - Q(\frac{1.232d}{\sigma})\Big)\Big] \end{aligned} \tag{4.32}$$

For the outermost circle, or the four points $\{12, 13, 14, 15\}$. The decision boundary is shown in Fig. C.6. The probability of a correct decision is given by

$$\begin{aligned} P_{c4} &= \Big[1 - P(n_I \leq -\frac{0.232d}{\sigma})\Big]\Big[1 - P(n_Q \leq -\frac{1.232d}{\sigma})\Big] \\ &= \Big[1 - Q(\frac{0.232d}{\sigma})\Big]\Big[1 - Q(\frac{1.232d}{\sigma})\Big] \end{aligned} \tag{4.33}$$

Then, the probability of error for Type IV is

$$\begin{aligned} P_{e4} &= 4 \times \Big[1 - P_{c4}\Big] \\ &= 4\Big[1 - \Big(1 - Q(\frac{0.232d}{\sigma})\Big)\Big(1 - Q(\frac{1.232d}{\sigma})\Big)\Big] \end{aligned} \tag{4.34}$$

Combining the equations (4.28), (4.30), (4.32) and (4.34), the average probability of error for the circular 16-QAM scheme is expressed as follows

$$\begin{aligned} P_{cir} &= \frac{1}{16} \times \Big(P_{e1} + P_{e2} + P_{e3} + P_{e4}\Big) \\ &= \frac{1}{16}\Big(4\Big[1 - \Big\{1 - 2Q(\frac{d}{2\sigma})\Big\}^2\Big] \\ &\quad +2\Big[1 - \Big\{1 - 2Q(\frac{d}{2\sigma})\Big\}\Big\{1 - Q(\frac{0.232d}{\sigma})\Big\}\Big] \\ &\quad +6\Big[1 - \Big\{1 - 2Q(\frac{0.5d}{\sigma})\Big\}\Big\{1 - Q(\frac{1.232d}{\sigma})\Big\}\Big] \\ &\quad +4\Big[1 - \Big\{1 - Q(\frac{0.232d}{\sigma})\Big\}\Big\{1 - Q(\frac{1.232d}{\sigma})\Big\}\Big]\Big) \end{aligned} \tag{4.35}$$

After some manipulations, we have

$$P_{cir} = \frac{1}{8}\Big[8A(2 - A - \frac{1}{4}(B + 3C)) + 2B(\frac{3}{2} - C) + 5C\Big] \tag{4.36}$$

where $A = Q(\frac{0.5d}{\sigma})$, $B = Q(\frac{0.232d}{\sigma})$ and $C = Q(\frac{1.232d}{\sigma})$. Using

$$d = \sqrt{\frac{3\log_2 M \cdot E_b}{2(M-1)}} \tag{4.37}$$

from [54] where M=16, and

$$\sigma = \frac{1}{2}\sqrt{\frac{N_0}{5}} \tag{4.38}$$

A, B and C in (4.36) can also be written as

$$\begin{aligned} A &= Q(0.5(\gamma)) \\ B &= Q(0.232(\gamma)) \\ C &= Q(1.232(\gamma)) \end{aligned} \tag{4.39}$$

where $\gamma = \frac{d}{\sigma} = 4\sqrt{\frac{1}{2}\frac{E_b}{N_0}}$. (4.36) can be expressed in terms of energy per bit over noise density ratio ($\frac{E_b}{N_0}$) when the variables in (4.39) are substituted into it. Simulation results for circular 16-QAM from (4.36) as well as for other M-ary QAM are obtained and compared with the square scheme as shown in Fig. 4.3. To simulate the square scheme, the analysis provided by (17) in [54] is used, and is rewritten as follows

$$\begin{aligned} P_{sq} &= \frac{\sqrt{M}-1}{\sqrt{M}log_2(\sqrt{M})}Q\left(\sqrt{\frac{3log_2(\sqrt{M})\cdot E_b}{2(M-1)N_0}}\right) \\ &\quad + \frac{\sqrt{M}-2}{\sqrt{M}log_2(\sqrt{M})}Q\left(\sqrt{\frac{3log_2(\sqrt{M})\cdot E_b}{2(M-1)N_0}}\right) \end{aligned} \tag{4.40}$$

From Fig. 4.3, it is shown that the circular 16-QAM slightly outperforms the counterpart scheme at most SNR values. The exact BER analysis for other circular M-ary is performed by changing the value of M in $d = \sqrt{\frac{3\log_2 M\cdot E_b}{2(M-1)}}$, and fix σ accordingly. When M is changed, the parameters A, B and C are consequently affected. Then, they are substituted into (4.36).

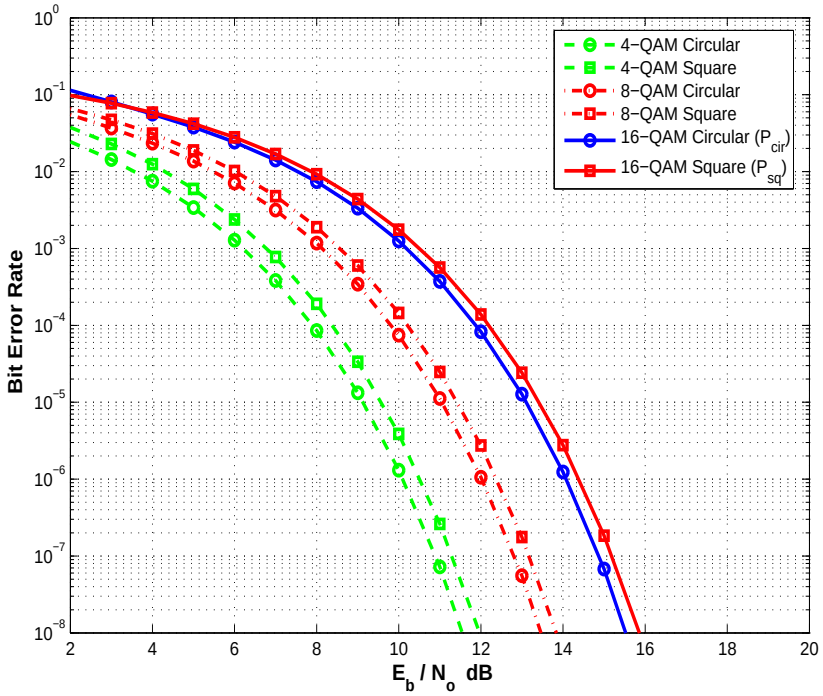

Figure 4.3: Exact BER of circular and square M-ary QAM.

Table 4.1 shows the summary of the arbitrary parameters due to varying M. The results of the circular schemes are slightly better than the square schemes in most SNR values. The simulation results also show that they met the theoretical analysis.

Table 4.1: Summary of parameters for circular M-ary ($M \leq 16$) QAM.

	$M=4$	$M=8$	$M=16$
d	$\sqrt{Eb}$	$\sqrt{\frac{9}{14}Eb}$	$\sqrt{\frac{2}{5}Eb}$
γ	$2\sqrt{5\frac{Eb}{No}}$	$2\sqrt{\frac{45}{14}\frac{Eb}{No}}$	$2\sqrt{2\frac{Eb}{No}}$
A	$Q(\sqrt{5\frac{Eb}{No}})$	$Q(\sqrt{\frac{45}{14}\frac{Eb}{No}})$	$Q(\sqrt{2\frac{Eb}{No}})$
B	$Q(b\sqrt{5\frac{Eb}{No}})$	$Q(b\sqrt{\frac{45}{14}\frac{Eb}{No}})$	$Q(b\sqrt{2\frac{Eb}{No}})$
C	$Q(c\sqrt{5\frac{Eb}{No}})$	$Q(c\sqrt{\frac{45}{14}\frac{Eb}{No}})$	$Q(c\sqrt{2\frac{Eb}{No}})$

Note: b=0.464, c=2.464 and $Q(\cdot) = erfc(\cdot)$

Both modulation schemes, square and circular 16-QAM are further applied to Fourier and wavelet based OFDM. This is discussed in sections 4.5.2 and 4.5.3.

4.5 Results and Discussions

We have divided the simulation results into three categories: comparisons of the transmitted power, performance in Fourier OFDM and performance in wavelet based OFDM. All sections include discussion for both square and circular 16-QAM constellations. Table 4.2 illustrates the parameters used for our simulations.

Table 4.2: Simulations' Parameters.

Parameters	Fourier based	Wavelet based
OFDM symbol T_o	1e-4	1e-4
Carrier spacing $\frac{1}{T_o}$	11.11 kHz	11.11 kHz
Signal bandwidth Bw ($Bw = f_s = N \times \frac{1}{T_o}$)	7.11e5	7.11e5
Number of symbols N_s	10000	10000
Number of carriers N	64	64
Cyclic Prefix length	16	0
Wavelet families	-	db, coif, bior, rbior

4.5.1 Transmitted Power Comparisons

Table 4.3 shows a summary of the average QAM power transmission for both modulations with the same dm and equal probability of obtaining the correct symbols between the transmitter and receiver. The calculation of the power in Table 4.3 is considered using

$$P_x = \overline{|S_{QAM}|^2} \tag{4.41}$$

where S_{QAM} can be replaced by S_{sq} in (4.12) or S_{cir} in (4.24) respectively. Since S_{QAM} consists of real and imaginary components, the absolute value has

to be considered. P_x will obtain a single numerical mean because (4.41) gives an average of the constellation points in a vector form.

Table 4.3: Summary of the average QAM power.

	Circular 16-QAM	Square 16-QAM
Minimum distance, d_m	2	2
Average QAM power, P_x	9.4641	10

As shown in Table 4.3, the circular 16-QAM consumes less power for a similar dm by 0.5359 W or -2.71 dB. Since the power is less, the bit error rate (BER) for the circular 16-QAM constellation has a better performance than the square 16-QAM constellation. This result will be further discussed in the next sections. Fig. 4.4 and Fig. 4.5 are the simulation results of square and circular 16-QAM constellation points for the transmitted and received signals respectively. In an ideal situation there would be no errors in the received signals, however, this is not happening in reality. In this particular case, the received OFDM symbols had errors due to additive white Gaussian noise. This is shown by the blue dots spread around the green dots referring to the incorrect decisions made by the receiver.

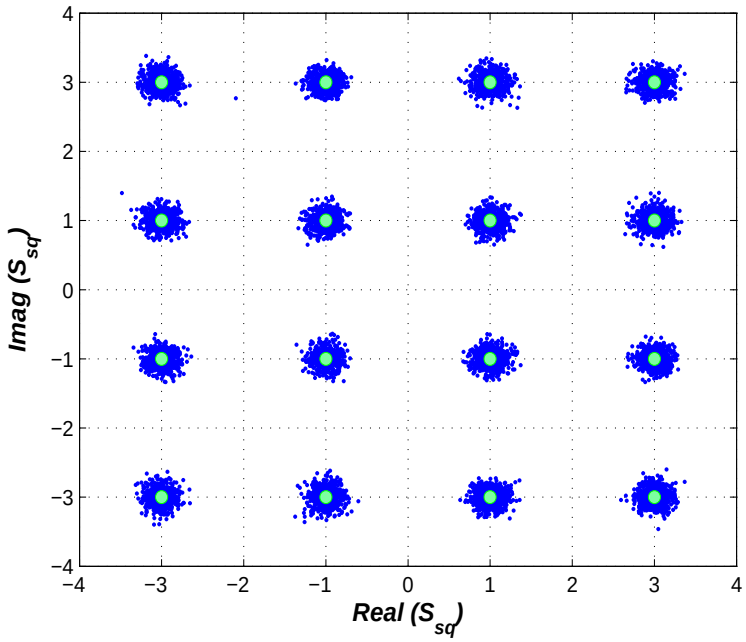

Figure 4.4: Square 16-QAM constellation signals. The green dots are referring to the transmitted symbols while the blue dots are referring to the received symbols.

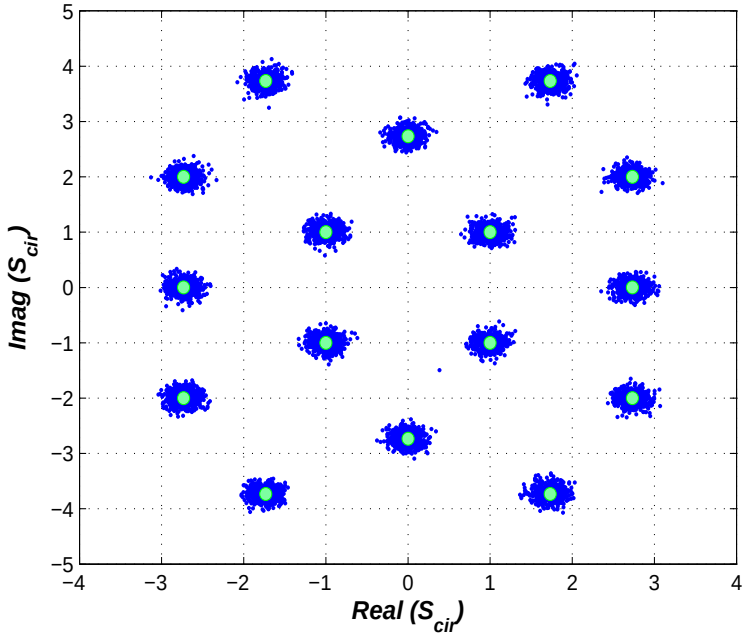

Figure 4.5: Circular 16-QAM constellation signals. The green dots are referring to the transmitted symbols while the blue dots are referring to the received symbols.

4.5.2 Performance in Fourier Based OFDM

Both modulation schemes are applied to Fourier based OFDM with a different number of subcarriers N ranging from 32 to 256. From Fig. 4.6, it can be observed that the circular constellation has performed slightly better than the square, at any particular BER, the circular 16-QAM has out-performed the square by about 1 dB. Our result is correct since the transmitted power for a circular constellation is less than the square constellation. It is interesting to note that the sidelobes of the frequency spectrum become closer to each other as the number of subcarriers increases [108]. This is also the reason for having less errors in performance within different numbers of subcarriers.

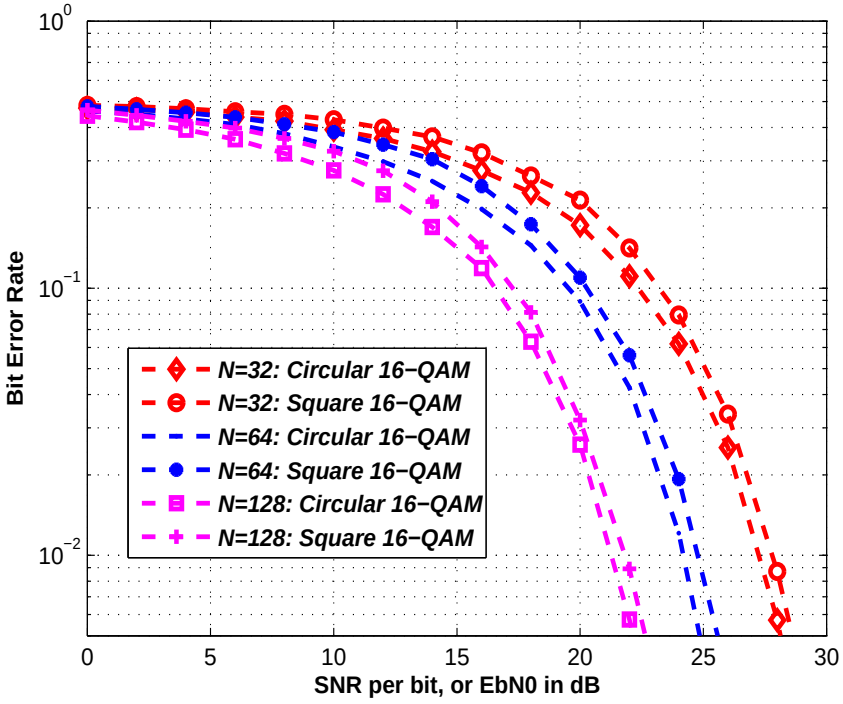

Figure 4.6: BER performance for circular and square 16-QAM in Fourier Based OFDM system using different subcarriers N.

4.5.3 Performance in Wavelet Based OFDM

To simulate the system using wavelet based OFDM, we need to choose the wavelet families satisfying the discrete transform's property since we are using IDWT and DWT as specified in Matlab's Wavelet Toolbox. The wavelet families that satisfies these properties are Daubechies, Coiflets, Biorthogonal and Reverse-Biorthogonal. The results obtained are shown in Figs. 4.7 to 4.10. Overall, the circular 16-QAM constellation has shown slightly better BER performance than the square. Our expectation is correct since the average QAM power of the circular constellation signal is less. The circular scheme for Daubechies and Coiflets' families for the filter length of 3 to 5 respectively is slightly better by about 1 dB at any particular SNR values as shown in Figs. 4.7 and 4.8 accordingly. In addition, the results of Biorthogonal and Reverse-Biorthogonal families are shown in Figs. 4.9 and 4.10. These families obtain slightly less errors when using the circular scheme as compared to when using the square scheme. For example, referring to Fig. 4.9, bior3.3 using circular scheme has less error about 0.01 at SNR of 8 dB. It is also interesting to observe that the reverse-biorthogonal family results are the opposite of the biorthogonal family as shown in Fig. 4.10.

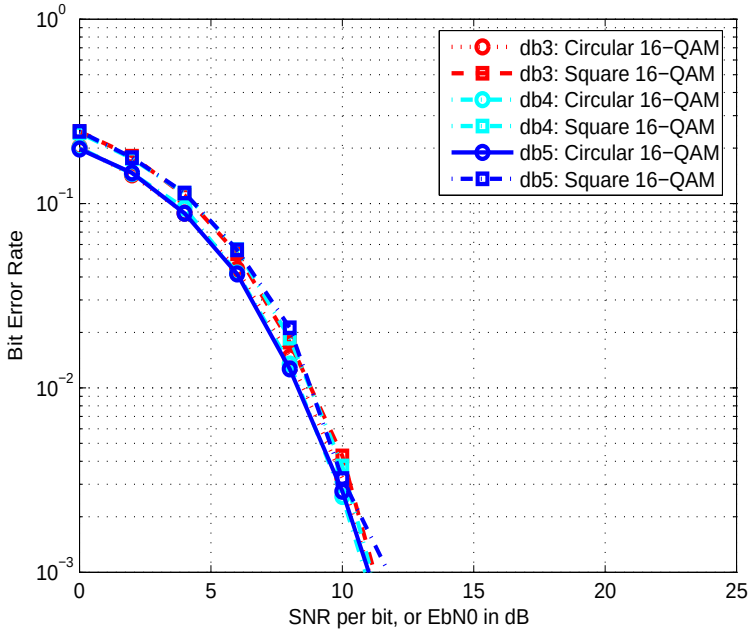

Figure 4.7: BER performance for circular and square 16-QAM in wavelet based OFDM system using Daubechies.

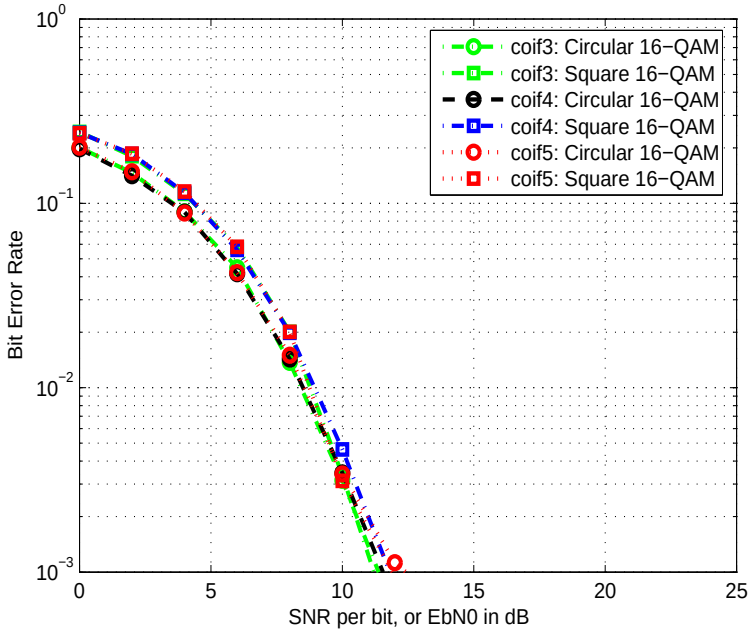

Figure 4.8: BER performance for circular and square 16-QAM in wavelet based OFDM system using Coiflets.

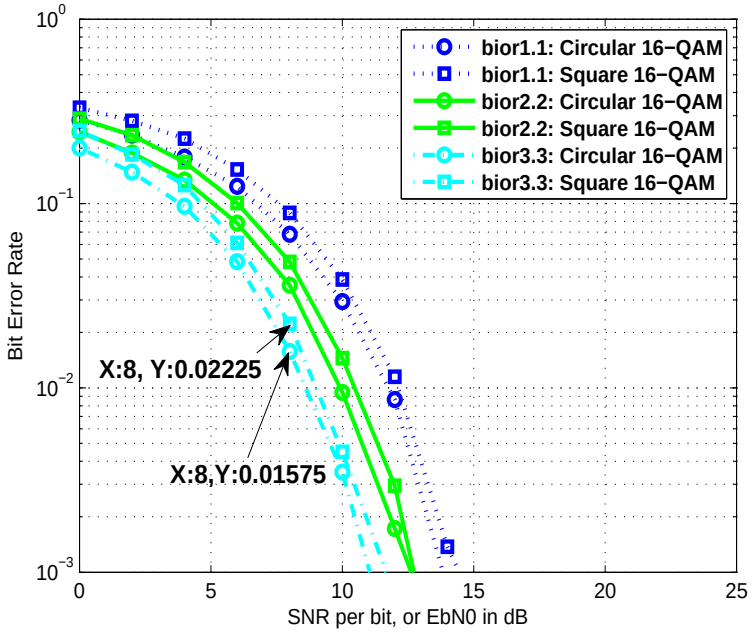

Figure 4.9: BER performance for circular and square 16-QAM in wavelet based OFDM system using Biorthogonal.

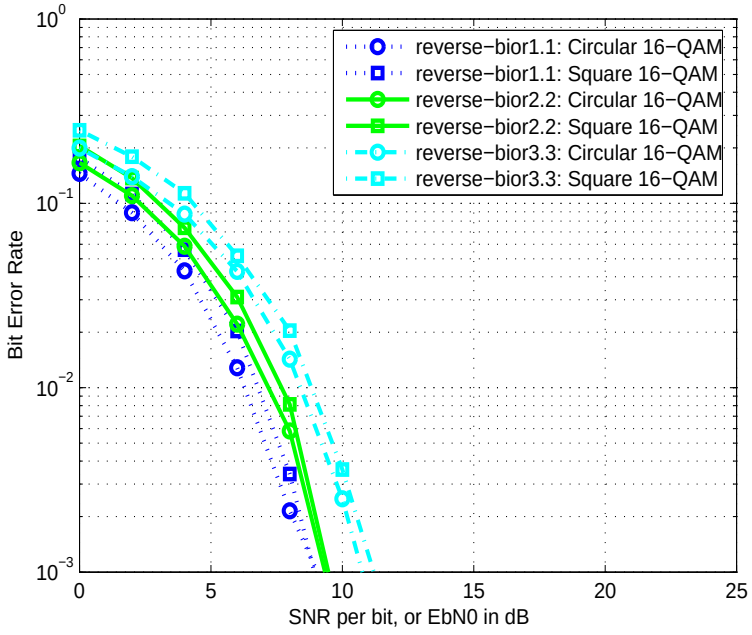

Figure 4.10: BER performance for circular and square 16-QAM in wavelet based OFDM system using Reverse-Biorthogonal.

4.6 Summary

A new approach of closed form BER expression for the circular 16-QAM constellation was derived. The work has been applied to Fourier and wavelet based OFDM systems to compare the two modulation schemes. The average QAM power of the circular 16-QAM is less as compared to the counterpart scheme. In Fourier based OFDM system, the circular scheme showed slightly better BER performance than the square scheme using different number of subcarriers. The results were also obtained for the wavelet based OFDM system using different wavelet families. The error rates showed that the circular 16-QAM was also slightly better compared to the square 16-QAM.

Chapter 5

Narrowband Interference Models and Mitigation Techniques

5.1 Introduction

Interferences can be categorised as narrowband and broadband [96]. This classification can be best described by the sources from where it comes from. Sources of narrowband interference potentially come from other sources with frequency bands below 5MHz [119]. The sources of narrowband interference are produced from intentional transmissions such as radio and TV stations, pager transmitters, and cell phones [96]. [2] indicates the sources are from other unlicensed systems such cordless phones, remote controlled of a garage and baby monitors that share with OFDM spectrum. On the other hand, broadband interference is caused by the devices with a rich harmonic content which interferes over a very broad spectrum, due to this characteristics, the interference spectra is embedded within almost every subcarrier in an OFDM symbol [96]. Because of this characteristic, the receiver will be less effective to filter the interference. Therefore, this dissertation focusses mainly on mitigating the narrowband interference. The broadband interference mitigation may be left for future research.

In the literature, there is considerable amount of work regarding narrowband interference (NBI) in Ultra-Wideband (UWB) system, and, OFDM system is a part of UWB. Because a UWB system ranges in a very wide frequency

band, the NBI may reside within the same band. This NBI may exist at close to the center frequency of any channel of a frequency band. If the power level of the interference higher than the average power level of UWB system, the side lobes of the sinc function of the interference may significantly affect to adjacent frequencies. For example, the UWB system which is assigned the frequency band of 3.1 GHz to 10.6 GHz by the Federal Communications Unions (FCC) has coexisted interferer from an IEEE 802.11a system [81]. This NBI may exist at close to the center frequency of any channel between 5.15 to 5.825 GHz bands, and, it is assumed that it has higher power levels than UWB system.

In this chapter, the NBI models and mitigation techniques are discussed. The narrowband interference effect is studied and its parameters such as the amplitude, frequency, and phase are discussed to observe the interference characteristics. By investigating these parameters or the interference characteristics, the interference can be estimated using a simple mitigation technique. This leads to the proposed suppression algorithm which is discussed in details in next chapter.

This chapter also includes the previous works of mitigation techniques. Various types of mitigation techniques have been introduced in much literatures. Interference suppression for OFDM using pre-coding has been proposed in [22], [16], [77], spread spectrum OFDM [110], [23], post-detection receiver involving equalizers and windowing technique [119]. Other literature reports NBI mitigation techniques for spread spectrum systems [63], [113], [47], including excision-based methods [92], [84], [41], [118]. There are much literatures about interference suppressions, therefore, they can be categorised into three major types; frequency domain cancelation, excision filtering and receiver windowing technique. These types will be discussed in section 5.4.

5.2 System Models

The system model for OFDM system consists of a received signal with an additive white Gaussian noise and narrowband interference at the front OFDM receiver [2], [19], [140]. In general, the system model is shown in Fig. 5.1.

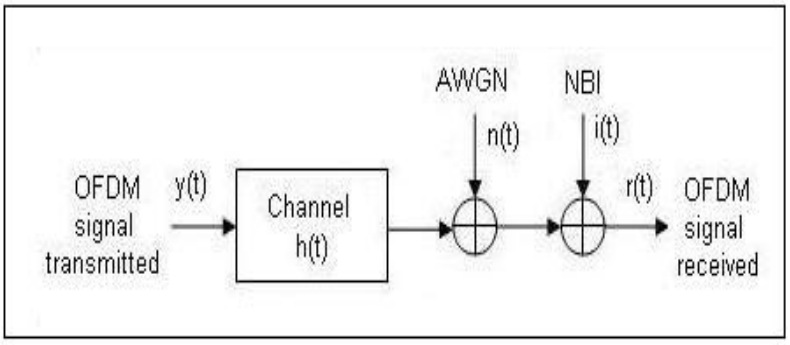

Figure 5.1: The system model showing the presence of NBI component.

The received signal, $r(t)$ can be expressed as follows [2], [19], [140]:

$$r(t) = h(t) * y(t) + i(t) + n(t) \tag{5.1}$$

where $h(t)$ is the channel impulse response, $y(t)$ is the transmitted signal in discrete time domain, $i(t)$ is the narrowband interference and n(t) is an additive white Gaussian noise. [19] presents the narrowband interference by modeling $i(t) = d(t)e^{j\omega_c t+\theta}$ where $d(t)$ is the message signal, ω_c is the carrier frequency and θ is the phase angle. The details about this model will be discussed in next section. Equation (5.1) can also be expressed by having a discrete frequency domain representation after FFT operation as following

$$R_k = H_k Y_k + I_k + N_k \tag{5.2}$$

The signals in (5.1) are time domain, whereas, the signals in (5.2) are frequency domain. The convolution between the channel impulse and the transmitted signal in the time domain is a multiplication between those two signals in the

frequency domain. The research in [19] is aiming to estimate the narrowband interference by subtracting to the left and right of equation (5.2) as following:

$$R_k - I'_k = H_k Y_k + (I_k - I'_k) + N_k \tag{5.3}$$

where I'_k is the estimated narrowband interference.

Another system model is introduced by [2]. He models the interference in different way compared to [19] by introducing the sampled period into the system with time, frequency and phase offsets to indicate the channel dispersion. The model is presented as follows

$$r_n = h(\tau; nT) * y(nT - \tau_s)e^{-j[2\pi f(nT-\tau_s)+\theta]} + \sum_{i=1}^{N} b_i e^{-j[2\pi f_i nT+\theta_i]} + n(nT) \tag{5.4}$$

The channel response $h(\tau; nT)$ having fading channel by indicating time dispersion τ with sample index nT, convolved with the transmitted signal $y(nT)$ which had time offset τ_s, frequency offset f and phase offset θ. The second term in equation (5.4) is the narrowband interference and this will be further discussed in next section. The last term is the additive white Gaussian noise.

The other different system model can be reviewed in [140]. This model indicates the channel dispersion with the sum of complex amplitude α_k for any k^{th} path in the channel impulse response as given by

$$h(\tau) = \sum_{k=0}^{L-1} \alpha_k \delta(\tau - \tau_k) \tag{5.5}$$

5.3 Narrowband Interference Models

The narrowband interference models in OFDM systems have been discussed in much literatures. By performing the study of the narrowband interference model and estimating it at the receiver, analysis and simulation can be less complexity because the NBI parameters such as amplitude, frequency and phases are defined and identified before a process of mitigation is per-

formed. Some literatures include the models (for example, [19]; [2] ; [81]; [119]), whereas, others did not (for example, [66]; [110]).

Zhang et al. present the narrowband interference $i(t)$ by modeling [19]

$$i(t) = d(t)e^{(j\omega_c t+\theta)} = \sum_{i=0}^{q} P_i g(t - i \cdot T_d)e^{(j\omega_c t+\theta)} \tag{5.6}$$

where ω_c is the carrier frequency with initial phase θ and $d(t)$ is a narrowband signal with time domain response of a narrowband filter $g(t)$ having symbol duration T_d and the instantaneous symbol value P_i. The constraint of the q value based on the bandwidth, frequency sampling and subcarrier is concerned because it specify the number of sinusoidal pulse representing the interferer. The matrix calculation to obtain the relationship between i and p in frequency domain before applying the subtraction to estimate the interference in (5.3) is also been demonstrated.

Another study about the model is in [2] and is rewritten as follows

$$I_{k,i} = \sum_{n=0}^{L-1} b_i e^{-j[2\pi f_i nT+\theta_i]} e^{-j2\pi k\frac{n}{L}} = b_i \Psi_k(f_i, \theta_i) \tag{5.7}$$

where

$$\Psi_k(f_i, \theta_i) = e^{-j[\pi(L-1)(\frac{k}{L}+f_i T)+\theta_i]} \frac{\sin \pi L(\frac{k}{L} + f_i T)}{\sin \pi(\frac{k}{L} + f_i T)} \tag{5.8}$$

where L is the number of point of discrete Fourier transform being processed, and $\Psi_k(f_i, \theta_i)$ is the circular sinc function sampled at the centre of the interferer frequency. b_i, f_i and θ_i are the amplitude, phase and frequency of ith of N demodulated narrowband interferers respectively. Note that $\Psi_k(f_i, \theta_i)$ has f_i and θ_i to indicate the frequency and phase effects of the multipath channel for the ith narrowband interferer.

5.4 Mitigation Techniques

Mitigation techniques are tools that are necessary to suppress narrowband interference (NBI) in OFDM systems. In this section, mitigation techniques can be divided generally into three categories [1]; frequency domain cancellation, receiver windowing and excision filtering. Examples of the previous works are discussed in this section followed by the proposed mitigation technique in the next section and chapter.

5.4.1 Frequency Domain Cancelation

Work in [19] performs an estimation of NBI based on the transmitted data and measures it on certain unmodulated subcarriers, then, the subtraction of the estimated disturbance is done in the frequency domain. This is done by introducing the amplitude of the interference which has time varying function based on the sinc function filter to mitigate NBI. The maximum likelihood estimation and narrowband filter with sinc function are determined. Using 16-QAM modulation, the performance analysis is further determined by comparing the ratio of bandwidth of NBI with the overall bandwidth of OFDM signal. The simulation result can be improved if the study performs a comparative analysis of bit error probability for signal noise ratio per bit for different type of modulations.

[105] developes a mitigation technique based on linear minimum mean-square error (LMMSE) which can estimate the spectral leakage by measuring the NBI on a few OFDM subcarriers close to its centre frequency. Using the model of the NBI power spectral density (PSD) as a priori information and the optimal rank reduction to reduce the complexity of the technique, the performance analysis is quite good. This technique uses a model of the NB signal's power spectral density as a priori information. Using a frequency invariant design it is possible to cancel NBI from signals whose frequency locations are changing with significantly reduced complexity overhead. The operational

complexity of the canceler can be lowered by using the theory of optimal rank reduction and using the time-bandwidth product of the narrowband (NB) signal. Compared to [19], the work is more complex and longer duration of simulation because it requires priori information and rank reduction method locating the NBI frequency. Work in [19] only requires maximum likelihood estimation and filtering the NBI with sinc function.

5.4.2 Excision Filtering

An interference suppression technique based on excision (notch) filtering is proposed in [2]. This work is presented to estimate the NBI carrier frequency without the estimation of amplitude and phase [2]. Using signal constellations such as BPSK, the study compares the results under three conditions; when there is interference, when the interference is suppressed by applying his proposed technique and when there is no interference. The obtained results showed an improvement when applying this method. However, the work has limitation in terms of modulation technique since [2] considers only BPSK. The study could have been more variations when considering other modulation scheme such as 4-QAM or 16-QAM.

Another work, which can be categorised as an excision filtering, is the prediction-error filter (PEF) introduced by [1]. The PEF acts an erasure insertion mechanism by inserting erasures via a notch around the tones closest to the interference, while leaving the surrounding tones unaffected. The study has included the work into two conditions; uncoded and coded cases. In the uncoded case, the PEF is shown to mitigate the interference, however, the performance is limited by an irreducible error floor due to the data subcarriers that are notched out. In the coded case, the coding provides a way for recovering the removed subcarriers. This method also has some weakness in terms of number of taps that are required for an optimum NBI suppression, and algorithm complexity due to filtering processing in time domain especially before removal the cyclic prefix at the front receiver.

5.4.3 Receiver Windowing Technique

One example of a receiver windowing mitigation technique can be found in [119]. The use of windowing techniques such as time and frequency windowing techniques are discussed to suppress the interference. A time windowing block is placed before the FFT in the receiver, whereas, a frequency windowing block is performed after the FFT. Time windowing is performed when the received signal is multiplied sample by sample with the window coefficients per symbol duration. Windowing can be implemented equivalently in the time or frequency-domains depending on the window type, computational constraints and convenience of implementation [119]. The goal of the receiver windowing is to enable suppression of the side-lobes of the DFT frequency response and consequently obtain a better performance against crosstalk and NBI while keeping the transmitter unchanged [119]. Frequency windowing is less complex and easier to implement since it deals with the signal in the frequency domain after FFT operation and locating the NBI frequency.

Another example is the work presented in [4]. The technique introduced by [4] uses the receiver windowing samples from the cyclic prefix to construct a window which effects the noise component of the received signal without effecting the data component. The result is that the noise is convolved in frequency with a window which has lower sidelobes than the sinc-like function, which limits the spreading to neighboring subchannels. The study proposes a design algorithm which minimizes the noise power of the demodulated multicarrier signal for DMT system including an OFDM signal. Simulations demonstrate the effectiveness of the windows on a variety of different channels and noise sources. The shape of the designed window is adapted for the observed channel and noise conditions to minimize the mean square error of the equalized signal in the frequency-domain. It is interesting to study this technique because it requires cyclic prefix constructing the window. However, this study does not aware about NBI power level contaminated in the spreading noise. The receiver windowing has been proposed as a computationally efficient technique

for reducing noise spreading, but, it does not consider when NBI presence with high level of power than that of an OFDM spectrum and background noise.

5.4.4 Other Techniques

Other suppression technique is presented by [16]. The study, namely called interference suppression(IS)-OFDM, encodes each transmitted symbol in all frequency bins. Each frequency bin will contain all the transmitted symbols which are distinguished and separated from each other by orthogonal Hadamard sequences. The IS-OFDM can provide a point-to-point wireless link without spreading the incoming data rate.

A method of compensating for the interference signal is also introduced by [110]. This work incorporates a variation of a frequency hopping spread spectrum technique that spreads the interference signal and an additive sinusoidal interference signal. A spread spectrum technique is selected to perform this mitigation technique over other methods (i.e an equaliser) because the sub-channels required are very narrow with an addition that it simplifies the acquisition algorithm.

5.5 Summary

All discussions in this chapter are the overview from other works about narrowband interference in terms of the system models, the NBI models and mitigation techniques. However, previous studies are not aware of other alternative platform of OFDM system which is wavelet based OFDM. Therefore, an interference cancelation algorithm has been proposed to work for both platforms. This mitigation technique is discussed in the next chapter.

Chapter 6

The Proposed Interference Cancelation Algorithm

6.1 Introduction

Literatures about mitigation techniques in the previous chapter are related to the conventional OFDM system without considering DWT-OFDM. Our approach is also to consider interference suppression in wavelet-based OFDM, therefore, we propose an interference cancelation algorithm (ICA) that can be implemented in both Fourier and wavelet-based OFDM systems. To develop and design the proposed mitigation technique, a simple model of NBI, a sinusoidal signal, is considered. A sinusoidal interference which is an unknown signal component is considered to affect both OFDM systems. An interference cancelation algorithm (ICA) is developed to minimise or mitigate that unknown signal. For this problem of study, we propose two situations; an ideal case where the received signal is mixed with a known interference signal, and a non-ideal case where the received signal is contaminated with an unknown interference signal. The reason of having these two cases is to follow the guide lines by [129] about the performance evaluation requiring the test observation (non-ideal) and comparing to the desired observation (ideal). Performance results are obtained to observe both cases. This chapter is organised as follows. The proposed NBI model and the NBI effects using that model are presented in sections 6.2 and 6.3 respectively. The system model for the ICA, followed

by the description of it in both OFDM schemes are discussed in sections 6.5 and 6.5. Then, performances of BER results are obtained at the end of this chapter considering both cases, ideal and non-ideal.

6.2 The Proposed Model

The baseband signal component, $i(n)$ can be modeled as follows:

$$i(n) = A\sin(2\pi f\frac{n}{N} + \phi) \tag{6.1}$$

where A, f and ϕ are the amplitude, frequency and phase of the signal respectively, and the discrete-time signal $i(n)$ has n samples with N sub-carriers. The model in equation 6.3 is relatively simple and requires little complex mathematics to extract and minimize the interference signal. Previously, a very similar model was used in [49], [68], and [125]. The work in [68], however, included multiple parameters indicated by the subscript i in A_i, f_i and ϕ_i and there was no indication that this model was used for OFDM systems. On the other hand, in [49] the similar model was used without parameter ϕ for a direct-sequence spread spectrum system. A similar model as in (6.1) is used in [125] but it was also no indication for OFDM systems as well.

6.3 NBI Effect using the Proposed Model

As shown in Fig.5.1, the system block diagram shows the effect of NBI. The received OFDM signals, , $r(t)$, is the results of the transmitted OFDM signal $y(t)$ together with AWGN, $n(t)$ and NBI, $i(t)$. In this proposed system, we assume that the NBI is a single sinusoidal signal and it is uncorrelated to AWGN and OFDM signal. The NBI model is discussed in the previous section. The simulation plots showing this effect can be found in Figs. 6.1, 6.2 and 6.3 respectively. When there is NBI presence, the receiver decodes incorrectly the received bit due to the NBI parameters such as its frequency that offsets the

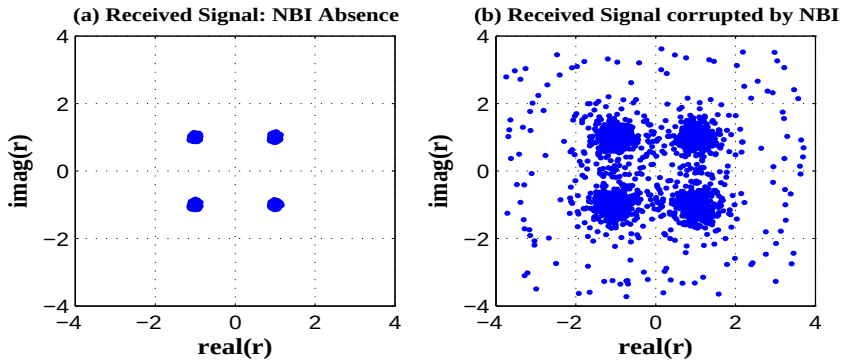

Figure 6.1: NBI effect when the system use 4-QAM.

carrier frequency, and its phase. This condition becomes worst when the power level of NBI is higher than the transmitted average power of the OFDM signal and the background noise power. The BER as a function of SNR to observe the performance of the OFDM system with the effect of the NBI presence is shown in Fig. 6.4. It is shown that the OFDM system of BER performance becomes degraded when NBI is present for 4-QAM, 16-QAM and 64-QAM modulation schemes. Specifically, the performance is degraded because the OFDM system required 6 dB of SNR per bit to achieve about 0.04 of BER using 4-QAM. However, the performance is better when NBI is absent because it required less SNR per bit, about 2 dB to achieve the same BER target, which is 0.04, using the same modulation system.

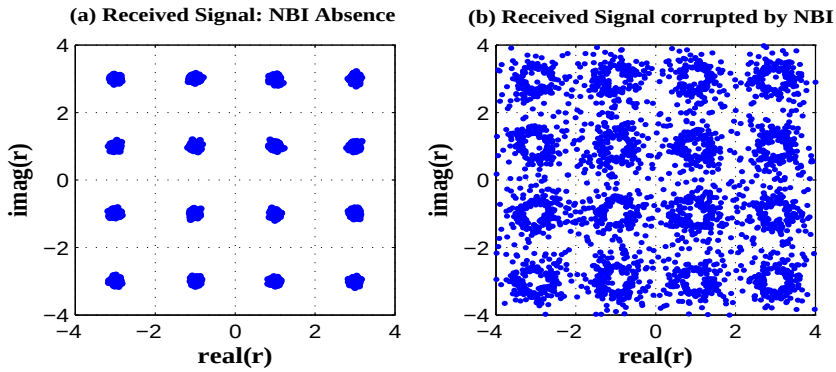

Figure 6.2: NBI effect when the system use 16-QAM.

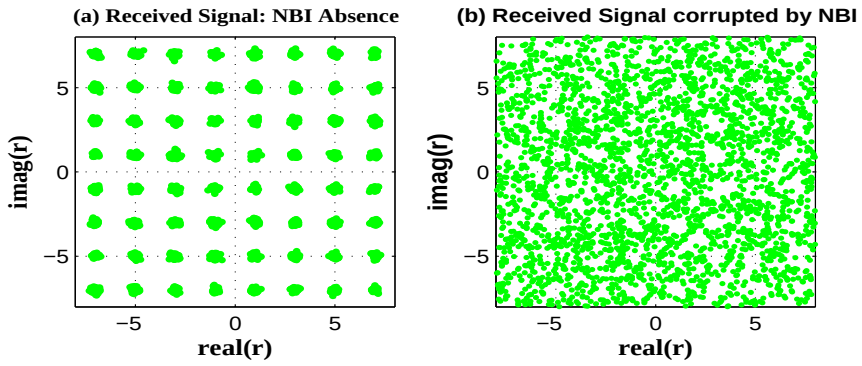

Figure 6.3: NBI effect when the system use 64-QAM.

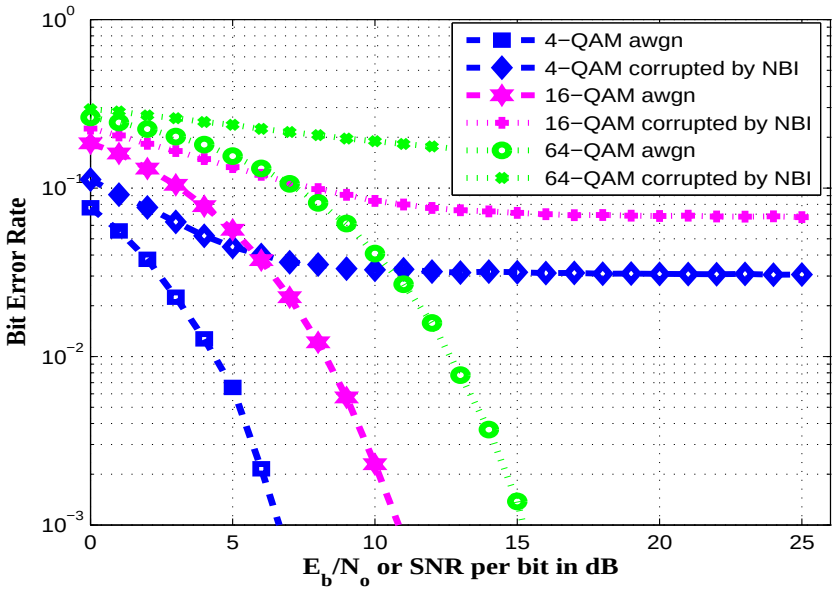

Figure 6.4: BER performance due to NBI effects in different QAM schemes.

6.4 System Model with ICA

A typical OFDM transmitter was discussed in Sections 2.3 and 3.3. In this chapter, we also include an ICA component before the signal is processed by the FFT/DWT block. This is shown in Fig. 6.5.

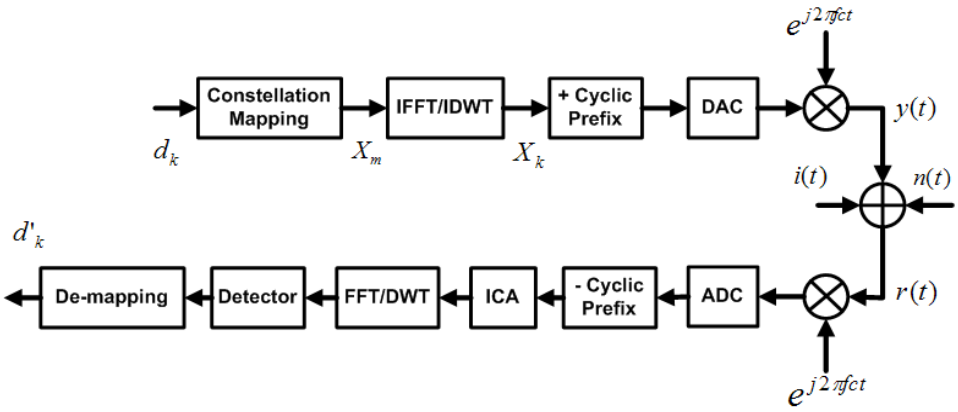

Figure 6.5: A Typical model of an OFDM transceiver with an insertion on the proposed ICA [56].

A discrete-time domain baseband signal at the front-end of the receiver can be modeled as follows:

$$y(n) = r(n) + g(n) + i(n) \tag{6.2}$$

where $y(n)$ is the received OFDM signal in the discrete time domain and consists of the OFDM transmitted signal $r(n)$ corrupted with additive white Gaussian noise $g(n)$ and an unwanted sinusoidal signal, $i(n)$. Note that $g(n)$ is used in (6.2) instead of $n(n)$ to avoid confusion term in other equations representing discrete time signal. We assume that the sinusoidal signal, $i(n)$, is the dominant part that corrupts the OFDM signal. The baseband signal component, $i(n)$, is modeled as follows:

$$i(n) = A\sin(2\pi f\frac{n}{N} + \phi) \tag{6.3}$$

where A, f and ϕ are the amplitude, frequency and phase of the signal respectively, and the discrete-time signal $i(n)$ has n samples with N sub-carriers. The model in equation (6.3) is relatively simple and requires little complex mathematics to extract and minimize the interference signal. Previously, a very similar model was used in [49], [68], and [125]. The work in [68], however, included multiple parameters indicated by the subscript i in A_i, f_i and ϕ_i and there was no indication that this model was used for OFDM systems. On the other hand, in [49] the similar model was used without parameter ϕ for a direct-sequence spread spectrum system. A similar model as in (6.3) is used in [125] but it was also no indication for OFDM systems as well.

6.5 The ICA in Fourier-Based and Wavelet-Based OFDM

When the system receives the signal, $y(n)$, all three components in (6.2) are serial signals. If Fourier-based OFDM is implemented then the signal will also

comprise of a Cyclic Prefix (CP) which will inevitably need to be removed before further processing [55], [88], [118].

At this point the serial data is passed into the ICA block where the main task is to isolate the unknown signal component, $i(n)$, corrupting the data stream. A flow-chart of the proposed ICA algorithm used in this work is detailed in Fig. 6.6.

Before the ICA can perform the task of detecting the unknown signal component, all the variables such as the length of the test signal, k, the error signal, e, the error squared, $\overline{e}^2$ and the mean-squared error, E have to be initialized. Next the ICA will call the testing signals consisting of the estimating parameters $\widehat{A}$, $\widehat{f}$ and $\widehat{\phi}$ as follows:

$$\widehat{i}_{test}(n) = [\widehat{A}_{test}]\sin(2\pi[\widehat{f}_{test}]\frac{n}{N} + [\widehat{\phi}_{test}]) \tag{6.4}$$

where $\widehat{A}_{test} = [\widehat{A}_{k=1:K}]$, $\widehat{f}_{test} = [\widehat{f}_{k=1:K}]$ and $\widehat{\phi}_{test} = [\widehat{\phi}_{k=1:K}]$, and K is chosen to have an odd number greater or equal to 3. For a better understanding, we can further describe the process by expanding (6.4) as follows:

$$\widehat{i}_{test}(n) = [\widehat{A}_{est} \in \widehat{A}_1, \widehat{A}_2, ..., \widehat{A}_K]\sin(2\pi[\widehat{f}_{test}]\frac{n}{N} + [\widehat{\phi}_{test}]) \tag{6.5}$$

where $\widehat{A}_{est}$ is the desired amplitude estimated by $\widehat{A}_{test}$. After the processing and detection in (6.5), the ICA will continue to detect the frequency, the equation will then be updated to:

$$\widehat{i}_{test}(n) = [\widehat{A}_{est}]\sin(2\pi[\widehat{f}_{est} \in \widehat{f}_1, \widehat{f}_2, ..., \widehat{f}_K]\frac{n}{N} + [\widehat{\phi}_{test}]) \tag{6.6}$$

where $\widehat{f}_{est}$ is the desired frequency estimated by $\widehat{f}_{test}$.

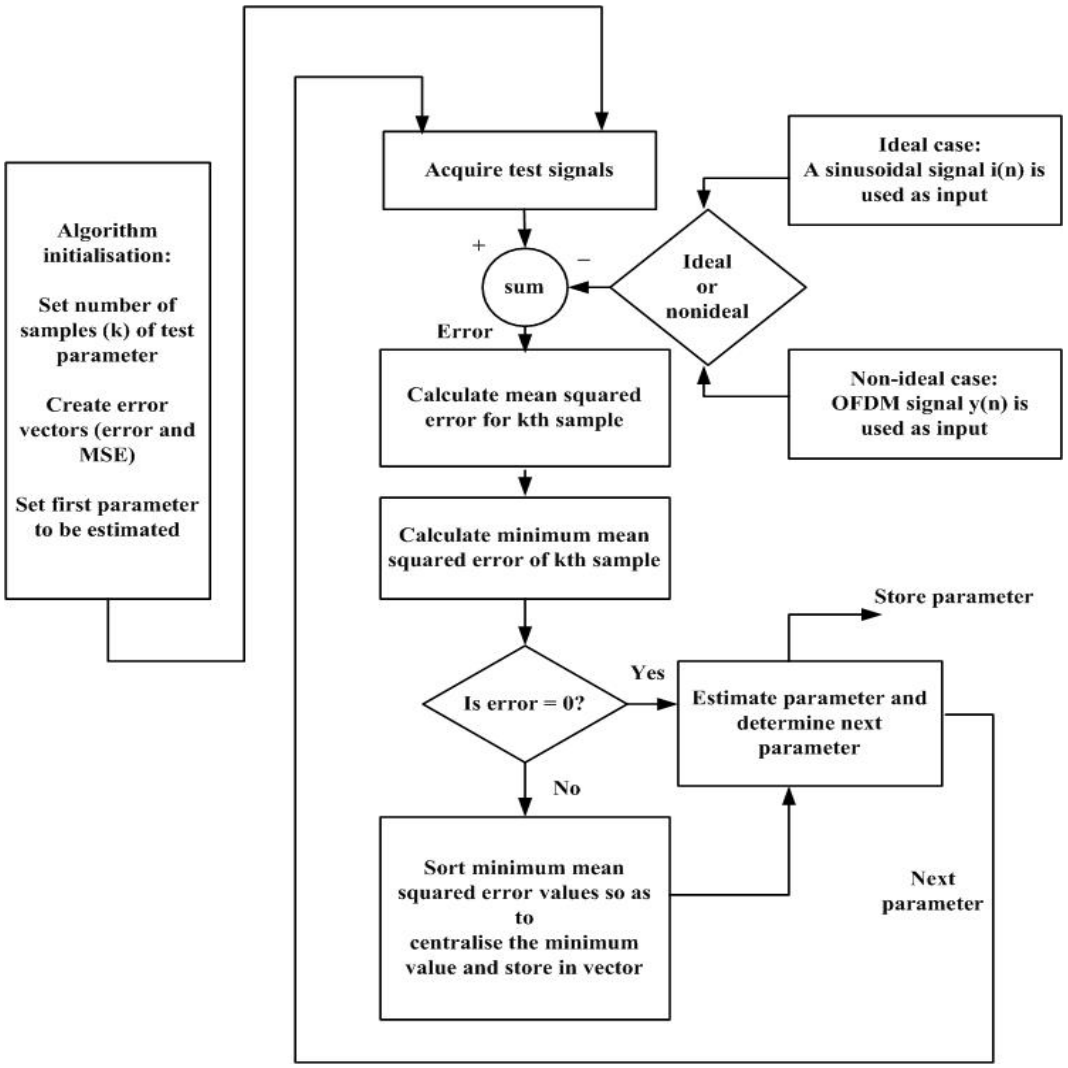

Figure 6.6: The proposed Interference Cancelation Algorithm (ICA).

Next the ICA will update the task to get the estimations $\widehat{A}_{est}$ and $\widehat{f}_{est}$, it will then proceed to estimate the last parameter, $\widehat{\phi}_{est}$. We will then have the following equation:

$$\widehat{i}_{test}(n) = [\widehat{A}_{est}]\sin(2\pi[\widehat{f}_{est}]\frac{n}{N} + [\widehat{\phi}_{est} \in \widehat{\phi}_1, \widehat{\phi}_2, ..., \widehat{\phi}_K]) \tag{6.7}$$

The ICA will finalize the estimated interference signal having all estimated

parameters as follows

$$\widehat{i}_{test}(n) = [\widehat{A}_{est}]\sin(2\pi[\widehat{f}_{est}]\frac{n}{N} + [\widehat{\phi}_{est}]) \tag{6.8}$$

Sections 6.5.1 and 6.5.2 will describe how the ICA takes different steps to obtain (6.8) for both ideal and non-ideal cases.

6.5.1 Ideal Case

The ideal case occurs when the interference model $i(n)$ in equation (6.3) is used to subtract the testing signals. The purpose of this is to obtain a reference measurement to evaluate the performance of the ICA in a practical situation. The result of the subtraction of (6.3) and (6.5) will be:

$$\widehat{e}(n) = i(n) - \widehat{i}_{test}(n) \tag{6.9}$$

Note that (6.9) obeys the Bayes performance measure as indicated in [65]. Equation (6.9) can also be expressed as

$$\widehat{e}(n) = [A - \widehat{A}_{test}]\sin(2\pi[\widehat{f}_{test}]\frac{n}{N} + [\widehat{\phi}_{test}]) \tag{6.10}$$

$$\widehat{e}(n) = [A - \widehat{A}_{est} \in \chi]\sin(2\pi[\widehat{f}_{test}]\frac{n}{N} + [\widehat{\phi}_{test}]) \tag{6.11}$$

where $\chi = [\langle A - \widehat{A}_1\rangle, \langle A - \widehat{A}_2\rangle, ..., \langle A - \widehat{A}_K\rangle]$. Taking the mean square error of (6.11) yields:

$$E[\widehat{e}^2(n)] = \{ \begin{smallmatrix} 0, & if\ A{=}\widehat{A}_{est} \\ \varepsilon, & if\ A{\neq}\widehat{A}_{est} \end{smallmatrix} \tag{6.12}$$

where ε is the residue of the subtraction in (6.11).

Referring to Fig. 6.6 it can be seen that the ICA is a mostly iterative algorithm that continues to loop while $E = \varepsilon$, as soon as the case occurs where $E = 0$ the ICA will stop the loop and store the result of the amplitude parameter estimation $\widehat{A}_{est}$, it will then look for the next desired parameter to be estimated and this, in turn, will re-initialise the loop. This same process

will be repeated to estimate all the desired parameters in the signal.

At the end of the algorithm $\widehat{A}_{est}$, $\widehat{f}_{est}$ and $\widehat{\phi}_{est}$ will be detected and stored. The results will then be passed into the demodulation block and a final error is calculated.

6.5.2 Non-Ideal Case

For the non-ideal case, we consider $y(n)$ (a received OFDM signal with cyclic prefix removed) as the input to the ICA. The reason it is called non-ideal is because it uses the received signal as the input to the ICA instead of $i(n)$. This is again illustrated in Fig. 6.6. In this non-ideal case, the equations from (6.4) to (6.8) are repeated as previously described, however, (6.9) is required to be changed to $\widehat{e}(n) = y(n) - \widehat{i}_{test}(n)$. Basically from now the same mathematical equations discussed in Section 6.5.1 can be used. $\widehat{e}(n)$ can be rewritten as:

$$\widehat{e}(n) = [\zeta + i(n) - \widehat{A}_{test}]\sin(2\pi[\widehat{f}_{test}]\frac{n}{N} + [\widehat{\phi}_{test}]) \tag{6.13}$$

Since we are interested in cancelling out $i(n)$, (6.13) can be expanded to:

$$\widehat{e}(n) = [\zeta + \langle A - \widehat{A}_{test}\rangle \in \chi]\sin(2\pi[\widehat{f}_{test}]\frac{n}{N} + [\widehat{\phi}_{test}]) \tag{6.14}$$

where, $\chi = [\langle A - \widehat{A}_1\rangle, \langle A - \widehat{A}_2\rangle, ..., \langle A - \widehat{A}_K\rangle]$. Then taking the mean square error of (6.14) yields:

$$E[\widehat{e}^2(n)] = \{\overline{\sigma}, \widehat{A}_{est} \in [\langle A - \widehat{A}_1\rangle, \langle A - \widehat{A}_2\rangle, ..., \langle A - \widehat{A}_K\rangle] \tag{6.15}$$

where $\overline{\sigma} = min(E[\widehat{e}^2(n)])$ and $\overline{\sigma}$ are complex.

For simplicity, the ICA will sort the elements of $\overline{\sigma}$ and arrange its minimum value into the mid-index location. It can be assumed that the actual parameters are approximately in the mid-index location of the testing parameter range since K is assumed to be odd, the ICA will determine the estimated parameter based on the index corresponding to the minimum value in the mid-index

location. Again as discussed in Section 6.5.1 the ICA will determine $\widehat{A}_{est}$, $\widehat{f}_{est}$ and $\widehat{\phi}_{est}$ and store them before passing them to the FFT or DWT block.

6.6 Performance of the ICA

For this performance simulation, the results are obtained from the ideal and non-ideal cases. MATLAB was used to perform the simulation. All the OFDM parameters were simulated according to the values indicated in Table 3.2 in section 3.4 considering FFT-OFDM and DWT-OFDM for Fourier and wavelet based OFDM respectively in each case.

6.6.1 The Ideal Case

Figure 6.7 shows the performance for an ideal case. This shows that wavelet-based OFDM outperforms Fourier-based OFDM. This again can be seen in the case of SNR = 5 dB where an error of 0.01812 was obtained for wavelet-OFDM and 0.03277 for the Fourier-OFDM. As SNR increases, the wavelet-OFDM continues to outperform Fourier-based OFDM. This was true since the input for the subtraction from the acquired test signals was the sinusoidal interference itself. Because of this, the minimum mean square error (MMSE) obtained would be zero.

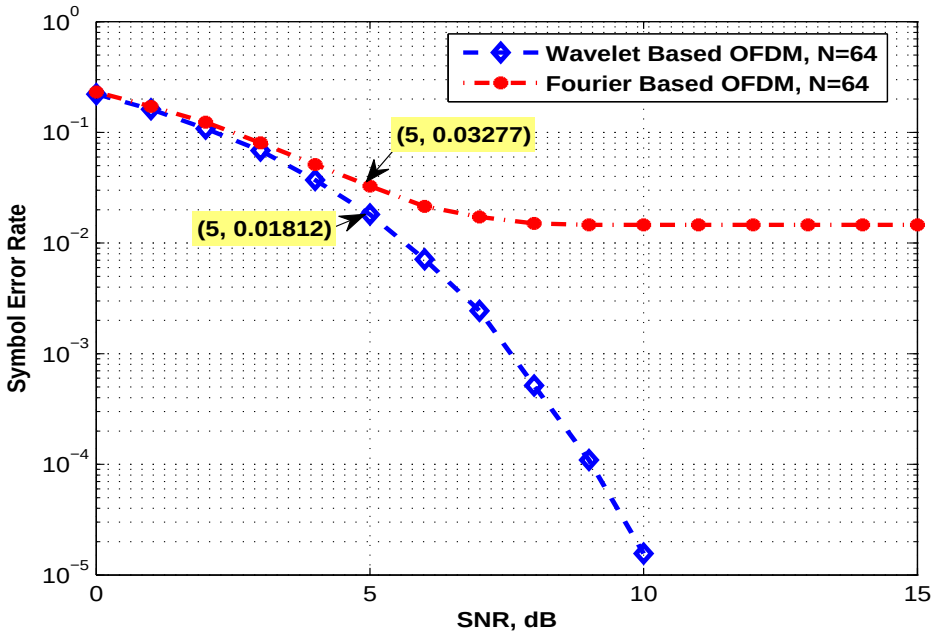

Figure 6.7: Performance of Fourier- and wavelet-based OFDM: the ideal case.

6.6.2 The Non-Ideal Case

For the non-ideal case, we assume that all testing parameters are positive. This is important since our interference model is a sine wave which is an odd function. We also assume that the number of samples are odd. This is because the ICA performs the task of sorting and centralising the minimum value after determining MMSE. Figure 6.8 shows the performance of the non-ideal case. In this case, the wavelet-based OFDM has also outperformed Fourier-based OFDM. At SNR = 5 dB, an error of 0.01817 was obtained as compared to 0.03167. The difference of about 1.35 % was due to the fact that the wavelet transform has the property as described in the previous section. The system also shows that the ideal and non-ideal cases have approximately the same curve. This means that the proposed ICA algorithm has a good performance.

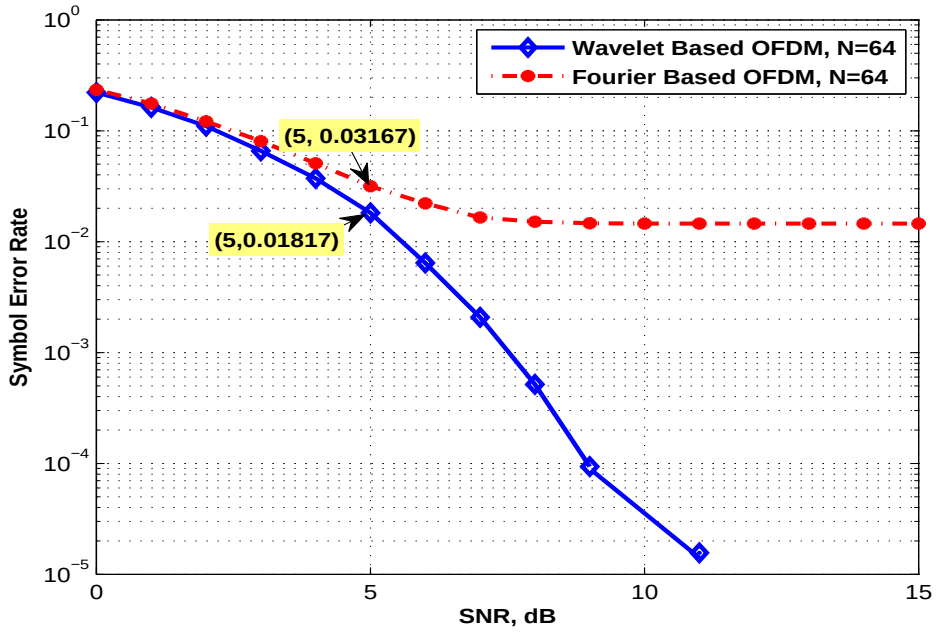

Figure 6.8: Performance of Fourier- and wavelet-based OFDM: the non-ideal case.

6.7 Summary

We proposed an interference cancelation algorithm (ICA) that has shown outstanding performance for both ideal and non-ideal system cases where it reached almost the same error. A sinusoidal interfering signal was considered. In addition, the wavelet-based OFDM outperformed Fourier-based OFDM in both cases. This chapter considers an estimation of a single type of interference. Future work may include the model described in this work and may consider multiple interferences as mentioned in the work in [6].

Chapter 7

Impulsive Noise Interference effects in OFDM Systems

7.1 Introduction

In general, the definition of impulsive noise is a random burst of noise [46]. Another term that can be used for impulsive noise is short burst [53] and occurs randomly over a period of time. Compared to Gaussian noise, this noise is mainly due to man-made and/or atmospheric-made noise [111]. This term is also being defined in [18] and it is a natural electromagnetic interference and highly non-Gaussian random processes. This man-made noise interference can be classified into three major types [18]:

1. Class A interference: This noise is typically narrower spectrally than the receiver's front-end bandwidth when a source emission terminates. This type is described by a 3-parameter model; the impulsive index, the ratio of the intensity between Gaussian and non-Gaussian components, and the intensity of impulsive (non-Gaussian) component.
2. Class B Interference: This type requires a more extensive analytical model. Here the bandwidth of the incoming noise is larger than that of the receiver's front-end stages, so that transient effects, both in the build-up and decay, occur, with the latter predominating. The receiver is to varying degrees "shock-excited," particularly for inputs of very short duration, so that the receiver is said to "ring." (broad band vis-

a-vis the receiver), Class B noise is described by a 6-parameter model which are including the 3-parameters in class A with another 3 additional parameters; the effective impulsive index, the spatial density-propagation parameter and the scaling factor for correcting the mean square error envelope of the class B impulsive component.

3. Class C Interference: This is the sum of Class A and Class B interference.

Details for each type can be found in [18]. The purpose of presenting the above category is to see that our impulsive noise interference is laid in the first type. The reason is that the class A interference type, or, a Middleton Class A is a statistical-physical impulse noise model [25]. Its occurrence has approximately a Poisson distribution, which means the arrival of the impulsive noise follows the Poisson process with a rate of units per second, so that the event of arrivals in seconds has the probability distribution which follows the equations of (3) in [25], and (6) in [135].

In discrete time the Bernoulli-Gaussian impulse noise model is used as an equivalent to the continuous-time model of Poisson distribution of arriving delta functions with random area distributed according to the Rayleigh probability density function.

A recent work has focussed on the effect of impulsive noise when wavelet packet division multiplexing (WPDM) is used [62]. Some discussions are related to the performance comparison between OFDM and time division multiplexing (TDM), however, there is no indication of a comparative study of performance using DWT and WPT as an alternative to FFT. Although the studies in [135] provide strong analysis of impulsive noise and its effect on the performance of OFDM system, its purpose is for the specific area of power line communications (PLC). Characteristic of impulsive noise in time and frequency domain analysis is studied in [87], but, the study also applied for PLC. To the best of the authors' knowledge, there is no work showing the steps of how to simulate flexible transformed models of DWT- and WPT-OFDM

as alternative replacements of FFT-OFDM under the effect of impulse noise. This chapter is divided into two main sections: section 7.2 discusses the impulse noise effects on the OFDM system, section 7.3 presents the flexibility models of FFT-, DWT- and WPT-OFDM, and section 7.4 obtains the results for the bit error rate (BER) performance considering two different scenarios of impulse noise effects.

7.2 Impulsive Noise Interference Model

The effect of impulsive noise on OFDM systems has been discussed in many literatures [62], [75], [87], [135]. In this section, we describe the general principles of impulse noise when it affects an OFDM system. We also mention the recurrence parameter of Poisson distribution which will affect the system performance. Let y_k be the transmitted signal, then the received signal can be written as follows

$$r_k = y_k + g_k \qquad k = 0, 1, 2, ...L-1 \tag{7.1}$$

where g_k is the noise consisting of AWGN and impulsive noise, and is given by

$$g_k = w_k + i_k \tag{7.2}$$

where w_k is the additive Gaussian process with mean zero and variance σ_w^2 and i_k can be expressed as

$$i_k = \beta_k z_k \tag{7.3}$$

In this case, β_k is the Poisson process indicating the arrival of impulsive noise and z_k is the white Gaussian process with mean 0 and variance σ_z^2. It is generally assumed that σ_z^2 is much larger than σ_w^2. Note that the impulsive noise having variance σ_z^2 amplitude occurs during the length of L samples. The occurrence of the impulsive noise generally follows the Poisson distribution of

a random variable X and can be expressed as [135]

$$P(k) = P(X = k) = \exp[-a(\frac{a^k}{k!})] \qquad k = 0, 1, 2, ..., L-1 \qquad (7.4)$$

where a is the Poisson parameter which is the average value of Poisson random variables. A general illustration of relationship between impulse noise interference, OFDM received symbol and AWGN can be found in Fig. 7.1.

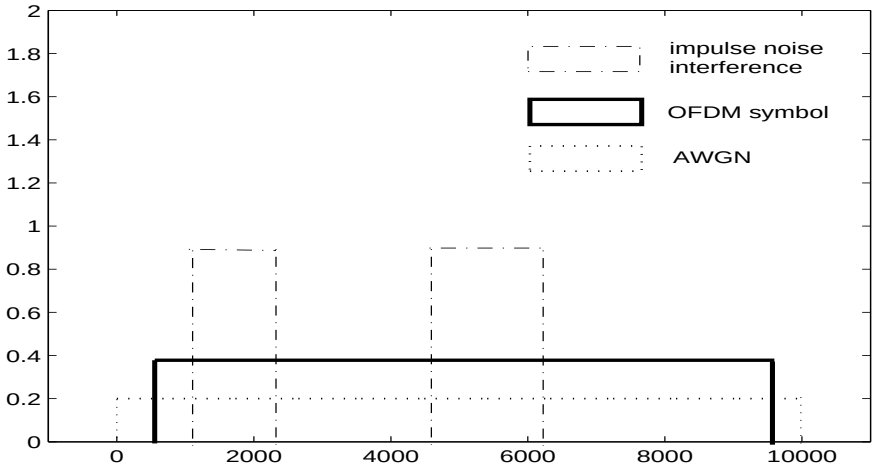

Figure 7.1: General relationship, impulse noise interference, OFDM symbol and AWGN [135].

7.3 Flexibility Transformed Models

The flexibility transformed models in this section is referred to the components, namely inverse transform and forward transform, in the transmitter and receiver of the block diagram of Fig. 2.3. The inverse and forward block transforms are flexible and can be substituted with FFT-, DWT- or Wavelet Packet (WPT)-OFDM [57]. The three transformed platform has been discussed in chapter 2 and 3. It is interesting to observe in [57] that the authors show the works on how to simulate flexible transformed models of DWT- and WPTOFDM as alternative replacements of FFT-OFDM under the effect of

impulse noise. The detail of each model, either DWT-OFDM or WPT-OFDM is discussed in section 3.3.1 and section 3.3.2 accordingly. The models are also described and shown in Figs. 3.6 and 3.8 respectively. The MATLAB commands for each model has also been provided in those sections. However, FFT-OFDM model and block diagram are not discussed because they are available in much literatures.

7.4 Experimental Results and Discussion

All of the transformed models in FFT-,DWT- and WPT-OFDM systems use the parameters as shown in Table 7.1. The number of samples for the subcarriers N is 64, and the number of samples for the symbols ns is 1000. Other variables are listed according to their use as a flexible model platform, either a FFT-, DWT- or WPT-OFDM.

Table 7.1: Simulation variables and their matrix values.

	FFT-OFDM	**DWT-OFDM**	**WPT-OFDM**
Variables	**Matrix Values**	**Matrix Values**	**Matrix Values**
N	64	64	64
ns	1000	1000	1000
CP	8	0	0
wv	-	bior5.5	bior5.5
d $(N \times ns)$	64×1000	64×1000	64×1000
$X_m(N \times ns)$	64×1000	64×1000	64×1000
xx	1×64000	1×64000	1×64000
X_k	64000×1	128000×1	64000×1
U_k	64000×1	128000×1	64000×1
uu	1×64000	1×64000	1×64000
U_m $(N \times ns)$	64×1000	64×1000	64×1000
$d^{'}$ $(N \times ns)$	64×1000	64×1000	64×1000

The signal-to-noise ratio (SNR) for all the simulations is determined as

$$SNR = \frac{P_x}{P_n} = \frac{P_x}{\sigma_w^2 + P_i} \tag{7.5}$$

where P_x is the mean power of the transmitted OFDM signal, σ_w^2 is the mean power of the Gaussian noise and P_i is the mean impulsive noise power. The ratio r between P_i and σ_w^2 is defined as $r = P_i/\sigma_w^2$. Since the impulsive noise follows the Poisson distribution in timing, the equation (7.5) can be rewritten as

$$SNR = \frac{P_x}{P_n} = \frac{P_x}{\sigma_w^2 + \frac{1}{a}\sigma_z^2} \tag{7.6}$$

where a is the Poisson parameter as indicated in equation (7.4) or it is the average value for Poisson random variables occurring during $L = N \times ns$ length of samples. In our simulation, we are interested in varying the values of a with the value of $r = 10$. When a is small, the received OFDM signal r_k has many impulsive noise samples as compared to when a is large. Examples of typical samples of the received OFDM signals having different a small value (i.e. $a = 5$) and a large value (i.e. $a = 50$) are shown in Figs. 7.2 and 7.3. We have divided this section in two parts; scenario I: $a = 5$ and $r = 10$, and scenario II: $a = 50$ and $r = 10$. Note that the value of r, which is the ratio value of P_i over P_n, is not varied because it will not make much impact on the BER results even though the three platforms are different. On the other hand, a will have a significant impact on performance since it is related to the exponential function as indicated in equation (7.4).

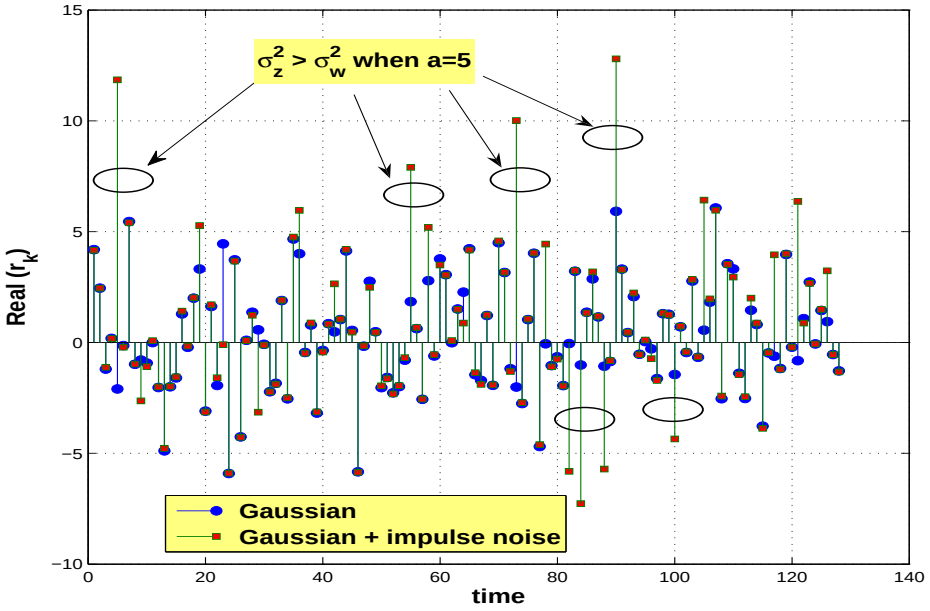

Figure 7.2: Sequence Samples of two OFDM symbols with impulsive noise effect when $a = 5$.

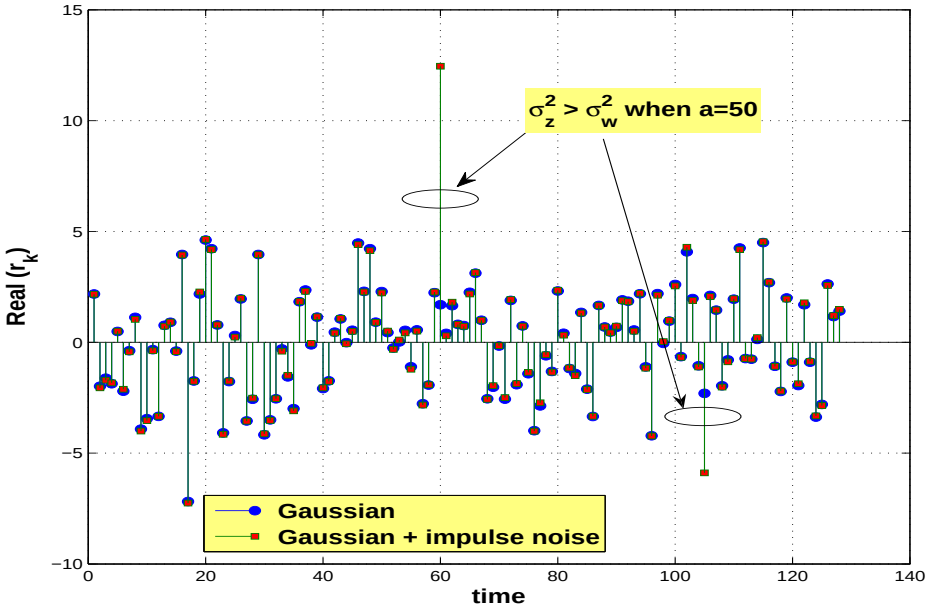

Figure 7.3: Sequence Samples of two OFDM symbols with impulsive noise effect when $a = 50$.

7.4.1 Results: Scenario I

Fig. 7.4 shows the results of Scenario I when $a = 5$ and $r = 10$ for all platforms. This condition can be referred to as heavily disturbed since the system has more frequent impulsive noise peaks as indicated in Fig. 7.2. It is interesting to see that WPT-OFDM signal shows minimal BER when there is no impulse noise; also when the impulse noise is present. At SNR of 20 dB, the BER of WPT-OFDM is about 0.07 as compared to 0.1 and 0.18 of DWT and FFT-OFDM respectively when there is impulse noise ($\sigma_z^2 >>> \sigma_w^2$). This also means that WPT-OFDM produces about 3 and 11 % less errors in the OFDM received samples as compared to DWT- and FFT-OFDM respectively. This is due to the fact that the wavelet packet tree produces wavelet basis functions at the terminal of level 3 having about the same basis functions at the same terminal as in the transmitter satisfying the perfect reconstruction and orthonormal bases properties. The DWT-OFDM also satisfies those properties when it deals with the LPF and HPF coefficients in the transmitter and receiver. However, the WPT-OFDM has the characteristics of forming the tree structure of wavelet basis function which is the result of the splitting process of scaling and wavelet coefficients corresponding to the LPF and HPF coefficients as discussed in section 3.3.2.

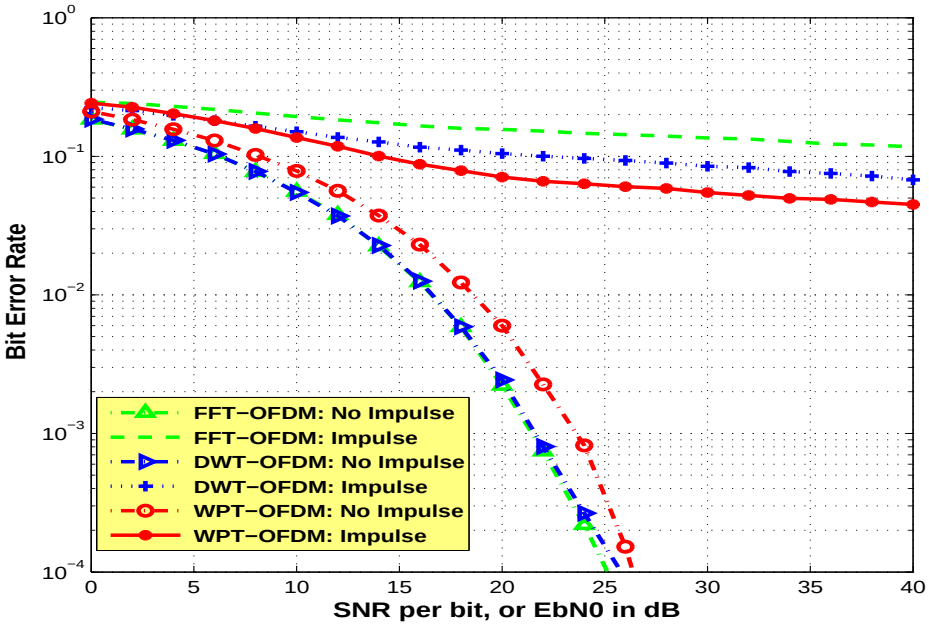

Figure 7.4: BER performance of Scenario 1 for all the three transforms when $a = 5$ and $r = 10$.

7.4.2 Results: Scenario II

The results of Scenario II when $a = 50$ and $r = 10$ for all platforms are shown in Fig. 7.5. In this scenario, the condition of impulsive noise effect has less impact since the value of a is large as illustrated in Fig. 7.3. It is shown that WPT-OFDM is superior to all as discussed in the previous section. To be specific, the BER of WPT-OFDM is about 0.015 as compared to 0.03 and 0.1 of DWT and FFT-OFDM respectively at SNR of 20 dB in the presence of impulse noise. This also shows that the WPT obtain about 1.5 % and 8.5 % less errors of the OFDM received samples as compared to DWT and FFT platforms respectively. Comparing the BER of Scenarios I and II, we can point out that the performance for this section is better since it obtained the result of 0.015 as compared to 0.07 in Scenario I within the same SNR value. This shows that our results match with the values of a as discussed in section 7.2 because the effect of the impulsive noise is less when the value of a is large.

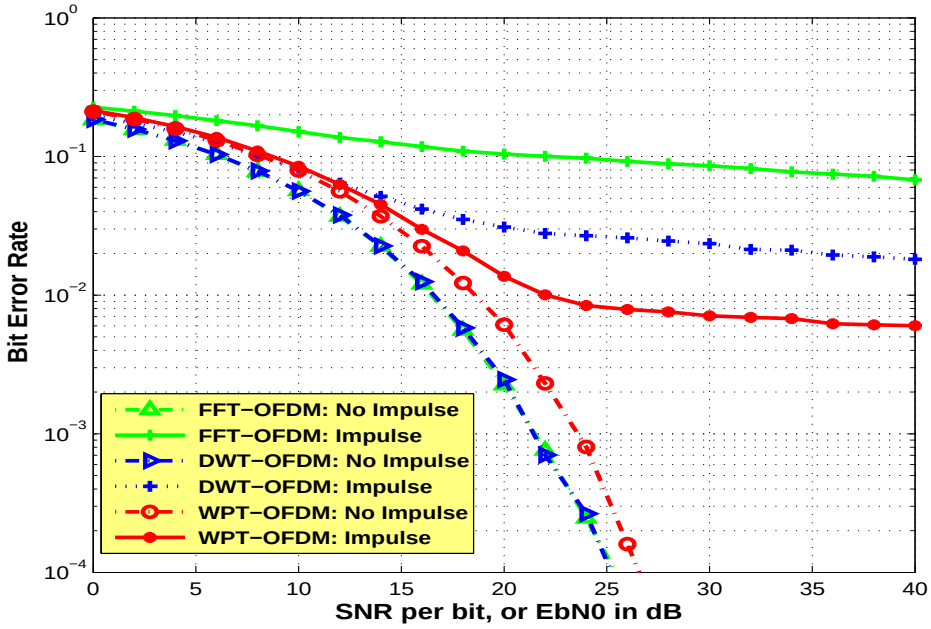

Figure 7.5: BER performance of Scenario 2 for all the three transforms when $a = 50$ and $r = 10$.

7.5 Summary

In this chapter, a performance study on DWT-OFDM and WPT-OFDM as substitutions for FFT-OFDM, with focus on the effects of impulse noise is presented. The flexibility models regarding FFT-OFDM, DWT-OFDM and WPT-OFDM platform models are discussed. These models are described in more details in chapter 3. Performance in terms of BER is also obtained for all of these techniques while varying the Poisson distribution parameters. The results showed that impulsive noise has less impact on the system when its recurrence parameter a is large. The BER performance of the WPT-OFDM system is shown to be superior to others due to its characteristics of forming the tree structure of wavelet basis function splitting LPF and HPF coefficients.

Chapter 8

Performance OFDM Systems in DVB-T and FER

8.1 Introduction

An OFDM system is a multi-carrier system which processes signals to be transmitted in parallel at different frequencies simultaneously from the same source. The conventional OFDM system, Fourier based OFDM, employs guard interval or cyclic prefix (CP) so that the delay spread of the channel becomes longer than the channel impulse response to minimize inter-symbol interference between symbols. However, the CP brings the disadvantage to the spectral containment of the channels. Much literatures have studied the use of wavelet based to replace Fourier based OFDM and found out that the wavelet based has more advantages than Fourier based OFDM. Some researchers have made comparisons between discrete multitone (DMT) and discrete wavelet multitone (DWMT) systems. However, to the best of author's knowledge, not much literature consider the applications of digital video broadcasting-terrestrial (DVB-T) in their investigations. There is only one literature, which is [55], discusses both OFDM systems with the DVB-T system. More discussions of FFT-OFDM and wavelet based OFDM are available in chapter 2 and 3 respectively.

This chapter is divided into two main sections. The first part of this chapter considers the performances of Fourier-Based and Wavelet-Based OFDM for

DVB-T Systems in section 8.2. The use of DVB-T in which that the bandwidth of the transmission is 8 MHz compliance with ETSI standard for 2k mode has been considered. We made comparisons based on BER Monte Carlo simulation for AWGN and Rayleigh fading channels. Section 8.2 contains the effect of NBI in section 8.2.1, followed by the presentation of the experimental results of DVB-T in AWGN channel in section 8.2.2 as well as the experimental results of the BER performance in multipath channel in section 8.2.3.

The second part presents the QAM comparisons of OFDM and FER application. In this research work, the BER performance of QAM over OFDM channel with facial expression recognition application is studied in section 8.3. The QAM scheme using FFT-OFDM is presented in section 8.3.1, whereas, the modulation comparisons using DWT-OFDM is discussed in section 8.3.2. The experimental results are described in section 8.3.3 and 8.3.4 respectively.

8.2 DVB-T and OFDM systems: Performance Simulation in DVB-T System

In this section, the performance of wavelet-based OFDM is compared with Fourier-based OFDM. Assumptions are made that the simulation is performed without the consideration of the channel equalization or channel estimation. For the system simulation, the OFDM parameters for DVB-T system are used with compliance of ETSI standard. This is shown in Table 8.1. Note that the term 2k mode refers to the number 1705 of subcarriers in ETSI standard above.

8.2.1 NBI Effect in DVB-T

Fig. 8.1 shows the frequency response of the system at the front end receiver of OFDM (DVT-B system) in AWGN channel. The top part shows the signal with carrier frequency about 90 MHz. The bottom part shows the signal if there is an unwanted signal or an interference within the same 8 MHz

Table 8.1: OFDM parameters for the 2k mode from [132].

Parameter	**2k mode**
Duration OFDM symbol period, T_u	224e-6
Baseband elementary period, T_b	$T_u/2048$
Number of carriers K	1705
Value of carrier number $K_{\max}$	1704
Value of carrier number $K_{\min}$	0
Carrier Spacing $1/T_u$	4464 Hz
Spacing between carriers $K_{\max}$ and $K_{\min}$, $(K-1)/2$	7.61 MHz
Allowed guard interval	1/4 1/8 1/16 1/32
Duration of symbol part T_u	$1048 \times T_b = 224$e-6
Duration of guard interval Δ	$512 \times T_b = 56$e-6 $256 \times T_b = 28$e-6 $128 \times T_b = 14$e-6 $64 \times T_b = 7$e-6
Symbol duration $T_s = \Delta + T_u$	$2560 \times Tb = 280$e-6 $2304 \times T_b = 252$e-6 $2176 \times T_b = 238$e-6 $2112 \times Tb = 231$e-6

bandwidth. In this case, we showed the unwanted signal having the carrier frequency of about 91 MHz. To simulate the signal to satisfy the transmission bandwidth of 8 MHz for DVT-B system, the sampling frequency has to satisfy Nyquist criterion, considering at least twice of the carrier frequency. In this simulation, we used a carrier frequency of about 90 MHZ for VHF channel, making the sampling frequency (f_s) of at least 180 MHz or the sampling time (t_s) was reciprocal of it, about 5.47 nano seconds.

In the presence of narrowband interference, the performance of OFDM in terms of E_b/N_o was also shown. In Fig. 8.2, the comparison was made when the narrowband interference may co-exist within the DVB-T spectrum and also when it was absence for both systems, the wavelet-OFDM (db32-OFDM) and FFT-OFDM with 25% of the total OFDM symbol period. Assumption

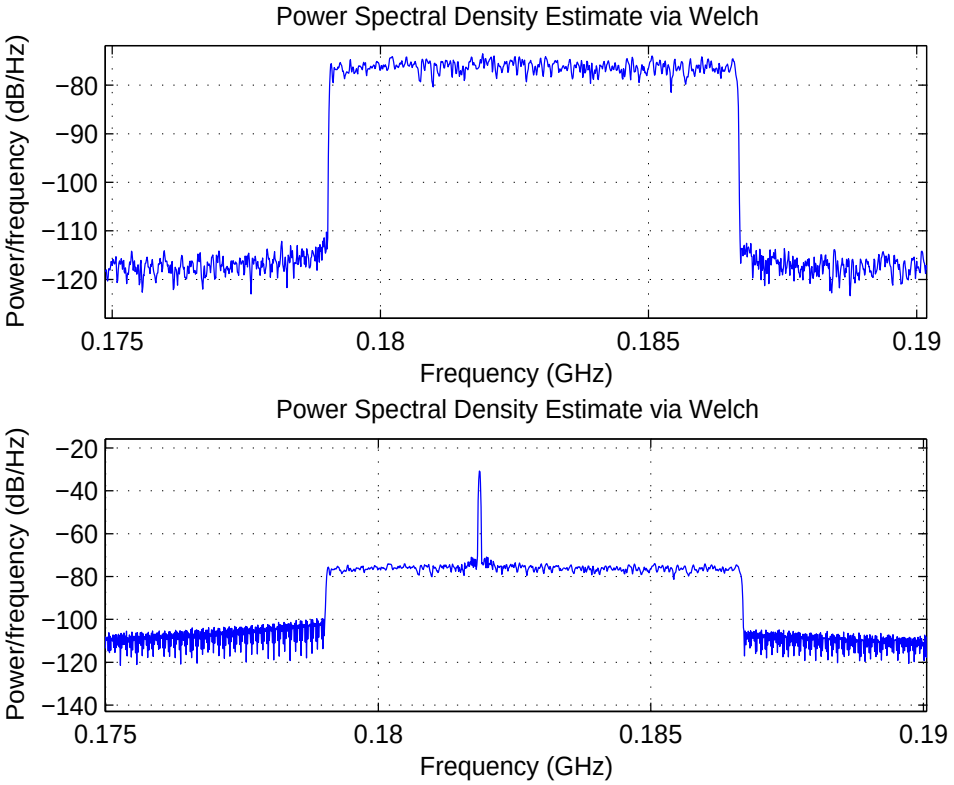

Figure 8.1: Frequency response of 2k mode signal (number of subcarriers: 1705) at the front-end receiver of (FFT-16-QAM with CP 1/4 th of symbol period) OFDM (DVT-B system) in AWGN channel without (Top figure) and with (Bottom) interference.

was made that the carrier frequency of the narrowband interference was 91 MHz next to the OFDM transmission frequency carrier for both systems. We used a simple method, time windowing technique as mentioned in [119] to suppress the interference. Time-domain windowing (TDW) is performed when the received signal sample is multiplied by a sample-by-sample in each symbol time with the window coefficients. In this case, rectangular pulse windowing is used. The wavelet-based OFDM with db32 showed a significant performance improvement of about 6 dB at BER of 0.01 over FFT-OFDM when the suppression method was applied.

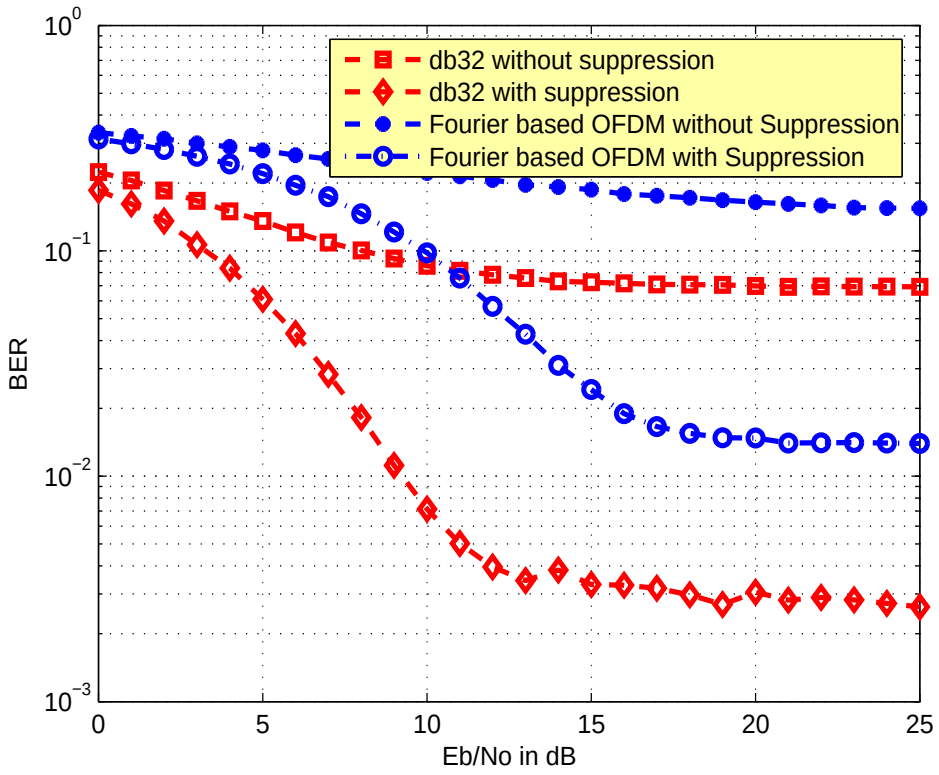

Figure 8.2: Performance of BER of FFT-OFDM and db8/db1 (Haar) - OFDM over AWGN channel using 16-QAM in the presence of narrowband interference.

8.2.2 AWGN Channel

The Daubechies' DWT-OFDM family outperform the Fourier-based FFT-OFDM as shown in Fig. 8.3. In this simulation, we used CP of 25% of the total OFDM symbol period for the FFT-OFDM system. The DWT-OFDM families do not require cyclic prefix due to the overlapping nature of their properties. The Haar or db1 wavelet outperformed the FFT-OFDM by E_b/N_o margin of 5 dB, for the same BER of 0.001 on AWGN channel. Other members of the Daubechies family such as db8, db16, and db32 also outperformed the FFT-OFDM by 7 dB, 10 dB, and 11 dB, respectively, at the same BER.

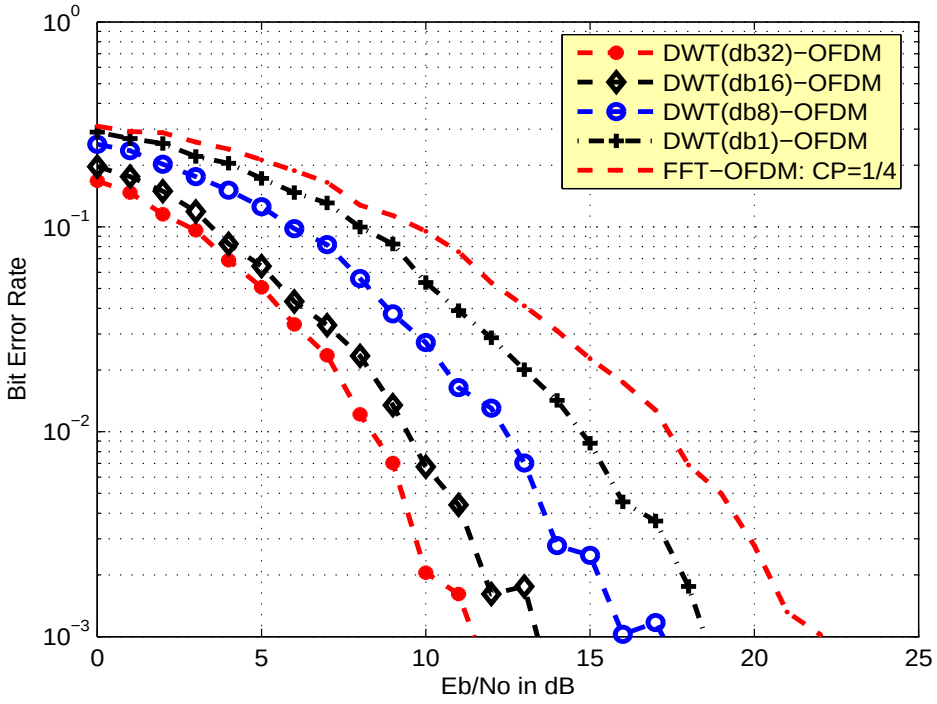

Figure 8.3: Performance of Bit error rate (BER) of Fourier-based OFDM and different Daubechies DWT-OFDM's over AWGN channel using 16-QAM.

8.2.3 Multipath Fading Channel

A comparison of BER was also observed in a multipath flat-fading channel in Fig. 8.4. We considered that the channel is static or the maximum Doppler

shift is 0. The DWT-OFDM's with db8 and Haar outperformed Fourier-based OFDM by 7 dB and 2 dB, respectively, at BER of 0.01. Performance in multipath frequency-selective fading was also simulated. In this case, we assumed that the receiver is a pedestrian with a walking speed of 1 m/s in an urban area. Using the formula $f_d = (v * f_c)/C$ ($C = 3 \times 10^8$ m/s), a maximum doppler shift (f_d) of about 0.3 Hz was obtained. The difference in time between path delays was approximately 6 micro seconds. In Fig. 8.5, the performance curves of Haar wavelet and db8 were almost the same as that of FFT-OFDM at low E_b/N_o (less than 10 dB). However, the results showed significant improvement by DWT-OFDM with E_b/N_o higher than 10 dB. The system might be further improved at low E_b/N_o if we could use a single-tap channel equalizer to compensate the performance due to the Rayleigh fading.

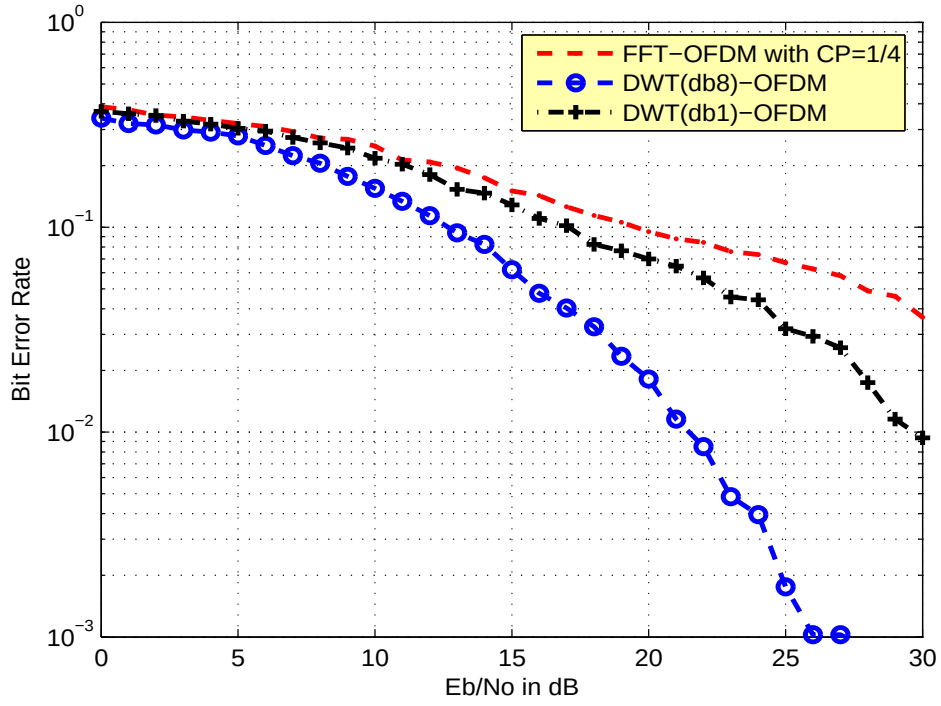

Figure 8.4: Performance of BER of FFT - OFDM and db8/db1 Haar -OFDM and over multipath fading.

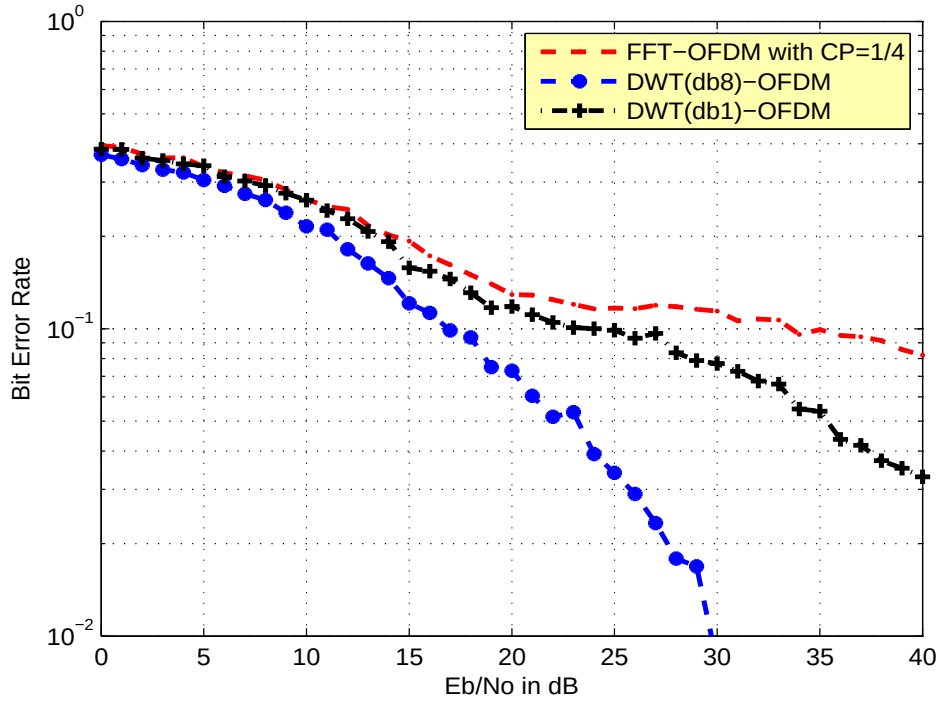

Figure 8.5: Performance of BER of FFT-OFDM and db8/Haar-OFDM over multipath (i.e multipath follows Rayleigh fading).

8.3 FER and OFDM Systems

In this system, facial image is used as the input data for the OFDM systems. An image pre-processing procedure is required to process the data before it is passed to the QAM modulation and OFDM channel. At the receiver, the image is recovered after applying facial expression recognition (FER). Several methods have been available in literatures including Higher-order local Auto Correlation (HLAC) to achieve an optimum image recovery. Details literature about FER can be found in [114] and [61].

8.3.1 The System Model of FER and FFT-OFDM Channel

The binary data is processed by M-ary quadrature amplitude modulation (QAM) to map the raw binary data to appropriate QAM symbols. The term M here means the number of binary input to the QAM. In the case of 4-QAM, M is 2 bit. There are four possible symbols that can be transmitted in parallel in an OFDM channel for that type of QAM. On the other hand, M is 4 bits if one considers 16-QAM. There are sixteen possible symbols that can be transmitted in parallel. These symbols are then input into inverse fast Fourier transform (IFFT). This involves taking N parallel streams of QAM symbols (N being the number of sub-carriers used in the transmission of the data) and performing an IFFT operation on this parallel stream. The IFFT and FFT have already been discussed in detail in section 2.5 and are not being described again in this section. The significant note from the figure is that the performance has been compared for two different QAM modulation using Fourier based OFDM and presented in further detail in section 8.3.3. In a typical communication link, the demodulated signal in the receiver will use the same modulation type as the modulated signal in the transmitter to achieve efficient use of bandwidth within optimal bit error rate. If the system uses 4-QAM in the transmitter, the receiver will also require to use 4-QAM demodulator in order to recover back the signal with 2 bits of data.

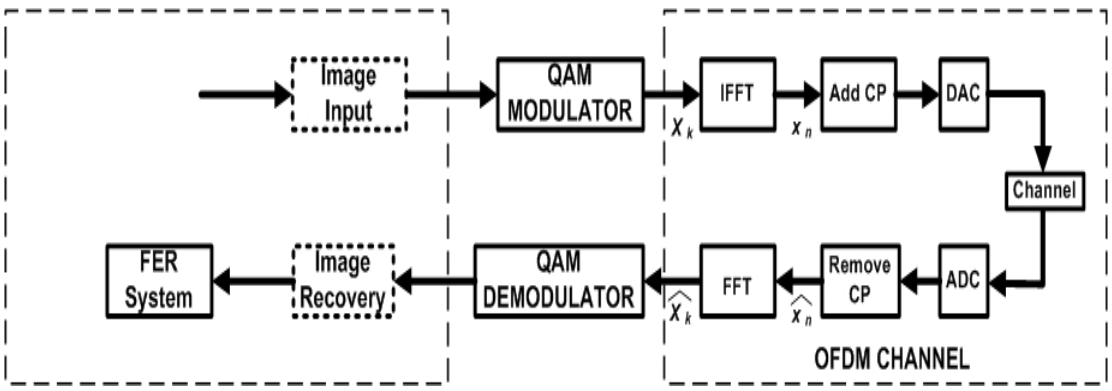

Figure 8.6: An overall system when FER is applied to conventional OFDM Channel.

8.3.2 The System Model of FER and DWT-OFDM Channel

Fig. 8.7 shows the system block diagram when considering wavelet based OFDM. QAM modulator and demodulator perform similar operations as described in previous section. In this case, two QAM types, 4-QAM and 16-QAM are used for obtaining the results in section 8.3.4. All functional components perform similar tasks as described in section 8.3.1 except the IDWT and DWT blocks. The operation of these two components is not described in this section. Their input and output signals processing have been discussed in chapter 3. The significant point from the figure is that the system has performed experimental results between 4-QAM and 16-QAM within two different wavelet families, orthogonal i.e. db2 and biorthogonal i.e bior5.5. Further wavelet families discussion can be found in section 8.3.4. These two wavelet families have been simulated because they showed better BER performance among orthogonal and biorthogonal families as described in section 3.4 shown in Fig. 3.13.

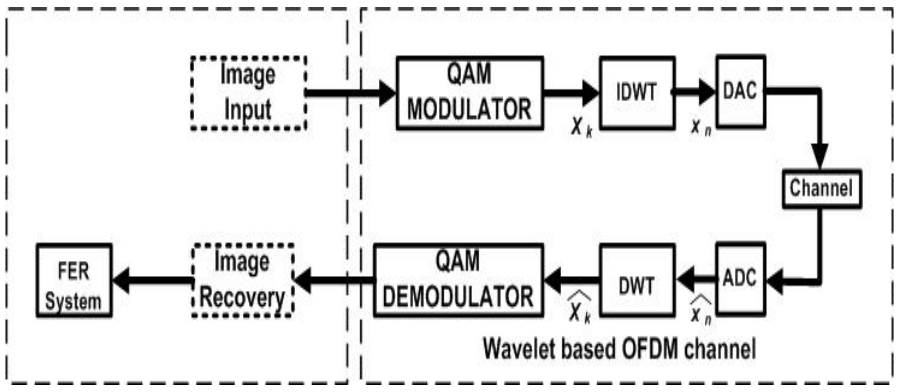

Figure 8.7: An overall system when FER is applied to Wavelet based OFDM Channel.

8.3.3 QAM Modulation Performance Comparisons: FER-Fourier based OFDM

Fig. 8.8 shows the error rate for 4-QAM and 16-QAM based on different SNRs. When the system uses 4-QAM, there is only 2 bits of transmission. As a result, the error rate oscillates within a small gap of error difference, which is between 0.15 to 0.22, to achieve a stable rate of error between 0 to 16 dB of SNR. On the other hand, the error rate oscillates within a big gap of error difference when the system uses 16-QAM. , there is only 2 bits of transmission. It takes a longer values of SNR from 0 to 30 dB to reach a stable rate of error since it has 4 bits of transmission.

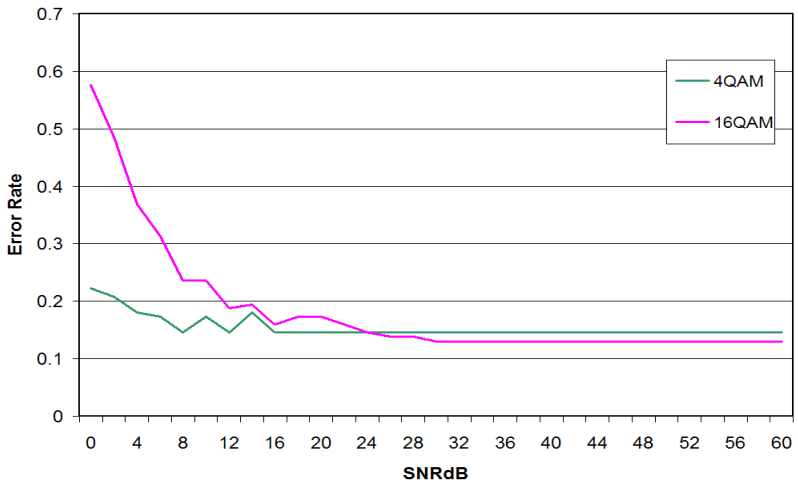

Figure 8.8: Error rate versus signal to noise ratio for different QAM modulation.

In Fig. 8.9, the theoretical value was obtained from equations (14) and (15) in [99]. The result shows that the image as input source has been correctly detected by the receiver as expected. This is because 4-QAM always show less BER error compared to 4 bits per symbol for 16-QAM [48].

It is shown that the empirical results has merged to obtain about the same as the theoretical results for 16-QAM modulation scheme. In addition, when the system uses 4-QAM, it has achieved an excellent performance as its empirical value performs inline with theoretical value. Moreover, when comparing 4 and 16-QAM, there is a marginal difference of about 6 dB SNR gain between

those two QAMs at BER target of 10^{-4}.

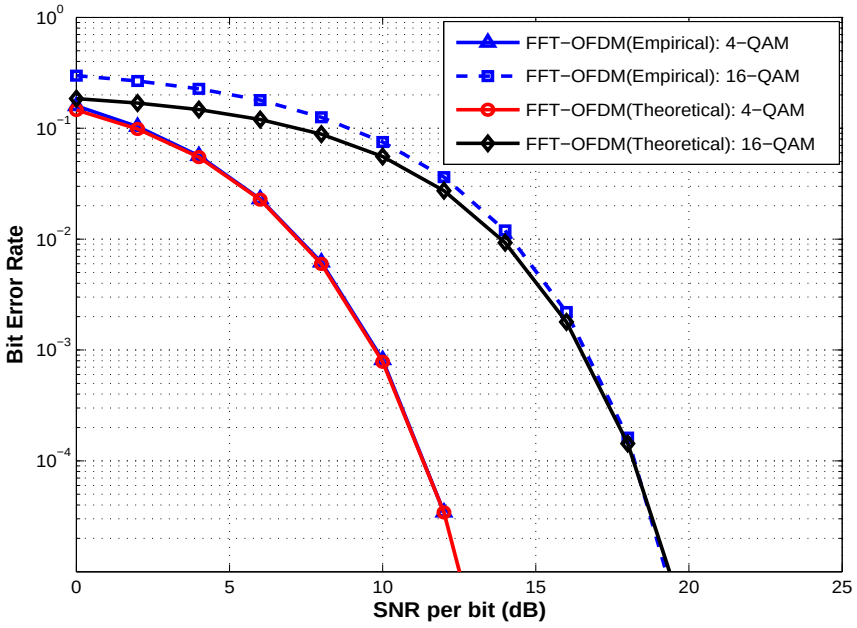

Figure 8.9: Bit error rate versus signal to noise ratio for different QAM modulation.

8.3.4 QAM Modulation Performance Comparisons: FER-Wavelet based OFDM

Fig. 8.10 shows the error rate for 4-QAM and 16-QAM based on different SNRs when wavelet based OFDM has been considered with FER. The result is correct because the error would be less if the number of level QAM is small. It is interesting to observe that bior5.5 has less error rate compare to db2 in both QAM schemes. This is possible since biorthogonal wavelet offers extra advantage in which that it has symmetrical scaling and wavelet coefficients as explained in chapter 3.

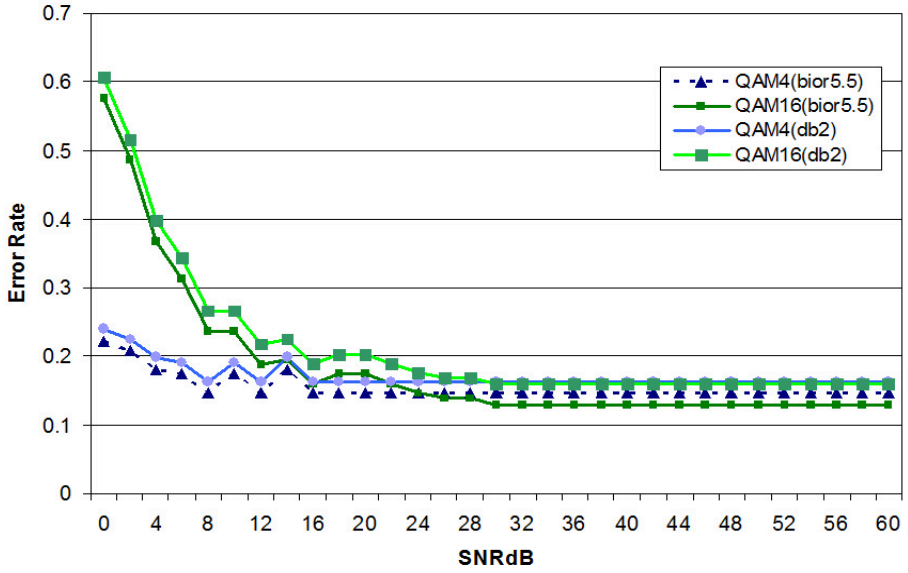

Figure 8.10: Error rate versus signal to noise ratio for different QAM modulation.

In Fig. 8.11, the result shows that the image as input source has again been correctly detected by the receiver as expected. Specifically, at BER target of 10^{-4}, there is a marginal difference of about 6 dB SNR gain between those two QAMs. It also interesting to observe that bior5.5 has better BER performance than db2 in both modulation schemes because of its characteristics having symmetrical scaling and wavelet coefficients.

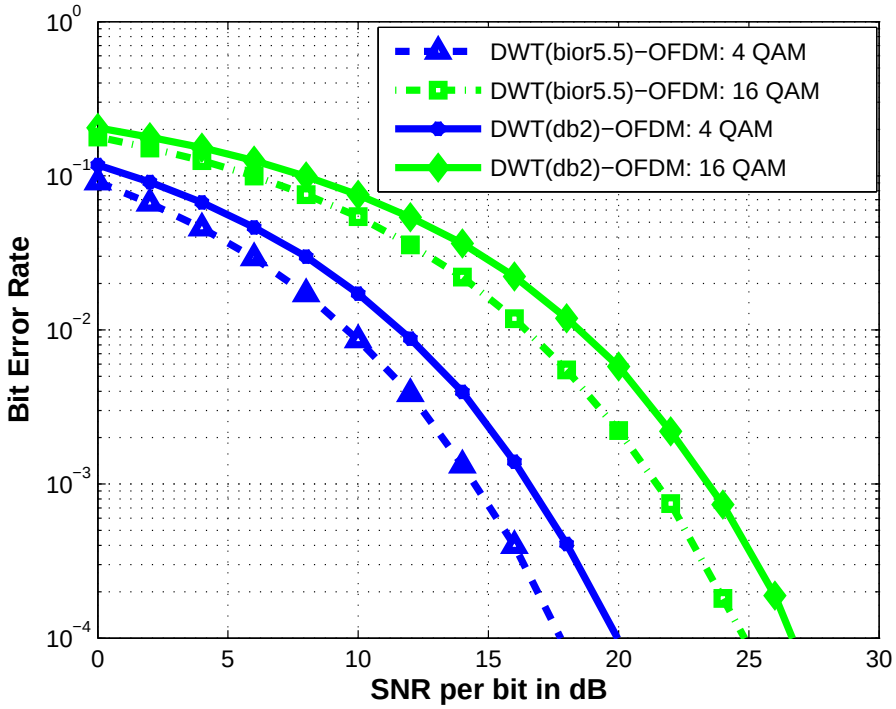

Figure 8.11: Bit error rate versus signal to noise ratio for different QAM modulation.

8.4 Summary

In this chapter, we studied DVB-T system using two OFDM platforms and facial expression recognition over OFDM channel for two different modulation methods within two OFDM systems. It is shown that the wavelet-based OFDM (DWT-OFDM) out-performs Fourier-based OFDM (FFT-OFDM) in terms of E_b/N_o for the same bit error rate (BER) target of 0.001 in DVB-T system. As the order of Daubechies filter increases from 1 (haar) to 32, the E_b/N_o gain also increases and all showed improvement over Fourier-based OFDM. In the presence of narrowband interference, the performance of OFDM in terms of E_b/N_o was also shown. The wavelet-based OFDM with db32 showed a significant performance of improvement of about 6 dB at BER of 0.01 over FFT-OFDM when the time windowing technique was applied. Further simulation were also done in Rayleigh fading channels under multipath flat-fading and frequency

- selective fading. In both cases, the performance of the DWT-OFDM also shows improvement over the performance of FFT-OFDM in DVB-T system.

Furthermore, when considering the second part of this chapter, two main sections are discussed, considering FFT-OFDM with FER and DWT-OFDM with FER. In FFT-OFDM with FER application, 4-QAM has an excellent performance since its empirical value performs inline with theoretical value. On the other hand, bior5.5 has obtained better BER performance as compared to an orthogonal family db2 because it has shown less error rates in both QAM modulations.

Chapter 9

Conclusions and Future Directions

The purpose of this chapter is to summarise the results of each chapter and to include the future directions. The second and third chapters discussed the overview of Fourier based OFDM as well as wavelet based OFDM. The results are included to study the components of transceivers in typical OFDM systems. The alternative platform of having wavelet OFDM can be applied in many systems. Wavelet based OFDM has outperformed the conventional OFDM since it offers many advantages. Due to offering many advantages, it has bright prospect for future research. Using wavelet packet transform, we can optimise the system by finding the best level of tree using different type of QAM modulations. This idea can be performed in two different schemes, circular and square modulations, as discussed in chapter 4.

The overviews of interference models and mitigation techniques are presented in chapter 5. Previous works show that they use conventional platform, which is Fourier based OFDM, without considering wavelet based OFDM. Therefore, an interference cancelation algorithm, which is explained in chapter 6, has been proposed to work in both OFDM systems. Further interference studies about an impulsive noise has been presented in chapter 7. This type of interference is one of the most popular topics in an OFDM system. Much literature studies the effect of an impulsive noise in conventional OFDM system. There are few investigations about it in wavelet based OFDM. Thus,

this dissertation develops a flexible models to function within three different OFDM platforms, FFT-OFDM, DWT-OFDM and WPT-OFDM. Appropriate MATLAB commands have to be performed correctly in order to function each model. The final chapter, which is chapter 8, deals with DVB-T system and FER application for Fourier and wavelet based OFDMs. When considering DVB-T with OFDM systems, the 2k mode of parameters following the ETSI standard are simulated for obtaining the experimental results. The effect of narrowband interference has been considered. When performing the NBI effect, the narrowband interference frequency must be properly simulated within the DVB-T frequency range in which that it is an offset value from the frequency carrier. The second part of the final chapter considers the FER application with two OFDM channels within two comparisons of QAM schemes (4-QAM and 16-QAM). The system block diagram containing inverse and forward transforms have been identified as crucial components to indicate that they works as Fourier or wavelet based OFDM. When the system considers Fourier based OFDM, the inverse and forward transform consider IFFT and FFT operations respectively. On the other hand, IDWT and DWT are the operational blocks replacing IFFT and FFT respectively.

9.1 Summary of Results

In chapter 4, we have derived the circular 16-QAM constellation in a programming-like language environment and proved that its power consumption is less as compared to the square 16-QAM scheme. The work has been applied to Fourier and wavelet based OFDM systems to compare the two modulations. In Fourier based OFDM system, the circular scheme showed slightly better results of BER performance than the square using different number of subcarriers. The results were also obtained for the wavelet based OFDM system using different wavelet families. The error rates showed that the circular 16-QAM were also slightly better as compared to the square 16-QAM.

An interference cancellation algorithm (ICA) that has shown outstanding performance for both ideal and non-ideal system cases where it reached almost the same error is proposed in chapter 6. A sinusoidal interfering signal was considered. In addition, the wavelet-based OFDM outperformed Fourier-based OFDM in both cases. This thesis considered an estimation of a single type of interference but it is expected that in future work the model described in this work can be expanded to consider multiple interferences as mentioned in work by [6]. It is also good if this work can be extended to include other interference cancelation or suppression algorithms in future work.

In chapter 7, performance studies on DWT-OFDM and WPT-OFDM as substitutions for FFT-OFDM, with the focus on the effects of impulsive noise interference are presented. The details about the DWT-OFDM and WPT-OFDM platform models including the MATLAB commands are discussed. Performance in terms of BER was also obtained for all of these techniques while varying the Poisson distribution parameters. Our results showed that impulse noise has less impact on the system when its recurrence parameter a is large. The BER performance of the WPT-OFDM system is shown to be

superior to others.

The performances of DVB-T in both OFDM systems, and application of facial expression recognition over two OFDM channels for two different modulation methods are considered in chapter 8. In the first part of this chapter, the performance of DVB-T has been obtained. It is shown that the wavelet-based OFDM (DWT-OFDM) out-performs Fourier-based OFDM (FFT-OFDM) in terms of E_b/N_o for the same bit error rate (BER) target of 0.001 in DVB-T system in AWGN channel. As the order of Daubechies filter increases from 1 (haar) to 32, the E_b/N_o gain also increases and all showed improvement over Fourier-based OFDM. In the presence of narrowband interference, the performance of OFDM in terms of E_b/N_o was also shown. The wavelet-based OFDM with db32 showed a significant performance of improvement of about 6 dB at BER of 0.01 over FFT-OFDM when the time windowing technique, rectangular window, was applied. Further simulation were also done in Rayleigh fading channels under multipath flat-fading and frequency - selective fading. In both cases, the performance of the DWT-OFDM also shows improvement over the performance of FFT-OFDM in DVB-T system.

When considering the second part of this chapter, which is the application of OFDM system in facial expression recognition over OFDM channel for different modulation methods, two subsections are discussed; FFT-OFDM with FER and DWT-OFDM with FER. In FFT-OFDM with FER application, 4-QAM has an excellent performance since its empirical value performs inline with theoretical value. On the other hand, bior5.5, has obtained better BER performance as compared to an orthogonal family, db2, because it has shown less error rates in both QAM modulations.

9.2 Future Directions

There are several areas in this dissertation that can be extended for further research. These can be itemised as follows:

- One of the drawbacks OFDM system is the peak-to-average power ratio (PAPR) problem. PAPR can be defined when the OFDM transmitting signal produce high peaks and drive the power amplifiers to operate near non linear saturation regions. As a result, the power efficiency becomes weak and causes performance degradation. Therefore, it is necessary to reduce PAPR. It is no doubt that there are many techniques introduce by many literatures using conventional Fourier based OFDM. On the other hand, wavelet based OFDM is a strong candidate as alternative platform instead of the conventional one to reduce PAPR. The significant feature of wavelet based OFDM is its orthogonality is satisfied by wavelet filters [24]. In addition, guard interval is also unnecessary, consequently, the bandwidth efficiency of WOFDM is enhanced by 20 percent better than the conventional OFDM systems [78], [98]. Works in [127] reduces the peak-to-average power ratio (PAPR) in Daubechies (Db) wavelet-based OFDM (WOFDM) by searching better wavelet packet tree (BWPT) structures. These BWPT structures are obtained by using a brute force search algorithm. The study uses BPSK modulation to obtain the results. Therefore, future research may include to use this BWPT structures with different modulation types. By performing this method, the results would be more novelty because of the variations of performances with different modulations.

- BER performances can be further improved if we apply error control coding [117]. An error control code can be defined as a redundancy code that is inserted in the transmitted data stream so that the receiver

can possibly detect the error and correct it during the signal transmission. A code rate R is normally expressed to indicate the amount of the redundancy code of insertion. A coding gain term is also important when discussing the error control code. It refers to the difference of the additional transmitted power that is required to obtain the same performance without coding. An example of a very famous type of coding is hamming code. It is a new approach of study to include such as a hamming code in wavelet based OFDM system to improve BER performances. It is a novelty work when comparisons of coding can be made and also performed in Fourier based OFDM.

- Chapter 5 discusses mitigation methods without considering a mitigation technique for broadband interference. The broadband interference mitigation would be hard to develop because its spectra is embedded within almost every subcarrier in an OFDM symbol [96]. Because of this characteristic, it results synchronization and timing errors. However, this interference would be possible to mitigate using wavelet based OFDM system. According to [28], a wavelet based system is more robust against synchronization errors could be developed without compromising on spectral efficiency or receiver complexity. The design and development of new wavelets which handle timing offset can be performed in order to mitigate the broadband interference.

- An estimation of a sinusoidal interference has been considered in chapter 6. This work could be extended to include other interference cancelation or suppression algorithms. Mitigation techniques described in chapter 5 can be simulated and compared with the proposed ICA. Furthermore, the proposed sinusoidal model described in chapter 6 can be extended to consider multiple sinusoidal interferences as mentioned in [6] and the OFDM systems, considering Fourier and wavelet based, should be de-

veloped to estimate and mitigate them.

- In chapter 7, the effect of impulsive noise interference in OFDM schemes is explained. Future works may develop mitigation techniques to minimise the impulsive noise. Example of works to mitigate the impulsive noise in a multicarrier modulation is in [124]. This work presents coding techniques in which that RS code is applied to techniques such as time domain clipping and MSE monitoring. The time domain clipping technique is begun with the assumption that some of the impulses magnitude are larger than the received ADSL signal. In order to detect them, monitoring of sudden drops in AGC level, clipping in the ADC and indicating the presence of large voltages at the input to the receiver are the tasks of the decoder. If this event occurs for some time domain samples, the decoder has to declare that an impulsive noise is present and it should erase the corresponding multitone symbol accordingly. The mitigation technique introduced by [124] considered only for Fourier based OFDM. The wavelet based OFDM has not yet been considered. Thus, a DWT-OFDM model as an alternative platform can be considered with consideration of the mentioned techniques. Furthermore, this technique coupled with the proposed ICA described in chapter 6 can be studied. The performance results would be a novelty because this work is new and it cannot be found in any available literature.

- Chapter 8 presents the application DVB-T in OFDM systems using 2k mode of ETSI standards. The BER performance simulated in Fig. 8.2 showed the effects of NBI. The time windowing technique, rectangular window, to suppress the interference was used. Future work should consider the ICA presented in chapter 6. The time widowing technique such as Hanning window, raise cosine window and Hamming window can be also used. Comparisons of BER performances can then be evaluated. In

the second part of chapter 8, the FER application with comparisons of QAM modulations for FFT- and DWT- OFDM was considered. It is interesting to observe the experimental results about BER performances for the two types of QAM modulations of FFT-and DWT-OFDM with FER application. It was not included the NBI effects in these systems. Thus, future work would be beneficial to have the effects of NBI in both systems with different modulation techniques within the FER application.

- The application of DVB-T system in chapter 8 and FER with OFDM channels can be furthered studied when the systems consider 16-QAM circular modulation scheme as described in chapter 4. In fact, the impulsive noise interference effects can also be simulated using this modulation scheme as well. The performance results can be obtained and compared with available square schemes. This work would become more interesting when considering different mitigation techniques to suppress the impulsive noise interference.

Appendix A

Orthogonality in an OFDM System

Appendix A: Orthogonal Integration between Two Subcarriers(2.6)

From equation 2.6, consider two different integers, $n = \xi$ and $m = \chi$ with the assumptions that $\{\xi \neq \chi\}$, $\{0 < \xi \leq N\}$ and $\{0 < \chi \leq N\}$ where N is the number of subcarrier. Then, we have two signals such as $\sin(\xi\omega t)$ and $\sin(\chi\omega t)$ fulfill the orthogonality by determining the integration over an effective OFDM symbol period T_s and $\omega = \frac{2\pi}{T_s}$ as shown in the following steps:

$$\begin{aligned}
\int_0^{T_s} \sin(\xi\omega t)\sin(\chi\omega t)dt &= \int_0^{T_s} \tfrac{1}{2}[\cos(\xi\omega t - \chi\omega t) - \cos(\xi\omega t + \chi\omega t)]dt \\
&= \int_0^{T_s} \tfrac{1}{2}[\cos(-\xi\omega t) - \cos((\chi+1)\omega t)]dt \\
&= \tfrac{1}{2}\int_0^{T_s} [\cos(-\xi\omega t) - \cos((\chi+1)\omega t)]dt \\
&= \tfrac{1}{2\omega}[\sin(\xi\omega t)\mid_0^{T_s} - \tfrac{1}{6\omega}[\sin((\chi+1)\omega t]\mid_0^{T_s} \\
&= \tfrac{1}{2\omega}[\sin(\xi\omega t)\mid_0^{T_s} - \tfrac{1}{6\omega}[\sin((\chi+1)\omega t]\mid_0^{T_s} \\
&= 0
\end{aligned}$$

The above derivation can also be treated in complex exponential by using Euler's identity

$[\sin(\theta) = \frac{1}{2j}(e^{j\theta} - e^{-j\theta})]$ and $[\cos(\theta) = \frac{1}{2}(e^{j\theta} + e^{-j\theta})]$

Appendix B

Perfect Reconstruction Properties

Appendix B: Perfect Reconstruction(3.3.3)

Orthogonal Wavelet

A simple construction of block diagram showing perfect reconstruction (PR) property is performed by a two-channel filter bank which is represented by the LPF and HPF is shown in Fig. 3.3.3. The first level of analysis filter in the receiver part can be folded and the decimator and the expander are cancelled out by each other. To satisfy a perfect reconstruction operation, the output $Y_{k(i)}$ is expected to be the same as $X_{k(i)}$. With the exception of a time delay, the input can be considered as $Y_{k(i)} = X_{k(i-n)}$ where n can be substituted as 1 to describe this simple task. The steps to perform the mathematical operation of PR can be summarised as follows [86]:

1. Selecting the filter coefficients for g_a, i.e., a and b. Thus, $g_a = \{a, b\}$.
2. h_a is a reversed version of g_a with every other value negated. Thus, $h_a = \{b, -a\}$. If the system has 4 filter coefficients with $g_a = \{a, b, c, d\}$, then $h_a = \{d, -c, b, -a\}$.
3. h_s is the reversed version of g_a, thus $h_s = \{b, a\}$.
4. g_s is also a reversed version of h_a, therefore $g_s = \{-a, b\}$.

The above steps can be rewritten as follows:

$$g_a = \{a, b\}, h_a = \{b, -a\}, h_s = \{b, a\}, g_s = \{-a, b\} \tag{B.1}$$

Considering that the input with delay are applied to h_a and g_a in Fig. **??**, then the output of these filters are

$$Z_{k(i)} = b(X_{k(i)} - a(X_{k(i-1)}) \tag{B.2}$$

$$W_{k(i)} = a(X_{k(i)} + b(X_{k(i-1)}) \tag{B.3}$$

Considering also that $Z_{k(i)}$ and $W_{k(i)}$ are delayed by 1, then the subscript i can be replaced by $(i-1)$ as follows

$$Z_{k(i-1)} = a(X_{k(i-1)} + b(X_{k(i-2)}) \tag{B.4}$$

$$W_{k(i-1)} = b(X_{k(i-1)} - a(X_{k(i-2)}) \tag{B.5}$$

The output $Y_{k(i)}$ can be written as

$$Y_{k(i)} = g_s Z_{k(i)} + h_s W_{k(i)} \tag{B.6}$$

or,

$$Y_{k(i)} = -aZ_{k(i)} + bZ_{k(i-1)} + bW_{k(i)} + aW_{k(i-1)} \tag{B.7}$$

Substituting equations (8), (9), (10) and (11) into (13) yields to

$$Y_{k(i)} = 2(a^2 + b^2)X_{k(i-1)} \tag{B.8}$$

The output $Y_{k(i)}$ is the same as the input $X_{k(i)}$ except that it is delayed by 1 if we substitute the coefficient factor $2(a^2 + b^2)$ by 1. The PR condition is satisfied.

Appendix C

Probability of Error Circular 16-QAM

Appendix C: Calculation Probability of Error (Pe) Expression (4.4)

Pe for binary PAM

Before we discuss the calculation of Pe for the circular 16-QAM, we provide the fundamental concept of binary pulse amplitude modulation (PAM) for general understanding. Consider Fig. C.1, we have the average probability of error Pe in terms of minimum distance d given by

$$\begin{aligned} P_e &= \frac{1}{2}P(y<0|_{x=\frac{d}{2}}) + \frac{1}{2}P(y>0|_{x=-\frac{d}{2}}) \\ &= \frac{1}{2}P(x+n<0|_{x=\frac{d}{2}}) + \frac{1}{2}P(x+n>0|_{x=-\frac{d}{2}}) \\ &= \frac{1}{2}P(n<-x|_{x=\frac{d}{2}}) + \frac{1}{2}P(n>x|_{x=-\frac{d}{2}}) \\ &= P(n>\frac{d}{2}) \quad or \quad P(n<-\frac{d}{2}) \\ &= P(z>\frac{d}{\sqrt{2N_0}}) \\ &= Q(\frac{d}{\sqrt{2N_0}}) \end{aligned} \tag{C.1}$$

where z is scaled by ratio of n over $\sqrt{\frac{N_0}{2}}$ or $z = \frac{n}{\sqrt{\frac{N_0}{2}}}$ and $Q(x) = \frac{1}{\sqrt{2\pi}}\int_x^\infty e^{\frac{-x^2}{2}}dx$.

Expressing P_e in terms of energy over noise spectral density, we need to consider the energy E for both points is the same amount since they are same distance to the centre or reference point 0. Thus, the energy for both points is $E = (\frac{d}{2})_2$, and also $d = \sqrt{4E} = 2\sqrt{E}$. By substituting E and d into equation C, we have

$$\begin{aligned} P_e &= Q(\frac{2\sqrt{E}}{\sqrt{2N_0}}) \\ &= Q(\sqrt{\frac{2E}{N_0}}) \end{aligned} \tag{C.2}$$

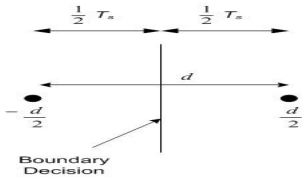

Figure C.1: The decision boundary Binary PAM. Note: T_s is a symbol period

Pe for Circular 16 QAM

This appendix has figures related to section 4.4 of Chapter 4.

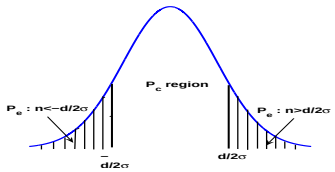

Figure C.2: The pdf curve illustrating the decision boundary process.

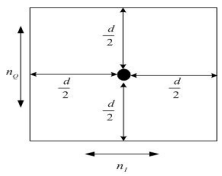

Figure C.3: Type I of decision boundary associated to the inner most circle of Figure 4.2.

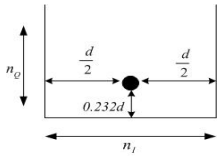

Figure C.4: Type II of decision boundary associated to the points {5, 7} in Figure 4.2

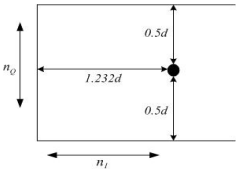

Figure C.5: Type III of decision boundary associated to the six points {4, 6, 8, 9, 10, 11} in Figure 4.2

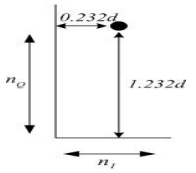

Figure C.6: Type IV of decision boundary associated to the four points located on the outermost circle in Figure 4.2

Bibliography

[1] A. Batra and J. R. Zeidler, "Narrowband interference mitigation in OFDM systems", *IEEE Military Communications Conference (MILCOM) 2008*, pp. 1-7, Nov 2008.

[2] A. J. Coulson, "Bit Error Rate Performance of OFDM in Narrowband Interference with Excision Filtering", *IEEE Transactions on Wireless Communications*, vol. 5, pp. 2484-2492, 2006.

[3] A. Jamin and P. Mahonen, "Wavelet packet Modulation for Wireless Communications", *Wireless Communications and Mobile Computing Journal*, John Wiley and Sons Ltd. Vol. 5, No. 2, pp. 123-137, Mar 2005.

[4] A. J. Redfern, "Receiver Window Design for Multicarrier Communication Systems", *IEEE Journal on Selected Areas in Communications*, Vol. 20, No. 5, June 2002.

[5] A. N. Akansu, "Wavelets and Filter Banks: A Signal Processing Perspective", *Tutorial in Circuit and Devices*, Nov 1994.

[6] A. N. Akansu, and L. Xueming, "A Comparative Performance Evaluation of DMT (OFDM) and DWMT (DSBMT) Based DSL Communications Systems for Single and Multitone Interference", *Proceedings of the IEEE International Conference on Acoustics, Speech and Signal Processing*, vol. 6, pp. 3269 - 3272, May 1998.

[7] A. N. Akansu, M. V. Tazebay, M. J. Medley, and P. K. Das, "Wavelet and subband transforms: fundamentals and communication applications," IEEE Communications Magazine, vol. 35, pp. 104-115, 1997.

[8] A. N. Akansu, P. Duhamel, L. Xueming, and M. de Courville, "Orthogonal transmultiplexers in communication: a review," IEEE Transactions on Signal Processing, vol. 46, pp. 979-995, 1998.

[9] A. N. Akansu and R. A. Haddad, *Multiresolution Signal Decomposition: Transforms, Subbands and Wavelets*, Second Edition, California: Academic Press, 2001.

[10] A. Peled, A. Ruiz, "Frequency Domain Data Transmission Using Reduced Computational Complexity Algorithms", *Proceedings IEEE Int. Conf. on Acoustics, speech and Signal Processing (ICASSP'80)*, Denver, pp. 964-967, 1980

[11] A. R. S. Bahai and B. R. Saltzberg, *Multi-Carrier Digital Communications - Theory and Applications of OFDM*, Kluwer, 1999.

[12] B. G. Negash and H. Nikookar,"Wavelet based OFDM for wireless channels", *Vehicular Technology Conference*, 2001.

[13] B. G. Negash and H. Nikookar, "Wavelet-based multicarrier transmission over multipath wireless channels," Electronics Letters, vol. 36, pp. 1787-1788, 2000.

[14] C. S Burrus, R. A Gopinath and H. Guo, *Introduction to Wavelets and Wavelet Transforms A Primer*, New Jersey: Prentice Hall, 1998.

[15] C. Valens: "A Really Friendly Guide to Wavelets", Available at: http://ergodic.ugr.es/statphys/bibliografia/reviews/wavelets.pdf

[16] D. Gerakoulis and P. Salmi, "An interference suppressing OFDM system for wireless communications," *IEEE International Conference on Communications*, New York, 2002.

[17] D. Karamehmedovic, M. K. Lakshmanan and H. Nikookar, "Performance of Wavelet Packet Modulation and OFDM in the Presence of Carrier Frequency and Phase Noise", *Proceedings of the 1st European Wireless Technology Conference*, Amsterdam, Oct 2008.

[18] D. Middleton, "Statistical-Physical Models of Electromagnetic Interference", *IEEE transaction on Electromagnetic Compatibility*, Vol. EMC-19, No. 3, Aug 1977.

[19] D Zhang, P. Fan and Z. Cao "A Novel Narrowband Interference Canceller for OFDM systems," *Wireless Communications and Networking Conference*, pp. 1426-1430, 2004.

[20] F. Adachi and M. Sawahashi, "Performance analysis of various 16 level modulation schemes under Rayleigh fading," *Electronics Letters*, vol. 28, pp. 1579-1581, 1992.

[21] F. Xiong, *Digital Modulation Techniques*, Second edition, Boston: Artech House, 2006.

[22] G. Carron et al., "Comparison of two modulation techniques using frequency domain processing in interference limited home networks", *International Conference Consumer Electronics(ICCE2002)*, pp. 296-297, June 2000.

[23] G. J. Saulnier, Z. Ye, and M. J. Medley, "Performance of a spread spectrum OFDM system in a dispersive fading channel with interference", *IEEE Military Communications Conference (MILCOM98)*, vol. 2, pp. 679-683, Oct 1998.

[24] G. Strang and T. Nguyen, *Wavelets and Filter Banks*, Wellesly/Cambridge Press, 1996.

[25] H. A. Suraweera, C. Chai, J. Shentu and J. Armstrong, "Analysis of Impulse Noise Mitigation Techniques for Digital Television Systems", *Proc.*

8th International OFDM Workshop (InOWo 2003), Hamburg, Germany, Sept. 2003. pp. 172-176.

[26] H. Nikookar and R. Prasad, "Waveshaping of Multicarrier Signal for data Transmission overWireless Channels", *IEEE 6th International Conference on Universal Personal Communications Record (ICUPC)*, October 1997.

[27] H. Nikookar and R. Prasad, "Optimal Waveform Design for Multicarrier Transmission Through a Multipath Channel", *Proceedings of the IEEE Vehi. Tech. Conf. (VTC)*, May 1997.

[28] H. Nikookar and M.K.Lakshmanan, "Comparison of Sensitivity of OFDM and Wavelet Packet Modulation to Time Synchronization Error", *The 19th Annual IEEE International Symposium on Personal, Indoor and Mobile Radio Communications (PIMRC'08)*, pp. 1-6, Sept 2008.

[29] H. Sari, G. Karam and I. Jeanclaude, "Transmission Techniques for Digital Terrestrial TV Broadcasting", *IEEE Communications Magazine*, pp. 100-109, Feb 1995.

[30] H. Steendam, M. Moeneclaey, "Analysis and Optimization of the Performance of OFDM on Frequency-Selective Time-Selective Fading Channels", *IEEE Transactions on Communications*, Vol. 47, No. 12, Dec 99, pp. 1811-1819.

[31] H. Zhang, D. Yuan, and M. Pätzold, "Novel study on PAPRs reduction in wavelet-based multicarrier modulation systems," *Digital Signal Processing*, vol. 17, pp. 272-279, 2007.

[32] H. Zhang, D. Yuan and C. X. Wang, "A study on the PAPRs in multicarrier modulation systems with different orthogonal bases", *Wireless Communications and Mobile Computing*, vol. 7, pp. 311-318, 2007.

[33] H. Zhang, D. Yuan, M. Jiang, and D. Wu, "Research of DFT-OFDM and DWT-OFDM on different transmission scenarios", *The 2nd International*

Conference on Information Technology for Application Proceedings, pp. 8-11 January 2004.

[34] IEEE Broadband Wireless Standard 802.16.3.

[35] I. Kalet, "The multitone Channel", *IEEE Transactions on Communications*, Vol. 37, no. 2, Feb. 1989, pp. 119-124

[36] I. Daubechies, *Ten Lectures on Wavelets*, Philapdelphia: Society for Industrial and Applied Mathematics, 1992.

[37] I. Daubechies, " Orthonormal Bases of Compactly Supported Wavelets", *Comm. in Pure and Applied Math.*, vol. 41, pp. 909-996, 1988.

[38] J. J. Van de Beek, P. Dling, S. K. Wilson and P. O. Brjesson, "Orthogonal Frequency Division Multiplexing (OFDM)", *URSI Review of Radio Science 1996-1999*, Oxford Publishers, pp. 177-206, 1999

[39] J. J. van de Beek, M. Sandell and P. O. Brjesson, "ML Estimation of Time and Frequency Offset in OFDM Systems", *IEEE Transactions on Signal Processing*, Vol. 45, no 7, Jul 1997, pp. 1800-1805

[40] J. A. C. Bingham, "Multicarrier Modulation for Data Transmission: An Idea Whose Time Has Come", *IEEE Communications Magazine*, Vol. 28, no 5, pp. 5-14, 1990.

[41] J. A. Young and J. S. Lehnert, "Analysis of DFT-based frequency excision algorithms for direct-sequence spread-spectrum systems", *IEEE Transactions Communications*, vol. 46, no. 8, pp. 1076Ű1087, Aug 1998.

[42] J. M Cioffi, "Class reader for EE379c-advanced digital communication: multichannel modulation", *Stanford University, Stanford, CA, 2005*, Chapter 4, available at: http:// www.stanford.edu/class/ee379c

[43] J. M Cioffi, G. P Dudevoir and M. V Eyuboglu, "MMSE decision-feedback equalizers and coding - Part I: Equalization results", *IEEE Transactions Communications*, 43, (10), pp. 2582-2594, 1995.

[44] J. M Cioffi, G. P Dudevoir and M. V Eyuboglu, "MMSE decision-feedback equalizers and coding - Part II: Coding results", *IEEE Transactions Communications*, 43, (10), pp. 2595-2604, 1995.

[45] J. C. Feauveau, "Analyse Multiresolution par Ondelettes Non-orthogonales et Bancs de Filtres numeriques", These, Univ Paris XI, 1990.

[46] J. Lago-Fernandez and J. Salter, "Modelling impulsive interference in DVB-T: statistical analysis, test waveforms and receiver performance", BBC Research and Development White Paper. Online. Available: http://www.bbc.co.uk/rd/pubs/whp/whp080.html

[47] J. G. Proakis, "Interference Suppression in Spread Spectrum Systems", The 4th IEEE International Symposium on Spread Spectrum Techniques and Application Proceedings, Vol. 1, pp. 259-266, Sept. 1996.

[48] J. G. Proakis and M. Salehi, *Communication Systems Engineering*, Second ed., New Jersey: Prentice Hall, 2002.

[49] J. G. Proakis, M. Salehi, and G. Bauch, *Contemporary Communication Systems Using MATLAB Second ed.*, Brooks Cole, 2004.

[50] J-P Kahane and P-Gilles L-Rieusset, *Fourier Series and Wavelets*, Volume 3, Luxembourg: Gordon and Breach Science, 1995.

[51] J. Wu, "Wavelet Packet Division Multiplexing", Dissertation for PhD, McMaster University, Hamilton, Ontario. pp. 1-171, 1998.

[52] K. Anwar, A. U. Priantoro, M. Saito, T. Hara, M. Okada and H. Yamamoto, "On the PAPR Reduction for Wavelet Based Transmultiplexer", *lnteniational Syinposiurri on Communications and Information Technologies (ISCW)*, Japan, Oct 26-29, 2004.

[53] K. L. Blackard, T. S. Rappaport and C. W. Bostian, "Measurements and Models of Radio Frequency Impulsive Noise for Indoor Wireless Commu-

nications," *IEEE Journal on Selected Areas in Communications*, vol. 11, pp. 991-1001, 1993.

[54] K. Cho and D. Yoon, "On the General BER Expression of One- and Two Dimensional Amplitude Modulations", *IEEE Transactions on Communications*, vol. 50, no. 7, pp. 1074Ű1080, July 2002.

[55] K. Abdullah and Z. M. Hussain, "Performance of Fourier-Based and Wavelet-Based OFDM for DVB-T Systems", *IEEE Australasian Telecommunication Networks and Applications Conference*, Dec 2007.

[56] K. Abdullah, K. L. Neville and Z. M. Hussain, "An Interference Cancelation Algorithm for Fourier-Based and Wavelet-Based OFDM Systems", *IEEE International Conference on Advance Technologies for Communications*, Oct 2008.

[57] K. Abdullah and Z. M. Hussain, "Impulsive Noise Effects on DWT- and WPTOFDM versus FFT-OFDM", *IEEE International Conference on Communication, Computer and Power*, Feb 2009.

[58] K. Abdullah and Z. M. Hussain, "Studies on DWT-OFDM and FFT-OFDM Systems", *IEEE International Conference on Communication, Computer and Power*, Feb 2009.

[59] K. Abdullah, N. A. Hinai, A. Z. Sadik and Z. M. Hussain, "Circular 16-QAM Modulation Scheme for Wavelet and Fourier Based OFDM Systems", *The 5th IEEE GCC Conference*, Mar 2009.

[60] K. Abdullah, A. Z. Sadik and Z. M. Hussain, "On the DWT- and WPT-OFDM versus FFT-OFDM", *The 5th IEEE GCC Conference*, Mar 2009.

[61] K. Abdullah, S. M. Lajervadi and Z. M. Hussain, "QAM Modulations over Wavelet based OFDM Channel for Facial Expression Recognition", *IEEE Australasian Telecommunication Networks and Applications Conference*, Nov 2009.

[62] K. M. Wong, W. Jiangfeng, T. N. Davidson, J. Qu and P. C. Ching, "Performance of wavelet packet-division multiplexing in impulsive and Gaussian noise", *IEEE Transactions on Communications*, vol. 48, no. 7,pp. 1083-1086, 2000.

[63] L. B. Milstein and P. K. Das, "An analysis of a real-time transform domain filtering digital communications system - part i: Narrow-band interference rejection", *IEEE Transactions Communications*, vol. COM-28, no. 6, pp. 816-824, June 1980.

[64] L. Cui, B. Zhai, and T. Zhang, "Existence and design of biorthogonal matrix-valued wavelets", *Nonlinear Analysis: Real World Applications*, vol. 10, pp. 2679-2687, 2009.

[65] L. C. Ludeman, *Random Processes: Filtering, Estimation and Detection*, New Jersey: John Wiley and Sons, 2003.

[66] L. de Clercq, M. Peeters, S. Schelstraete, and T. Pollet, "Mitigation of radio interference in xDSL transmission", *IEEE Communications Magazine*, pp. 168-173, Mar 2000.

[67] L. J. Cimini, "Analysis and Simulation of a Digital Mobile Channel Using Orthogonal Frequency Division Multiplexing", *IEEE Transactions on Communications*, Vol. COM-33, No. 7, pp. 665-675, 1985.

[68] L. Xu and Y. Yan, "Wavelet-based Removal of Sinusoidal Interference from a Signal", *IOP Electronic Journals: Measurement Science and Technology*, vol. 15, no. 9, pp. 1779-1786, 2004.

[69] M. A. Tzannes, M. C. Tzannes, and H. L. Resnikoff, "The DWMT A multicarrier transceiver for ADSL using M-band wavelets", ANSI Standard Committee TlE1.4 Contribution 93-067, Mar 1993.

[70] M. A. Tzannes, "System design issues for the DWMT transceiver", ANSI Standard Committee TlE1.4, Contribution 93-100, Apr 1993.

[71] M. A. Tzannes, M. C. Tzannes, J. Proakis, and P. N. Heller, "DMT systems, DWMT systems and digital filter banks", in Proc. ZCC, 1994.

[72] M. Baro and J. Ilow, "PAPR Reduction in OFDM Using Wavelet Packet Pre-Processing", *The 5th IEEE Consumer Communications and Networking Conference (CCNC)*,pp. 195-99, 2008.

[73] M. Baro and J. Ilow, "PAPR Reduction in OFDM Using Wavelet Packet Modulation Using Tree Pruning", *The 65th IEEE Vehicular Technology Conference (VTC)*,pp. 1756-1760, 2007.

[74] M. W. Frazier, *An Introduction to Wavelets through Linear Algebra*", New York: Springer-Verlag, 1999.

[75] M. Ghosh, "Analysis of the effect of impulse noise on multicarrier and single carrier QAM systems", *IEEE Transactions on Communications*, vol. 44, no. 2, pp. 145-147, 1996.

[76] M. Jeruchim, "Techniques for Estimating the Bit Error Rate in the Simulation of Digital Communication Systems," Selected Areas in Communications, IEEE Journal on, vol. 2, pp. 153-170, 1984.

[77] M. Kuhn, D. Benyoucef, and A. Wittneben, "Linear block codes for frequency selective PLC channels with colored noise and multiple narrowband interference", *IEEE Vehicle Technology Conference*, vol. 4, pp. 1756-1760, 2002.

[78] M. K. Lakshmanan and H. Nikookar, "A Review of Wavelets for Digital Wireless Communication " *Wireless Personal Communications*, vol. 37, pp. 387-420, 2006.

[79] M. R. Nakhai, "Multicarrier transmission," Signal Processing, IET, vol. 2, pp. 1-14, 2008.

[80] M. Oltean and M. Nafornita, "Efficient Pulse Shaping and Robust Data Transmission Using Wavelets," *IEEE International Symposium on Intelligent Signal Processing, WISP*, 2007.

[81] M. E. Sahin and H. Arslan, "A narrowband interference identification approach for UWB systems," presented at Milcom 2005, 2005.

[82] M. A. Tzannes and M. C. Tzannes, "Bit-by-bit channel coding using wavelets," in Global Telecommunications Conference, 1992. Conference Record., GLOBECOM '92. Communication for Global Users., IEEE, 1992, pp. 684-688 vol.2.

[83] M. A. Tzannes, M. C. Tzannes, J. G. Proakis, and P. N. Heller, "DMT Systems, DWMT Systems and Digital Filters," *Proceedings International Conference Communication*, New Orleans, LA, pp. 31-315, May 1-5, 1994.

[84] M. G. Amin, C. Wang, and A. R. Lindsey, "Optimum interference excision in spread spectrum system communications using open-loop adaptive filters", *IEEE Trans. Signal Processing Mag.*, vol. 47, no. 7, pp. 1966Ű1976, July 1999.

[85] M. Vetterli and J. Kovacevic, *Wavelets and Subband Coding*, New Jersey:Prentice Hall, 1995.

[86] M. Weeks, *Digital Signal Processing Using Matlab and Wavelets*, Infinity Science Press LLC, 2007.

[87] M. Zimmermann and K. Dostert, "Analysis and modeling of impulsive noise in broad-band powerline communications," *IEEE Transactions on Electromagnetic Compatibility*, vol. 44, pp. 249-258, 2002.

[88] N. Ahmed, "Joint Detection Strategies for Orthogonal Frequency Division Multiplexing", Dissertation for Master of Science, Rice University, Houston, Texas. pp. 1-51, April 2000.

[89] N. Neurohr and M. Schilpp, "Comparison of transmultiplexers for multi-carrier modulation", *Fourth International Conference on Signal Processing Proceedings, (ICSP '98)*, vol.1, pp. 35-38, 1998.

[90] O. G. Hooijen, "On the channel capacity of the residential power circuit used as a digital communications medium", *IEEE Commun. Letters*, Vol. 2, no. 10, pp. 267-268, Oct. 1998.

[91] P. A. Bello and R. Esposito, "A new method for calculating probabilities of errors due to impulsive noise", IEEE Transactions Communications Technology, Vol. COM-17, pp. 368Ű379, June 1969.

[92] P. J. Marshall, "The coexistance of DS-CDMA mobile radio systems and fixed services", Ph.D. dissertation, University of Auckland, 1997.

[93] P. J. Van Fleet, *Discrete Wavelet Transformations: An Elementary Approach with Applications*, New Jersey: Wiley-Interscience, 2008.

[94] P. S. Addison, *The Illustrate Wavelet Transform Handbook: Introductory Theory and Applications in Science, Engineering, Medicine and Finance*, London: Institute of Physics, 2002.

[95] P. P. Vaidyanathan, *Multirate Systems and Filter Banks*, New Jersey: Prentice Hall, 1993.

[96] RadioSky Journal. Available: http://www.radiosky.com/journal0901.html.

[97] Rainmaker Technologies, Inc.: ŚRM wavelet based PHY proposal for 802.16.3, Available: http://ieee802.org/16.

[98] Rainmaker Technologies, Inc.: ŚRM wavelet based (WOFDM) PHY proposal for 802.16.3, Technical Report IEEE 802.16.3c-01/12,2001. Available: http://ieee802.org/16.

[99] R. A. Pacheco and D. Hatzinakos, "BER analysis of self-heterodyne OFDM transmission scheme ", *Canadian Conference on Electrical and Computer Engineering*, Vol. 4, pp. 1953-1956, May 2004.

[100] R. Dilmirghani and M. Ghavami, "Wavelet Vs Fourier Based UWB Systems", *18th IEEE International Symposium on Personal, Indoor and Mobile Radio Communications*, pp.1-5, Sep. 2007.

[101] R. E. Blahut, *Fast Algorithms for Digital Signal Processing*, Reading, MA: Addison-Wesley, 1985.

[102] R.E. Ziemer, W.H. Tranter, and D.R. Fannin, *Signals and Systems: Continuous and Discrete*, Fourth Edition, New Jersey: Prentice-Hall, 1998.

[103] R. G. Gallager, *Information Theory and Reliable Communication*. New York: Wiley, 1968.

[104] R. K. Young, *Wavelet Theory and Its Applictions*, Massachusetts: Kluwer Academic, 1993.

[105] R. Nilsson, F. Sjoberg and J. P. LeBlanc,"A Rank-Reduced LMMSE Canceller for Narrowband Interference Suppression in OFDM-Based Systems", *IEEE Transactions on Communication*, Vol. 51, No. 12, Dec. 2003.

[106] R. Mirghani, and M. Ghavami, "Comparison between Wavelet-based and Fourier-based Multicarrier UWB Systems", *IET Communications*, Vol. 2, Issue 2, pp. 353-358, 2008.

[107] R.M. Rao and A.S. Bopardikar, *Wavelet Transforms: Introduction to Theory and Applications*, Massachusetts: Addison-Wesley, 1998.

[108] R. V. Nee and R. Prasad, *OFDM for Wireless Multimedia Communications*, Boston: Artech House, 2000.

[109] R.W. Chang, "Synthesis of Band-limited Orthogonal Signals for Multichannel Data Transmission", *Bell System Technical Journal*, Vol. 45, pp. 1775-1796, 1966.

[110] R. W. Lowdermilk and F. J. Harris, "Interference mitigation in orthogonal frequency division multiplexing (OFDM)," *The 5th IEEE International Conference on Universal Personal Communications*, California, USA, 1996.

[111] S. A. Kosmopoulos, P. T. Mathiopoulos, and M. D. Gouta, "Fourier-Bessel error performance analysis and evaluation of M-ary QAM schemes in an impulsive noise environment", *IEEE Transactions Communications*, vol. 39, pp. 398-404, Mar 1991.

[112] S. D. Sandberg, "Adapted demodulation for spread-spectrum receivers which employ transform-domain interference excision", *IEEE Transactions Communications*, Vol. 43, no. 9, pp. 2502-2510, Sept 1995.

[113] S. J. Howard, "Narrowband interference rejection using small FFT block sizes", *IEEE Military Communications Conference (MILCOM93)*, Vol. 2, pp. 608-612, Oct 1992.

[114] S. M. Lajervadi, K. Abdullah and Z. M. Hussain, "Modulation Comparison Over OFDM Channel Facial Expression Recognition", *IEEE International Conference on Advance Technologies for Communications*, Oct 2009.

[115] S. Oshita and K. Feher, "Performance of coherent PSK and DPSK systems in an impulsive and Gaussian noise environment", IEEE Transactions Communications, Vol. COM-30, pp. 2540-2546, Dec 1982.

[116] S.B. Weinstein, P.M. Ebert, "Data Transmission by Frequency- Division Multiplexing Using the Discrete Fourier Transform", *IEEE Transactions on Communications*, Vol. 19, no. 5, pp. 628-634, May 1971.

[117] S. B. Wicker, *Error Control Systems for Digital Communucation and Storage.* New Jersey: Prentice Hall, 1995.

[118] S. D. Sandberg, and M. A. Tzannes, "Overlapped Discrete Multitone Modulation for High Speed Copper Wire Communications", *IEEE Journal on Selected Areas in Communications*, vol. 13, no. 9, pp. 1571-1585, 1995.

[119] S. Kapoor, and S. Nedic, "Interference Suppressions in DMT Receiver Using Windowing", *IEEE International Conference on Communications*, vol. 2, pp. 778-782, June 2000.

[120] S. R. Baig, F. U. Rehman, and M. J. Mughal, "Performance Comparison of DFT, Discrete Wavelet Packet and Wavelet Transforms in an OFDM Transceiver for Multipath Fading Channel", *9th IEEE International Multitopic Conference,*, pp. 1-6, Dec 2005.

[121] T. K. Moon and W. C. Stirling, *Mathematical Methods and Algorithms for Signal Processing*, New Jersey: Prentice Hall, 2000.

[122] T. Pollet, H. Steendam, M. Moeneclaey, "Performance Degradation of Multicarrier Systems by an Insufficient Guard Interval Duration", *Proceedings Int. Workshop on Copper Wire Access Systems "Bridging the Last Copper Drop" CWAS'97* , Budapest, Hungary, pp. 265-270, 1997.

[123] T. Wang, J. G. Proakis, and J. R. Zeidler, "Performance analysis of high QAM OFDM system over frequency selective time-varying fading channel,", *14th IEEE International Symposium on Personal, Indoor and Mobile Radio Communications*, pp. 793-798, 2003.

[124] T. N. Zogakis, P. S. Chow, J. T. Aslanis, and J. M. Cioffi, "Impulse noise mitigation strategies for multicarrier modulation," *IEEE International Conference on Communications*,Geneva. Technical Program, Conference Record, vol.2., pp. 784-788. 1993

[125] V. K. Ingle and J. G. Proakis, *Digital Signal Processing Using MATLAB V.4*, Massachusts: PWS Publishing/ITP, 1997.

[126] V. Kumbasar and O. Kucur, "Better wavelet packet tree based OFDM for multipath powerline channel," *Computers and Electrical Engineering*, vol. In Press, Corrected Proof. Available Online by 21 May, 2009.

[127] V. Kumbasar and O. Kucur, "Better wavelet packet tree structures for PAPR reduction in WOFDM systems," *Digital Signal Processing*, vol. 18, pp. 885-891, 2008.

[128] W. Kozek, G. Pfander, J. Ungermann and G. Zimmermann, "A comparison of various MCM schemes", *The 5th International OFDM Workshop Proceedings*, pp. 20-1 to 20-4, 2000.

[129] W. H. Tranter and K. L. Kosbar, "Simulation of Communication Systems", *IEEE Communications Magazine*, pp. 26-35, July 1994.

[130] W. Yang, G. Bi, and T. S. P. Yum, "A multirate wireless transmission system using wavelet packet modulation", *The IEEE 47th Vehicular Technology Conference*, vol.1, pp. 368-372, 1997.

[131] W.Y. Zou, Y. Wu, "COFDM, an Overview", *IEEE Transactions on Broadcasting*, Vol. 41, no 1, pp. 1-8, 1995.

[132] X. D. Yang, Y. H. Song, T. J. Owens, J. Cosmas and T. Itagaki, "Performance analysis of the OFDM scheme in DVB-T", *IEEE CAS Symposium on Emerging Technologies: Mobile and Wireless Communications*, Shanghai, China, 2004.

[133] X. Zhang, P. Xu, G. Zhang, and G. Bi, "Study on complex wavelet packet based OFDM modulation (CWP-OFDM)", *ACTA Electronica SINICA*, 30(4): pp. 476-479, 2002.

[134] Y. J. Guo, *Advances in Mobile Radio Access Networks*, MA: Artech House, 2004.

[135] Y. H. Ma, P. L. So and E. Gunawan, "Performance analysis of OFDM systems for broadband power line communications under impulsive noise and multipath effects", *IEEE Transactions on Power Delivery*, vol. 20, no. 2, pp. 674-682, 2005.

[136] Y. Wang and X. P. Zhang, "Filter bank based interference suppression for fading channels", *IEEE Canadian Conference on Electrical and Computer Engineering*, vol. 2, pp. 961- 964, May 2003.

[137] Y. Zhang and S. Cheng, "A novel multicarrier signal transmission system over multipath channel of low-voltage power line", *IEEE Transactions on Power Delivery*, vol. 19, pp. 1668-1672, 2004.

[138] Z. Dan, F. Pingyi and C. Zhigang, "Interference cancellation for OFDM systems in presence of overlapped narrow band transmission system", *IEEE Transactions on Consumer Electronics*, vol. 50, pp. 108-114, 2004.

[139] Z. Rafique, N. Gohar, and M. J. Mughal, "Performance Comparison of OFDM andWOFDM Based V-BLAST Wireless Systems", *IEICE Transactions on Communications*, E88-B: 2207-2209, 2005.

[140] Z. Zhang, S.C. Chan, and H. Cheng, "Robust adaptive channel estimation of OFDM systems in time-varying narrowband interference," 2005.

VITA

Khaizuran Abdullah received the B. Sc. in Electrical Engineering from Ohio University, USA 1997. From 1997 to 2000, he works as an electrical engineer in an industrial company. He proceeded his study and obtained the Master degree in Electrical Engineering from Universiti Teknologi Malaysia in 2003. He works as a lecturer and taught for Signals and Systems. He joint RMIT university as a PhD candidate in 2007. During his candidature, he was a tutor for various subjects such as Digital Signal Processing, Introduction to Matlab, Electronic Design and Electric Circuit Theory. His research interests are digital signal processing communications and digital communications, including the use of wavelet transform in an OFDM system.